10. SITE 987[1]

Shipboard Scientific Party[2]

HOLE 987A

Position: 70°29.796′N, 17°56.243′W

Start hole: 0915 hr, 23 August 1995

End hole: 0815 hr, 24 August 1995

Time on hole: 23.00 hr (0.96 days)

Seafloor (drill pipe measurement from rig floor, mbrf): 1683.0

Total depth (drill pipe measurement from rig floor, mbrf): 1882.3

Distance between rig floor and sea level (m): 11.4

Water depth (drill pipe measurement from sea level, m): 1671.6

Penetration (mbsf): 199.3

Coring totals:
Type: APC
Number: 10
Cored: 83.7 m
Recovered: 75.26 m, 89.9%

Type: XCB
Number: 12
Cored: 115.6 m
Recovered: 97.75 m, 84.6%

Total:
Number: 22
Cored: 199.3 m
Recovered: 173.01 m, 86.8%

Formation:
Unit I: 0–199.3 mbsf; Pleistocene to late Pliocene; silty clay, sandy turbidites

HOLE 987B

Position: 70°29.798′N, 17°56.216′W

Start hole: 0815 hr, 24 August 1995

End hole: 1845 hr, 24 August 1995

Time on hole: 10.50 hr (0.44 days)

Seafloor (drill pipe measurement from rig floor, mbrf): 1683.3

Total depth (drill pipe measurement from rig floor, mbrf): 1782.5

Distance between rig floor and sea level (m): 11.4

Water depth (drill pipe measurement from sea level, m): 1671.9

Penetration (mbsf): 99.2

Coring totals:
Type: APC
Number: 11
Cored: 99.2 m
Recovered: 74.18 m, 74.8%

Formation:
Unit I: 0–99.2 mbsf; Pleistocene to late Pliocene; silty clay, sandy turbidites

HOLE 987C

Position: 70°29.787′N, 17°56.188′W

Start hole: 1845 hr, 24 August 1995

End hole: 2145 hr, 24 August 1995

Time on hole: 3.00 hr (0.13 days)

Seafloor (drill pipe measurement from rig floor, mbrf): 1681.9

Total depth (drill pipe measurement from rig floor, mbrf): 1725.5

Distance between rig floor and sea level (m): 11.4

Water depth (drill pipe measurement from sea level, m): 1670.5

Penetration (mbsf): 43.6

Coring totals:
Type: APC
Number: 5
Cored: 43.6 m
Recovered: 44.91 m, 103.0%

Formation:
Unit I: 0–43.6 mbsf; Pleistocene to late Pliocene; silty clay, sandy turbidites

HOLE 987D

Position: 70°29.798′N, 17°56.178′W

Start hole: 2145 hr, 24 August 1995

End hole: 2245 hr, 26 August 1995

Time on hole: 49.00 hr (2.04 days)

Seafloor (drill pipe measurement from rig floor, mbrf): 1684.2

Total depth (drill pipe measurement from rig floor, mbrf): 2057.2

Distance between rig floor and sea level (m): 11.4

Water depth (drill pipe measurement from sea level, m): 1672.8

Penetration (mbsf): 373.0

Coring totals:
Type: APC
Number: 11
Cored: 94.8 m
Recovered: 97.67 m, 103.0%

[1]Jansen, E., Raymo, M.E., Blum, P., et al., 1996. *Proc. ODP, Init. Repts.*, 162: College Station, TX (Ocean Drilling Program).

[2]Shipboard Scientific Party is given in the list preceding the Table of Contents.

Type: XCB
Number: 31
Cored: 278.2 m
Recovered: 170.79 m, 61.4%

Total:
Number: 42
Cored: 373.0 m
Recovered: 268.46 m, 72.0%

Formation:
Unit I: 0–305.6 mbsf; Pleistocene to late Pliocene; silty clay, sandy turbidites
Unit II: 305.6–369.2 mbsf; late Pliocene; silty clay with sand and gravel (debris flows)
Unit III: 369.2–373.0 mbsf; late Pliocene; silty clay, clayey silt with sand, tilted/contorted beds, dropstones

HOLE 987E

Position: 70°29.787′N, 17°56.188′W

Start hole: 2245 hr, 26 August 1995

End hole: 1215 hr, 1 September 1995

Time on hole: 133.50 hr (5.56 days)

Seafloor (drill pipe measurement from rig floor, mbrf): 1684.2

Total depth (drill pipe measurement from rig floor, mbrf): 2543.6

Distance between rig floor and sea level (m): 11.5

Water depth (drill pipe measurement from sea level, m): 1672.7

Penetration (mbsf): 859.4

Drilled interval (mbsf): 0–363.3

Coring totals:
Type: RCB
Number: 52
Cored: 496.1 m
Recovered: 308.83 m, 62.3%

Formation:
Unit II: 363.3–369.2 mbsf; late Pliocene; silty clay with sand and gravel (debris flows)
Unit III: 369.2–575.5 mbsf; late to early Pliocene; silty clay, clayey silt with sand, tilted/contorted beds, dropstones
Unit IV: 575.5–657.6 mbsf; early Pliocene; silty clay with sand and gravel (debris flows)
Unit V: 657.6–859.4 mbsf; early Pliocene to Miocene; silty clay, very indurated, dropstones, dipping/contorted beds

Principal results: Five holes were drilled at Site 987 (EGM-4), with a maximum penetration of 859.4 mbsf, estimated to be within a few meters of oceanic basement at this site. All major seismic sequence boundaries were penetrated with overall good recovery. Despite gas expansion problems in the upper few hundred meters of the section, offsets between holes could be determined for the upper ~180 mbsf, and a continuous spliced section was produced for the upper 100 mbsf (approximately the last 1 Ma). Paleomagnetic data provided time control, enabling detailed documentation of the glacial history of the Greenland Ice Sheet back to the late Miocene. Biostratigraphic age information is scarce due to predominance of fossil-barren intervals.

The recovered sediments are mostly fine- to coarse-grained siliciclastics. Evidence for glacial depositional environments prevails throughout the recovered section. Five lithostratigraphic units were defined.

Unit I (0–305.6 mbsf; Pleistocene to late Pliocene) consists of silty clays interbedded with silt and silt with sand and clay. Thick sandy turbidites with sharp erosional lower contacts and graded upper contacts are common. Turbidites are thicker and most common toward the top of the unit. Dropstones were identified throughout this unit. Sediments containing up to 35% carbonate occur in inorganic calcite-rich bands, but the average for the unit is only 4.9%. Unit I is characterized by low magnetic susceptibility.

Unit II (305.6–369.2 mbsf; late Pliocene) consists of predominantly silty clay with sand, silty clay with sand and gravel, sand-silt-clay, and clayey silt with sand and gravel. Carbonate content is very low, but some inorganic calcite layers occur at the base of the unit. The unit contains numerous clasts >1.0 cm (up to 91 clasts in Core 162-987E-40X) and randomly oriented gravel, interpreted as components of debris-flow deposits rather than as dropstones. Crystalline rocks are the dominant rock type of these clasts. The unit is primarily defined by the presence of numerous isolated clasts. The top of Unit II is marked by a sharp increase in magnetic susceptibility and sand-sized fraction, as well as a decrease in the clay-sized content.

Unit III (369.2–575.5 mbsf; late to early Pliocene) is composed of silty clay with sand, silty clay with sand and gravel, silty clay with gravel, and silty clay. It is defined by a downcore decrease in magnetic susceptibility and in sand-sized particles. This unit contains a few >1.0-cm clasts, mainly sedimentary and igneous rock fragments, interpreted to be dropstones. Distorted and dipping beds and laminations occur in various intervals within the unit.

Unit IV (575.5–657.6 mbsf; early Pliocene) is, like Unit II, mainly composed of silty clay with sand, silty clay with sand and gravel, silty clay with gravel, and silty clay. Various igneous, metamorphic, and sedimentary clasts >1.0 cm are present. It is defined by a downcore increase in magnetic susceptibility and sand-sized content.

Unit V (657.6–859.4 mbsf; early Pliocene to Miocene) is composed of silty clay interbedded with clayey silt, clay with silt and sand, and clayey silt with sand. A few graded sandy turbidites are present and sediments are highly indurated. Fine-scale structures, including flaser bedding, dipping beds, wavy laminae, convoluted structures, and folding interpreted to be slumps or water escape structures occur throughout the unit. The unit is characterized by low magnetic susceptibility and by a reduced number of gravel clasts.

Turbiditic downslope sediment transport seems to be an important sedimentary process during the Pleistocene and late Pliocene. Units II (late Pliocene) and IV (early Pliocene) are very similar. Most of the sediment of these units seems to represent gravity-driven debris flows. Unit III (late to early Pliocene) and Unit V (early Pliocene to late Miocene) appear to have a higher component of hemipelagic deposition with less downslope sediment transport than in Units I, II, and IV.

The high deposition rates at this site are reflected by the change from sulfate reduction to methanogenesis at shallow burial depth (30 mbsf). Methane content as high as 68,000 ppm was observed at 74 mbsf, decreasing somewhat downsection. No evidence for gas hydrates was found, and natural gas profiles reflect normal biogenic processes. The organic matter content is variable, primarily reflecting marine organic matter with low C/N ratios.

The seismic stratigraphy, lithostratigraphy, sediment physical properties, and wireline logging results at Site 987 reflect general variations in the frequency and amount of gravity-driven sediment transport from the East Greenland Shelf. This is in accordance with the site's location at the northeastern flank of the Scoresbysund glacial fan. Intervals of more frequent debris flows form the most distinct seismic reflectors. Results of the shipboard paleomagnetic studies indicate a late Miocene age for the lowermost drilled sediments, immediately above basement. Based on the paleomagnetic data, a main result of drilling at Site 987 is that new and younger ages than previously proposed can be assigned to the main build-up of the Scoresbysund Fan. The main phase of fan construction took place in the late Pliocene to Pleistocene. Although glacial marine deposition and downslope transport is characteristic of most of the drilled sequence, two phases, one in the early Pliocene, and another in the late Pliocene, are particularly pronounced. At these times, thick debris-flow sequences were deposited from an active ice margin presumably positioned at the shelf break.

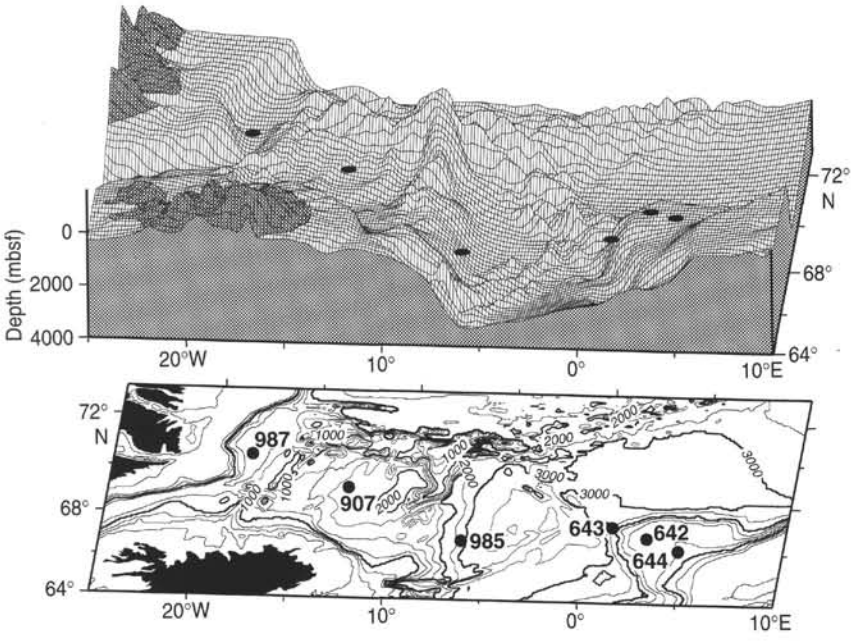

Figure 1. Bathymetry of the East Greenland–Norway transect margin showing the location of Leg 104, 151, and 162 drill sites.

BACKGROUND AND OBJECTIVES

Site 987 (EGM-4) was drilled on the Greenland Margin (Fig. 1) to examine the onset and history of glaciation in the North Atlantic region and to establish the history of the Greenland Ice Sheet, its inception, and possible phases of ice extension off the coast. Site 987 is also part of a paleoenvironmental transect from Norway to Greenland, designed to study the history of the advection of temperate, saline Atlantic waters into the Norwegian-Greenland Sea ("the Nordic heat pump"). This transect covers the climatically sensitive gradient between polar areas near east Greenland and temperate areas off Norway. Sites drilled on the Vøring Plateau during ODP Leg 104 anchor the eastern end of the transect, and Site 987 forms its western end (Fig. 1). By extending the late Pleistocene record available from piston cores back in time, we will be able to obtain a clearer understanding of the relationships between the Nordic heat pump, ocean circulation patterns, and the glaciation history on Milankovitch and longer time scales. This will provide insight into the climatic sensitivity of the Nordic Seas and its possible role as an early responder to orbital climate forcing.

It is important for our understanding of the transformation of the climate system into the ice-age world with increased sensitivity to orbital forcing to identify where and why ice sheets started to form. During the Pliocene–Pleistocene, three major ice sheets have terminated along the margins of the Nordic Seas: the Greenland, Scandinavian, and Svalbard–Barents Sea Ice Sheets. Information on the inception, variability, and dynamics of these ice masses needs to be assessed individually for each ice sheet, in order to understand which areas are the most sensitive to early ice-sheet growth, when glaciation style shifted from mountain-and-fjord-style glaciation to full-fledged ice sheets, and when marine-based ice sheets extending to the outer shelf area started to form. Drilling in relatively proximal areas of the ice masses is necessary to obtain this information. Sites 986 and 987 are therefore located on the lower continental slopes adjacent to the Svalbard–Barents Sea and Greenland Ice Sheets, respectively.

The initial phase of the late Cenozoic glaciation was most likely in the form of limited mountain, valley, and fjord glaciers reaching sea level. Due to its northern location on the western boundary of the Atlantic Ocean/Nordic Seas, with sufficient elevation and moisture supply, Greenland is the most likely location for the initiation of Cenozoic glaciation in the North Atlantic realm. Diamictites, interpreted to be basal tills, in shelf deposits drilled off southeast Greenland during ODP Leg 152, as well as land evidence, document that the Greenland Ice Sheet was previously much larger than at present, and in some periods reached to the shelf break (Funder, 1989; Larsen, Saunders, Clift, et al., 1994). This is also evident from the glacially sculpted shelf morphology with transverse troughs off major fjords and trough-mouth fans on the continental slope and rise. Site 987 was drilled on the lower part of the most prominent glacial trough-mouth fan complex on the East Greenland Margin off the Scoresbysund Fjord, which forms a major ice-drainage pathway from the central parts of the Greenland Ice Sheet. The fan is seen as a prominent positive expression in the bathymetry (Fig. 1).

Site 987 is located on supposed Anomaly 5 crust, about 10 Ma old (Vogt, 1986), and hence should enable documentation of the late Miocene to Holocene history of the area. The planned drilling to 800 mbsf was intended to penetrate and date the main seismic sequences, defining the phases of fan buildup and shelf progradation, and to date potential ice-rafting events within these units.

Basic information on the development of Neogene glaciations and late Cenozoic paleoclimatic history has been obtained from the results of the drilling on the Vøring Plateau in the Norwegian-Greenland Sea, ODP Leg 104 (Eldholm, Thiede, Taylor, et al., 1987), Iceland and Yermak Plateaus during Leg 151 (Myhre, Thiede, Firth, et al., 1995) and drilling shelf and slope regions off southeast Greenland during Leg 152 (Larsen, Saunders, Clift, et al., 1994). The oldest occurrences of dropstones off southeast Greenland were dated to about 7 Ma by Leg 152 (Larsen, Saunders, Clift, et al. 1994; Larsen et al., 1994). Stable isotope and ice-rafted debris (IRD) data from the Vøring and Iceland Plateaus indicate the onset of an early small-scale stage of glaciation and climatic cooling from about 12 Ma, with intensification at about 7 Ma. A major stage of intensified glaciations occurred in northern Europe from 2.72 Ma, and increased IRD deposition is documented in response to the shift to 100-k.y. cycles at about 1 Ma (Jansen et al., 1988; Jansen and Sjøholm, 1991; Wolf and Thiede, 1991; Myhre, Thiede, Firth, et al., 1995; Fronval and Jansen, in press). The location and size of pre-2.72-Ma ice sheets were poorly constrained prior to Leg 162. The location of pre-7-Ma ice masses was also not known. Data from Site 907 on the Iceland Plateau indicate that the western parts of the Nordic Seas experienced a marked

intensification of IRD deposition at about 3 Ma, about 200–300 k.y. before the eastern Nordic Seas and the North Atlantic, pointing to Greenland as a possible early responder to the major expansion of ice sheets in the 3–2.5-Ma period (Fronval and Jansen, in press).

OPERATIONS

While underway to Site 987 (EGM-4), the ice map data we received gave conflicting reports regarding the outer edge of the ice margin. The most recent SSMI data indicated that the ice edge was well to the west of proposed site EGM-4. Later, AVHRR and SAR data showed the site to be 10 nmi within closed ice. As a result, the first survey waypoint was selected well to the east along the 70°30.0′N latitude. At 2400 hr on 22 August 1995 the vessel slowed to survey speed (5.4 kt). In dense fog a seismic profile was begun toward the ice margin in the west. Repeated freezing of the water guns hampered the survey, and eventually all water guns were inoperative. The profile extended all the way to 18°9.89′W, well beyond what had been hoped for. This allowed a tie with an existing pre-cruise survey line which is crossing the proposed site EGM-4. The ice margin was estimated to be located approximately 10 nmi farther to the west or roughly at the coordinates of the original EGM-4 drill site. The vessel returned to a previously approved alternate site EGM-4B located on the site survey line using GPS coordinates. A cross line could not be shot over site EGM-4B due to the gun failures.

The operational plan for this site was similar to that for Site 986 (SVAL-1B). It called for two piston-cored holes to be drilled to refusal or approximately 200 m below the seafloor. One hole was to be deepened to XCB refusal, estimated to occur at about 500 mbsf. The third hole was to be drilled down just short of the XCB hole's total depth and then continuously RCB cored to a depth of 800 mbsf. This hole would terminate shy of basement but penetrate the glacial sediment package which constituted the major site objective. A minimum number of downhole temperature measurements were to be taken in the upper (APC) portion of the hole in order to establish a temperature gradient. A full suite of logging tools were to be deployed on the deepest site. Iceberg warning and hole abandonment procedures were put in effect. In addition, the Danish Greenland Command was advised of the vessel's arrival on site and anticipated departure from the area. Daily position reports were sent while on site.

Position, depths, and coring totals for each hole are summarized at the beginning of this chapter. All cores are listed in Table 1.

The positioning beacon was deployed at 0920 hr on 23 August, initiating Hole 987A. Routine piston coring continued through Core 987A-10H. Core 987A-3H recovered zero core when the core-catcher flapper stuck open, allowing the entire core to slip out of the liner. Since APC refusal occurred at such a shallow depth, coring operations was continued with the XCB system. XCB coring continued with excellent recovery until coring was halted after Core 987A-22X, when the scientific target for the hole was reached. Methane was encountered in all cores ranging from 7 to 67,760 ppm and ethane from 0 to 7 ppm. Propane was detected beginning with Core 987A-13H and ranged from 0 to 1 ppm. No higher hydrocarbons were detected.

After offsetting the vessel 15 m east, a bottom-water temperature was taken with the APC temperature tool before spudding Hole 987B. APC-coring continued through Core 987B-11H, when the scientific target depth for the hole had been reached. Cores 987B-3H through 5H again lost all core recovery due to the core-catcher flapper sticking open. Four successful downhole temperature measurements were taken on Cores 987B-4H, 6H, 8H, and 10H, yielding a temperature gradient of 96°C/km.

Because of the lost core interval on the first two holes, a third APC hole, Hole 987C, was drilled through the problem zone. This time the core-catcher flapper was supplemented with a dog-type core catcher as well. Running dual core catchers was successful. Coring was suspended when the target for the hole had been reached.

The ship was again offset 15 m east. Routine piston coring at Hole 987D continued through Core 987D-11H without incident. XCB coring was initiated with Core 987D-12X. The hard-formation XCB cutting shoe used on Core 987D-21X was severely damaged, apparently drilling through a large dropstone. Cores 987D-21X through 23X recovered zero core through an apparent mass flow deposit. Normal coring parameters were regained on Core 987D-24X, and coring was ultimately discontinued due to steadily deteriorating rate of penetration and core recovery. In addition, the cores were becoming increasingly more disturbed, with many core "biscuits" noticed. Cores 987D-24X through 42X had methane from 3162 to 21,087 ppm and ethane from 2 to 14 ppm. Propane ranged from 0 to 3 ppm. No higher hydrocarbons were detected.

During the course of drilling Hole 987D, the first indications of encroaching sea ice were identified on the radar. The progress of the floe was picked up at a range of approximately 6.3 nmi from the drill site, moving toward the site at approximately 0.25 kt. The closest point of approach was 5.5 nmi, however, and the ice never posed a danger to drilling operations.

The drill pipe was then tripped back to the drill floor for changing the bit/bottom-hole assembly (BHA) to that used in RCB coring in preparation for Hole 987E. During the pipe trip, the vessel was offset 50 m to the east. The upper several hundred meters of formation was to be drilled rather than cored. Therefore the seafloor depth from Hole 987D was used as a reference. This is more accurate than "feeling" for bottom with the RCB drilling assembly. Drilling ahead continued to a depth of 2047.5 mbrf (363.3 mbsf). The center bit was then recovered via wireline, and continuous RCB coring commenced. Coring was terminated after Core 987E-52R (859.4 mbsf). This was in excess of the original scientific target depth of 800 mbsf; however, permission had been obtained earlier to advance to 900 mbsf. Coring had to be abandoned only a few tens of meters short of the elusive basement so the logging program would not be compromised. Maximum methane identified was 70,787 ppm at a depth of 792.9 m and ethane was 62 ppm at a depth of 739.0 m.

During the following wiper trip, a tight spot requiring 30,000 lb of overpull was identified at 408.8 mbsf. While running back in the hole a hard spot was tagged with 30,000 lb of bit weight at 409.8 mbsf. The top drive was picked up at that point; however, advancement still could not be achieved so a center bit was dropped. Washing/reaming with the top drive continued from that point on until the original total depth for the hole was reached. An additional 60-barrel mud sweep was pumped during the reaming process. A total of 22 m of fill was found on the bottom of the hole which was swept a final time with 50 barrels of gel mud prior to recovering the center bit. Two additional wireline runs were then made to release the bit and reverse-shift the mechanical-bit-release sleeve. The pipe was placed at a logging depth of 2122.7 m (438.5 mbsf) because there was little confidence that the tools would be able to traverse the bad spot in the hole identified during the wiper trip. The logging equipment was rigged, and the first run, with the Quad combo suite of tools, was deployed to a depth of 2165.0 m (480.8 mbsf). This was only 42.3 m below the open-ended pipe. The logging tools were removed and the pipe was lowered to a depth of 2180.5 m (496.3 mbsf). The second run with the Quad combo tools reached a depth of 2184.0 m (499.8 mbsf) only 3.5 m below open-ended pipe. Further logging attempts were considered futile in the lower part of the hole. The tools were recovered, the logging sheaves were again partially rigged down, and the pipe was pulled to a depth of 1776.1 m (91.9 mbsf). A third run with the Quad combo suite of logging tools reached a depth of 2170.0 m (485.8 mbsf) or 394.0 m below open-ended pipe. The logging run was successfully completed at 1935 hr on 31 August.

The next logging run with the GHMT tool reached a depth of 2164.0 m (479.8 mbsf) or 387.9 m below open-ended pipe. This logging run was successfully completed at 2320 hr on 31 August. The final logging attempt was with the FMS, which reached a depth of 2092.0 m (407.8 mbsf) or 315.9 meters below open-ended pipe. Dur-

Table 1. Coring summary for Site 987.

Core	Date (Aug. 1995)	Time (UTC)	Depth (mbsf)	Length cored (m)	Length recovered (m)	Recovery (%)
162-987A-						
1H	23	1530	0.0–8.5	8.5	8.57	101.0
2H	23	1555	8.5–18.0	9.5	9.70	102.0
3H	23	1620	18.0–27.5	9.5	0.00	0.0
4H	23	1645	27.5–37.0	9.5	9.89	104.0
5H	23	1710	37.0–46.5	9.5	8.51	89.6
6H	23	1745	46.5–52.2	5.7	5.72	100.0
7H	23	1830	52.2–59.7	7.5	7.53	100.0
8H	23	1900	59.7–67.7	8.0	8.89	111.0
9H	23	1925	67.7–76.2	8.5	8.55	100.0
10H	23	1955	76.2–83.7	7.5	7.90	105.0
11X	23	2145	83.7–93.3	9.6	4.41	45.9
12X	23	2230	93.3–103.0	9.7	2.15	22.1
13X	23	2330	103.0–112.7	9.7	9.65	99.5
14X	24	0010	112.7–122.2	9.5	9.66	101.0
15X	24	0100	122.2–131.8	9.6	9.01	93.8
16X	24	0145	131.8–141.4	9.6	8.35	87.0
17X	24	0230	141.4–151.0	9.6	9.52	99.1
18X	24	0335	151.0–160.7	9.7	8.53	87.9
19X	24	0420	160.7–170.3	9.6	9.70	101.0
20X	24	0515	170.3–179.9	9.6	9.77	102.0
21X	24	0555	179.9–188.6	9.7	7.24	74.6
22X	24	0645	189.6–199.3	9.7	9.76	100.0
			Coring totals:	199.3	173.00	86.8
162-987B-						
1H	24	1005	0.0–4.2	4.2	4.26	101.0
2H	24	1035	4.2–13.7	9.5	9.40	98.9
3H	24	1115	13.7–23.2	9.5	0.01	0.1
4H	24	1210	23.2–32.7	9.5	0.00	0.0
5H	24	1240	32.7–42.2	9.5	0.00	0.0
6H	24	1400	42.2–51.7	9.5	10.22	107.6
7H	24	1430	51.7–61.2	9.5	9.83	103.0
8H	24	1545	61.2–70.7	9.5	10.16	106.9
9H	24	1615	70.7–80.2	9.5	10.20	107.3
10H	24	1715	80.2–89.7	9.5	9.90	104.0
11H	24	1755	89.7–99.2	9.5	10.20	107.3
			Coring totals:	99.2	74.20	74.8
162-987C-						
1H	24	1925	0.0–5.6	5.6	5.63	100.0
2H	24	1950	5.6–15.1	9.5	9.76	103.0
3H	24	2015	15.1–24.6	9.5	9.88	104.0
4H	24	2050	24.6–34.1	9.5	9.89	104.0
5H	24	2115	34.1–43.6	9.5	9.75	102.0
			Coring totals:	43.6	44.90	103.0
162-987D-						
1H	24	2215	0.0–1.3	1.3	1.30	100.0
2H	24	2235	1.3–10.8	9.5	9.77	103.0
3H	24	2305	10.8–20.3	9.5	9.79	103.0
4H	24	2330	20.3–29.8	9.5	9.81	103.0
5H	24	2355	29.8–39.3	9.5	9.85	103.0
6H	25	0035	39.3–48.8	9.5	9.82	103.0
7H	25	0110	48.8–58.3	9.5	9.82	103.0
8H	25	0145	58.3–67.8	9.5	9.90	104.0
9H	25	0215	67.8–76.6	8.8	8.80	100.0
10H	25	0255	76.6–86.1	9.5	10.10	106.3
11H	25	0400	86.1–94.8	8.7	8.71	100.0
12X	25	0615	94.8–103.4	8.6	5.12	59.5
13X	25	0700	103.4–113.0	9.6	9.63	100.0
14X	25	0800	113.0–122.6	9.6	4.61	48.0
15X	25	0900	122.6–132.3	9.7	9.69	99.9
16X	25	0945	132.3–141.9	9.6	8.11	84.5
17X	25	1050	141.9–151.6	9.7	9.14	94.2
18X	25	1140	151.6–161.2	9.6	9.58	99.8
19X	25	1225	161.2–170.9	9.7	7.46	76.9
20X	25	1345	170.9–176.5	5.6	7.73	138.0
21X	25	1440	176.5–180.5	4.0	0.02	0.5
22X	25	1530	180.5–190.2	9.7	0.00	0.0
23X	25	1615	190.2–199.8	9.6	0.00	0.0
24X	25	1720	199.8–209.4	9.6	1.86	19.4
25X	25	1820	209.4–219.0	9.6	9.67	101.0
26X	25	1920	219.0–228.6	9.6	9.80	102.0
27X	25	2015	228.6–238.2	9.6	9.46	98.5
28X	25	2100	238.2–247.9	9.7	4.30	44.3
29X	25	2150	247.9–257.5	9.6	9.04	94.1
30X	25	2245	257.5–267.1	9.6	9.66	100.0
31X	25	2350	267.1–276.8	9.7	9.57	98.6
32X	26	0110	276.8–286.4	9.6	7.36	76.6
33X	26	0215	286.4–296.0	9.6	0.17	1.8
34X	26	0350	296.0–302.6	6.6	3.60	54.5
35X	26	0600	302.6–305.6	3.0	0.54	18.0
36X	26	0820	305.6–315.2	9.6	9.51	99.0
37X	26	1055	315.2–324.8	9.6	0.76	7.9
38X	26	1400	324.8–334.4	9.6	1.60	16.6
39X	26	1610	334.4–344.0	9.6	1.68	17.5
40X	26	1755	344.0–353.7	9.7	3.20	33.0
41X	26	1950	353.7–363.3	9.6	6.63	69.0
42X	26	2120	363.3–373.0	9.7	1.29	13.3
			Coring totals:	373.0	268.50	72.0
162-987E-						
1R	27	2055	363.3–369.2	5.9	3.85	65.2
2R	27	2210	369.2–378.8	9.6	4.34	45.2
3R	27	2310	378.8–388.4	9.6	4.20	43.7
4R	28	0020	388.4–398.0	9.6	0.15	1.6
5R	28	0140	398.0–407.6	9.6	8.37	87.2
6R	28	0300	407.6–417.2	9.6	8.87	92.4
7R	28	0405	417.2–426.8	9.6	8.86	92.3
8R	28	0515	426.8–436.4	9.6	9.26	96.4
9R	28	0635	436.4–446.1	9.7	8.04	82.9
10R	28	0745	446.1–455.8	9.7	8.75	90.2
11R	28	0900	455.8–465.4	9.6	4.19	43.6
12R	28	1015	465.4–475.0	9.6	8.60	89.6
13R	28	1135	475.0–484.6	9.6	8.78	91.4
14R	28	1245	484.6–494.2	9.6	4.93	51.3
15R	28	1350	494.2–503.8	9.6	7.90	82.3
16R	28	1450	503.8–513.4	9.6	8.10	84.4
17R	28	1600	513.4–523.0	9.6	8.11	84.5
18R	28	1730	523.0–532.6	9.6	7.41	77.2
19R	28	1830	532.6–542.2	9.6	7.08	73.7
20R	28	1930	542.2–551.8	9.6	8.42	87.7
21R	28	2045	551.8–561.4	9.6	8.16	85.0
22R	28	2150	561.4–571.0	9.6	8.83	92.0
23R	28	2310	571.0–580.6	9.6	6.90	71.9
24R	29	0030	580.6–590.2	9.7	4.03	41.5
25R	29	0155	590.2–599.9	9.6	7.53	78.4
26R	29	0330	599.9–609.5	9.6	7.59	79.0
27R	29	0500	609.5–619.1	9.7	4.98	51.3
28R	29	0640	619.1–628.8	9.6	4.35	45.3
29R	29	0815	628.8–638.4	9.6	8.02	83.5
30R	29	1000	638.4–648.0	9.6	2.07	21.5
31R	29	1120	648.0–657.6	9.6	3.30	34.4
32R	29	1240	657.6–667.2	9.6	4.86	50.6
33R	29	1340	667.2–676.8	9.6	3.03	31.5
34R	29	1450	676.8–686.4	9.6	4.51	47.0
35R	29	1605	686.4–696.0	9.6	6.03	62.8
36R	29	1740	696.0–705.6	9.6	6.19	64.5
37R	29	1900	705.6–715.2	9.6	7.93	82.6
38R	29	2015	715.2–724.9	9.7	8.72	89.9
39R	29	2130	724.9–734.5	9.6	8.57	89.3
40R	29	2240	734.5–744.1	9.6	6.99	72.8
41R	30	0000	744.1–753.6	9.5	2.81	29.6
42R	30	0130	753.6–763.2	9.6	0.00	0.0
43R	30	0245	763.2–772.8	9.6	5.59	58.2
44R	30	0400	772.8–782.5	9.7	4.70	48.4
45R	30	0515	782.5–792.1	9.6	1.19	12.4
46R	30	0625	792.1–801.8	9.7	0.82	8.5
47R	30	0740	801.8–811.3	9.5	8.42	88.6
48R	30	0855	811.3–820.9	9.6	5.75	59.9
49R	30	1005	820.9–830.6	9.7	4.73	48.7
50R	30	1110	830.6–840.2	9.6	4.57	47.6
51R	30	1215	840.2–849.8	9.6	6.10	63.5
52R	30	1320	849.8–859.4	9.6	3.34	34.8
			Coring totals:	496.1	308.80	62.2

ing the final run, another set of data points was collected for the Borehole Research Group (LDEO-BRG), documenting the performance of the new wireline compensator control system. The tools were subsequently recovered on deck at 0400 hr and the logging equipment was rigged down.

The drill pipe knobbies were then laid out and the drill string was pulled clear of the seafloor at 0536 hr. During the subsequent pipe trip the beacon was released and recovered. The BHA components were broken down, cleaned, and stowed for transit. Thrusters and hydrophones were pulled and all remaining rig floor equipment was secured for the 1.7 day (455 nmi) transit to Reykjavik, Iceland. As the vessel got underway at half speed in moderate snow flurries, scattered bergy bits and a few isolated growlers, likely being discharged from Scoresbysund, littered the area. The ice margin was clearly vis-

ible to the west as the vessel sailed on a southerly course toward Iceland.

COMPOSITE DEPTHS

The sediments drilled at Site 987 were marked by intervals of gas expansion, dropstones, disturbance, and nonrecovery (see "Lithostratigraphy" section, this chapter). However, continuity of the sedimentary sequence was documented for approximately the upper 190 meters below seafloor (mbsf). Sufficient overlap between the APC cores from Holes 987A, 987B, 987C, and 987D allowed both a composite section and an uninterrupted spliced record to be developed over this interval, as described in the "Composite Depths" section, "Explanatory Notes" chapter (this volume). The depth offsets that comprise the composite depth section at Site 987 are given in Table 2.

Multisensor-track data used in the correlations are displayed on the composite depth scale in Figure 2 (see also back pocket). Magnetic susceptibility was the primary parameter used to develop the composite section. Gamma-ray attenuation porosity (GRAPE) density was used to confirm the hole-to-hole correlations.

The mcd scale grows, relative to the mbsf scale, in both holes over the range of the composite section. This "growth" is caused by physical expansion of the cores after recovery and by stretching of the sequence during the coring process. Because the loss of overlap below Core 987D-11H affects the relative offsets, the composite section "growth" is documented only for the APC-cored interval in Figure 3.

From the APC-cored interval of the Site 987 composite depth section, a single spliced record was developed according to the description in the "Explanatory Notes" chapter (this volume). The tie points between the cores used to construct the splice are given in Table 3. It was not possible to omit disturbed and anomalous intervals from the splice, as most cores showed some evidence of disturbance. Below the APC-cored interval, where overlaps between adjacent holes were not continuously maintained, the remainder of Hole 987D was appended to the composite. The spliced GRAPE density and magnetic susceptibility data are shown in Figure 4.

While overlap between adjacent holes and relative agreement of the sedimentary features present was maintained over the upper 190 mbsf, stretching and compression within the cored sequence was noted. Because much of this distortion was on a scale of less than 9 m, it was not possible to align every sedimentary feature using only the composite depth scale adjustments. Within-core, decimeter to centimeter-scale depth adjustments would be required to align all sedimentary features simultaneously.

LITHOSTRATIGRAPHY

Five holes were drilled at Site 987, with a maximum penetration of 859.4 mbsf. The sediments recovered are mostly fine- to coarse-grained siliciclastics. The dominant lithologies include silty clay, clayey silt, clay with silt, and silty clay with sand and gravel. More than 500 isolated clasts >1.0 cm in size are present throughout the section, most of which are interpreted as dropstones. Clasts are listed in Table 4.

Sandy turbidites and sandy layers occur in the upper sedimentary sequences primarily above 281.3 mbsf. Biocarbonate and biosilica do not exceed 10%. Isolated thin (<1 cm) to medium thickness (several centimeters) layers of inorganic calcite are observed from 37.3 to 740.5 mbsf. Contorted and dipping beds and thin dark clayey laminations are present toward the base of the sedimentary sequence. Authigenic sulfides, primarily in the form of disseminated pyrite, are present in minor amounts in both the upper and lower part of the sedimentary sequence.

The five lithostratigraphic units and two subunits at Site 987 are defined on the basis of data obtained from seven sources: (1) visual core descriptions, (2) smear slide examination, (3) bulk calcium carbonate measurements, (4) spectral reflectance measurements, (5) magnetic susceptibility measurements, (6) natural gamma-ray measurements, and (7) X-ray diffraction (XRD) of bulk sediments. Spectral reflectance measurements are of limited use, as there are no measurements in Hole 987E (Fig. 5). Lithostratigraphic unit boundaries occur at 305.6, 369.2, 575.5, and 657.6 mbsf. A subunit boundary within Unit III occurs at 465.4 mbsf. Detailed descriptions of these units follow and a summary of each lithostratigraphic unit is given in Table 5.

Description of Lithostratigraphic Units

Unit I

Interval:
Cores 162-987A-1H through 22X (base of hole)
Cores 162-987B-1H through 11H (base of hole)
Cores 162-987C-1H through 5H (base of hole)
Core 162-987D-1H through Section 35X-CC
Age: Pleistocene to upper Pliocene
Depth: 0 to 305.6 mbsf

Unit I is characterized by magnetic susceptibility values that consistently remain at the low end of the range of values at Site 987. The lower boundary of this unit is clearly marked by a sharp increase in magnetic susceptibility, a slight decrease in natural gamma radiation, an increase in the abundance of sand-sized particles and a decrease in the abundance of clay-sized particles (Fig. 5). Spectral reflectance values vary between 5% and 15% within the red band (650–700 nm) (Fig. 5) and are highest at the very top of the unit. Sediments containing up to 35% carbonate occur in the inorganic calcite-rich bands, but the average carbonate content for the unit is only 4.9% (see "Organic Geochemistry" section, this chapter).

Sediments of Unit I are predominantly dark gray, very dark gray, dark greenish gray, very dark greenish gray, and dark reddish gray silty clay interbedded with minor dark gray to dark greenish gray clay with silt and silt with sand and clay. Thick sandy turbidites with sharp erosional lower contacts and gradational upper contacts are common (Fig. 6). Other sandy and, to a lesser extent, silty layers also interpreted as turbidites are common in this unit, many occur as fining- and thinning-upward sequences (Fig. 7). Sandy layers are thicker toward the top of the unit (20–60 cm) and are less common and thinner (5–25 cm) in the lower part of the unit. Some dark gray, gray, light gray, brown, and dusky red silty clay with inorganic calcite, and inorganic calcite with silt and clay, occur as minor lithologies throughout the unit.

Several dropstones, some as large as 7.3 cm, were identified throughout this unit (Table 4). Crystalline rocks dominate, but sedimentary rocks are also common. Smear slide analysis reveals that quartz, feldspar, and inorganic calcite (up to 56%) are the most common terrigenous silt- to sand-sized components. XRD analysis indicates that amphibole and pyroxene are also common components.

Sulfides occur throughout the unit, primarily as disseminated pyrite and filled burrows. Two distinct volcanic ash layers are present (in Sections 162-987A-9H-3 and in 12X-9). Slight to moderate bioturbation is common at all depths. Disturbance due to gas expansion is common at the top of the unit.

Unit II

Interval:
Cores 162-987D-36X through 42X
Core 162-987E-1R
Age: upper Pliocene
Depth: 305.6 to 369.2 mbsf

Unit II is primarily defined by the presence of numerous isolated clasts >1.0 cm and randomly oriented gravel <1.0 cm. The top of Unit

Table 2. Site 987 composite depths.

Core, section	Length (cm)	Depth (mbsf)	Depth (mcd)	Offset (mcd – mbsf)
162-987A-				
1H-1	150	0.00	0.14	0.14
1H-2	150	1.50	1.64	0.14
1H-3	150	3.00	3.14	0.14
1H-4	150	4.50	4.64	0.14
1H-5	150	6.00	6.14	0.14
1H-6	88	7.50	7.64	0.14
1H-CC	19	8.38	8.52	0.14
2H-1	150	8.50	10.07	1.57
2H-2	150	10.00	11.57	1.57
2H-3	150	11.50	13.07	1.57
2H-3	150	11.50	13.07	1.57
2H-4	150	13.00	14.57	1.57
2H-5	150	14.50	16.07	1.57
2H-6	150	16.00	17.57	1.57
2H-7	46	17.50	19.07	1.57
2H-CC	24	17.96	19.53	1.57
4H-1	150	27.50	30.85	3.35
4H-2	150	29.00	32.35	3.35
4H-3	150	30.50	33.85	3.35
4H-4	150	32.00	35.35	3.35
4H-5	150	33.50	36.85	3.35
4H-6	150	35.00	38.35	3.35
4H-7	63	36.50	39.85	3.35
4H-CC	26	37.13	40.48	3.35
5H-1	100	37.00	41.49	4.49
5H-2	30	38.00	42.49	4.49
5H-3	150	38.30	42.79	4.49
5H-4	150	39.80	44.29	4.49
5H-5	150	41.30	45.79	4.49
5H-6	150	42.80	47.29	4.49
5H-7	96	44.30	48.79	4.49
5H-CC	25	45.26	49.75	4.49
6H-1	150	46.50	51.51	5.01
6H-2	150	48.00	53.01	5.01
6H-3	150	49.50	54.51	5.01
6H-4	95	51.00	56.01	5.01
6H-CC	27	51.95	56.96	5.01
7H-1	150	52.20	58.25	6.05
7H-2	150	53.70	59.75	6.05
7H-3	150	55.20	61.25	6.05
7H-4	150	56.70	62.75	6.05
7H-5	128	58.20	64.25	6.05
7H-CC	25	59.48	65.53	6.05
8H-1	150	59.70	67.15	7.45
8H-2	150	61.20	68.65	7.45
8H-3	150	62.70	70.15	7.45
8H-4	150	64.20	71.65	7.45
8H-5	150	65.70	73.15	7.45
8H-6	108	67.20	74.65	7.45
8H-CC	31	68.28	75.73	7.45
9H-1	150	67.70	74.76	7.06
9H-2	150	69.20	76.26	7.06
9H-3	150	70.70	77.76	7.06
9H-4	150	72.20	79.26	7.06
9H-5	150	73.70	80.76	7.06
9H-6	72	75.20	82.26	7.06
9H-CC	33	75.92	82.98	7.06
10H-1	151	76.20	83.99	7.79
10H-2	75	77.71	85.50	7.79
10H-3	41	78.46	86.25	7.79
10H-4	142	78.87	86.66	7.79
10H-5	150	80.29	88.08	7.79
10H-6	13	81.79	89.58	7.79
10H-7	150	81.92	89.71	7.79
10H-CC	74	83.42	91.21	7.79
11X-1	150	83.70	92.45	8.75
11X-2	150	85.20	93.95	8.75
11X-3	132	86.70	95.45	8.75
11X-CC	9	88.02	96.77	8.75
12X-1	150	93.30	98.69	5.39
12X-CC	65	94.80	100.19	5.39
13X-1	150	103.00	110.87	7.87
13X-2	150	104.50	112.37	7.87
13X-3	150	106.00	113.87	7.87
13X-4	150	107.50	115.37	7.87
13X-5	150	109.00	116.87	7.87
13X-6	150	110.50	118.37	7.87
13X-7	48	112.00	119.87	7.87
13X-CC	17	112.48	120.35	7.87
14X-1	150	112.70	121.35	8.65
14X-2	150	114.20	122.85	8.65
14X-3	150	115.70	124.35	8.65
14X-4	150	117.20	125.85	8.65
14X-5	150	118.70	127.35	8.65
14X-6	150	120.20	128.85	8.65
14X-7	18	121.70	130.35	8.65
14X-CC	48	121.88	130.53	8.65
15X-1	150	122.20	130.85	8.65
15X-2	150	123.70	132.35	8.65
15X-3	150	125.20	133.85	8.65
15X-4	150	126.70	135.35	8.65
15X-5	150	128.20	136.85	8.65
15X-6	109	129.70	138.35	8.65
15X-CC	42	130.79	139.44	8.65
16X-1	150	131.80	141.27	9.47
16X-2	150	133.30	142.77	9.47
16X-3	150	134.80	144.27	9.47
16X-4	150	136.30	145.77	9.47
16X-5	150	137.80	147.27	9.47
16X-6	54	139.30	148.77	9.47
16X-CC	31	139.84	149.31	9.47
17X-1	150	141.40	150.87	9.47
17X-2	150	142.90	152.37	9.47
17X-3	150	144.40	153.87	9.47
17X-4	150	145.90	155.37	9.47
17X-5	150	147.40	156.87	9.47
17X-6	150	148.90	158.37	9.47
17X-7	18	150.40	159.87	9.47
17X-CC	34	150.58	160.05	9.47
18X-1	150	151.00	160.99	9.99
18X-2	150	152.50	162.49	9.99
18X-3	150	154.00	163.99	9.99
18X-4	150	155.50	165.49	9.99
18X-5	150	157.00	166.99	9.99
18X-6	55	158.50	168.49	9.99
18X-CC	48	159.05	169.04	9.99
19X-1	150	160.70	171.55	10.85
19X-2	150	162.20	173.05	10.85
19X-3	150	163.70	174.55	10.85
19X-4	150	165.20	176.05	10.85
19X-5	150	166.70	177.55	10.85
19X-6	150	168.20	179.05	10.85
19X-7	33	169.70	180.55	10.85
19X-CC	37	170.03	180.88	10.85
20X-1	150	170.30	181.15	10.85
20X-2	150	171.80	182.65	10.85
20X-3	150	173.30	184.15	10.85
20X-4	150	174.80	185.65	10.85
20X-5	150	176.30	187.15	10.85
20X-6	150	177.80	188.65	10.85
20X-7	28	179.30	190.15	10.85
20X-CC	49	179.58	190.43	10.85
21X-1	150	179.90	190.75	10.85
21X-2	150	181.40	192.25	10.85
21X-3	150	182.90	193.75	10.85
21X-4	150	184.40	195.25	10.85
21X-5	87	185.90	196.75	10.85
21X-CC	37	186.77	197.62	10.85
22X-1	40	189.60	200.45	10.85
22X-2	142	190.00	200.85	10.85
22X-3	150	191.42	202.27	10.85
22X-4	150	192.92	203.77	10.85
22X-5	150	194.42	205.27	10.85
22X-6	150	195.92	206.77	10.85
22X-7	150	197.42	208.27	10.85
22X-CC	44	198.92	209.77	10.85
162-987B-				
1H-1	150	0.00	0.08	0.08
1H-2	150	1.50	1.58	0.08
1H-3	93	3.00	3.08	0.08
1H-CC	33	3.93	4.01	0.08
2H-1	150	4.20	4.69	0.49
2H-2	150	5.70	6.19	0.49
2H-3	150	7.20	7.69	0.49
2H-4	150	8.70	9.19	0.49
2H-5	150	10.20	10.69	0.49
2H-6	150	11.70	12.19	0.49
2H-7	18	13.20	13.69	0.49
2H-CC	22	13.38	13.87	0.49
3H-CC	1	13.70	14.19	0.49
6H-1	150	42.20	46.77	4.57
6H-2	150	43.70	48.27	4.57
6H-3	150	45.20	49.77	4.57
6H-4	150	46.70	51.27	4.57
6H-5	150	48.20	52.77	4.57
6H-6	150	49.70	54.27	4.57
6H-7	72	51.20	55.77	4.57
6H-CC	50	51.92	56.49	4.57
7H-1	150	51.70	56.69	4.99
7H-2	150	53.20	58.19	4.99
7H-3	150	54.70	59.69	4.99
7H-4	150	56.20	61.19	4.99
7H-5	150	57.70	62.69	4.99
7H-6	150	59.20	64.19	4.99
7H-7	57	60.70	65.69	4.99
7H-CC	26	61.27	66.26	4.99

Table 2 (continued).

Core, section	Length (cm)	Depth (mbsf)	Depth (mcd)	Offset (mcd – mbsf)
8H-1	150	61.20	67.58	6.38
8H-2	150	62.70	69.08	6.38
8H-3	150	64.20	70.58	6.38
8H-4	150	65.70	72.08	6.38
8H-5	150	67.20	73.58	6.38
8H-6	150	68.70	75.08	6.38
8H-7	88	70.20	76.58	6.38
8H-CC	40	71.08	77.46	6.38
9H-1	150	70.70	77.67	6.97
9H-2	150	72.20	79.17	6.97
9H-3	150	73.70	80.67	6.97
9H-4	150	75.20	82.17	6.97
9H-5	150	76.70	83.67	6.97
9H-6	150	78.20	85.17	6.97
9H-7	84	79.70	86.67	6.97
9H-CC	36	80.54	87.51	6.97
10H-1	150	80.20	89.12	8.92
10H-2	43	81.70	90.62	8.92
10H-3	150	82.13	91.05	8.92
10H-4	150	83.63	92.55	8.92
10H-5	150	85.13	94.05	8.92
10H-6	150	86.63	95.55	8.92
10H-7	110	88.13	97.05	8.92
10H-8	18	89.23	98.15	8.92
10H-CC	69	89.41	98.33	8.92
11H-1	150	89.70	102.75	13.05
11H-2	150	91.20	104.25	13.05
11H-3	150	92.70	105.75	13.05
11H-4	150	94.20	107.25	13.05
11H-5	150	95.70	108.75	13.05
11H-6	150	97.20	110.25	13.05
11H-7	86	98.70	111.75	13.05
11H-CC	34	99.56	112.61	13.05
162-987C-				
1H-1	150	0.00	0.00	0.00
1H-2	150	1.50	1.50	0.00
1H-3	150	3.00	3.00	0.00
1H-4	86	4.50	4.50	0.00
1H-CC	27	5.36	5.36	0.00
2H-3	150	8.60	8.38	–0.22
2H-4	150	10.10	9.88	–0.22
2H-5	150	11.60	11.38	–0.22
2H-6	150	13.10	12.88	–0.22
2H-7	51	14.60	14.38	–0.22
2H-CC	25	15.11	14.89	–0.22
3H-1	150	15.10	16.16	1.06
3H-2	150	16.60	17.66	1.06
3H-3	150	18.10	19.16	1.06
3H-4	150	19.60	20.66	1.06
3H-5	150	21.10	22.16	1.06
3H-6	150	22.60	23.66	1.06
3H-7	61	24.10	25.16	1.06
3H-CC	27	24.71	25.77	1.06
4H-1	150	24.60	26.31	1.71
4H-2	150	26.10	27.81	1.71
4H-3	150	27.60	29.31	1.71
4H-4	150	29.10	30.81	1.71
4H-5	150	30.60	32.31	1.71
4H-6	150	32.10	33.81	1.71
4H-7	64	33.60	35.31	1.71
4H-CC	25	34.24	35.95	1.71
5H-1	150	34.10	36.45	2.35
5H-2	150	35.60	37.95	2.35
5H-3	150	37.10	39.45	2.35
5H-4	150	38.60	40.95	2.35
5H-5	150	40.10	42.45	2.35
5H-6	150	41.60	43.95	2.35
5H-7	61	43.10	45.45	2.35
5H-CC	14	43.71	46.06	2.35
162-987D-				
1H-1	118	0.00	0.00	0.00
1H-CC	12	1.18	1.18	0.00
2H-1	150	1.30	3.40	2.10
2H-2	150	2.80	4.90	2.10
2H-3	150	4.30	6.40	2.10
2H-4	150	5.80	7.90	2.10
2H-5	150	7.30	9.40	2.10
2H-6	150	8.80	10.90	2.10
2H-7	51	10.30	12.40	2.10
2H-CC	26	10.81	12.91	2.10
3H-1	150	10.80	13.67	2.87
3H-2	150	12.30	15.17	2.87
3H-3	150	13.80	16.67	2.87
3H-4	150	15.30	18.17	2.87
3H-5	150	16.80	19.67	2.87
3H-6	150	18.30	21.17	2.87
3H-7	55	19.80	22.67	2.87
3H-CC	24	20.35	23.22	2.87
4H-1	150	20.30	23.91	3.61
4H-2	150	21.80	25.41	3.61
4H-3	150	23.30	26.91	3.61
4H-4	150	24.80	28.41	3.61
4H-5	150	26.30	29.91	3.61
4H-6	150	27.80	31.41	3.61
4H-7	55	29.30	32.91	3.61
4H-CC	26	29.85	33.46	3.61
5H-1	150	29.80	34.60	4.80
5H-2	150	31.30	36.10	4.80
5H-3	150	32.80	37.60	4.80
5H-4	150	34.30	39.10	4.80
5H-5	150	35.80	40.60	4.80
5H-6	150	37.30	42.10	4.80
5H-7	66	38.80	43.60	4.80
5H-CC	19	39.46	44.26	4.80
6H-1	150	39.30	44.95	5.65
6H-2	150	40.80	46.45	5.65
6H-3	150	42.30	47.95	5.65
6H-4	150	43.80	49.45	5.65
6H-5	150	45.30	50.95	5.65
6H-6	150	46.80	52.45	5.65
6H-7	63	48.30	53.95	5.65
6H-CC	19	48.93	54.58	5.65
7H-1	150	48.80	55.65	6.85
7H-2	150	50.30	57.15	6.85
7H-3	150	51.80	58.65	6.85
7H-4	150	53.30	60.15	6.85
7H-5	150	54.80	61.65	6.85
7H-6	150	56.30	63.15	6.85
7H-7	58	57.80	64.65	6.85
7H-CC	24	58.38	65.23	6.85
8H-1	150	58.30	66.14	7.84
8H-2	150	59.80	67.64	7.84
8H-3	150	61.30	69.14	7.84
8H-4	150	62.80	70.64	7.84
8H-5	150	64.30	72.14	7.84
8H-6	150	65.80	73.64	7.84
8H-7	67	67.30	75.14	7.84
8H-CC	23	67.97	75.81	7.84
9H-1	150	67.80	76.45	8.65
9H-2	150	69.30	77.95	8.65
9H-3	150	70.80	79.45	8.65
9H-4	150	72.30	80.95	8.65
9H-5	150	73.80	82.45	8.65
9H-6	61	75.30	83.95	8.65
9H-CC	8	75.91	84.56	8.65
10H-1	150	76.60	86.48	9.88
10H-2	150	78.10	87.98	9.88
10H-3	150	79.60	89.48	9.88
10H-4	150	81.10	90.98	9.88
10H-5	150	82.60	92.48	9.88
10H-6	150	84.10	93.98	9.88
10H-7	78	85.60	95.48	9.88
10H-CC	32	86.38	96.26	9.88
11H-1	38	86.10	97.20	11.10
11H-2	150	86.48	97.58	11.10
11H-3	150	87.98	99.08	11.10
11H-4	150	89.48	100.58	11.10
11H-5	150	90.98	102.08	11.10
11H-6	150	92.48	103.58	11.10
11H-7	50	93.98	105.08	11.10
11H-CC	33	94.48	105.58	11.10
12X-1	150	94.80	105.90	11.10
12X-2	150	96.30	107.40	11.10
12X-3	150	97.80	108.90	11.10
12X-4	44	99.30	110.40	11.10
12X-CC	18	99.74	110.84	11.10
13X-1	150	103.40	114.50	11.10
13X-2	150	104.90	116.00	11.10
13X-3	150	106.40	117.50	11.10
13X-4	150	107.90	119.00	11.10
13X-5	150	109.40	120.50	11.10
13X-6	150	110.90	122.00	11.10
13X-7	26	112.40	123.50	11.10
13X-CC	37	112.66	123.76	11.10
14X-1	123	113.00	124.10	11.10
14X-2	150	114.23	125.33	11.10
14X-3	150	115.73	126.83	11.10
14X-CC	38	117.23	128.33	11.10
15X-1	150	122.60	133.70	11.10
15X-3	150	125.60	136.70	11.10
15X-4	150	127.10	138.20	11.10
15X-5	150	128.60	139.70	11.10
15X-6	150	130.10	141.20	11.10
15X-7	23	131.60	142.70	11.10
15X-2	150	124.10	135.20	11.10
15X-CC	46	131.83	142.93	11.10

Table 2 (continued).

Core, section	Length (cm)	Depth (mbsf)	Depth (mcd)	Offset (mcd – mbsf)
16X-1	150	132.30	143.40	11.10
16X-2	150	133.80	144.90	11.10
16X-3	150	135.30	146.40	11.10
16X-4	150	136.80	147.90	11.10
16X-5	150	138.30	149.40	11.10
16X-6	18	139.80	150.90	11.10
16X-CC	43	139.98	151.08	11.10
17X-1	118	141.90	153.00	11.10
17X-2	102	143.08	154.18	11.10
17X-3	150	144.10	155.20	11.10
17X-4	150	145.60	156.70	11.10
17X-5	150	147.10	158.20	11.10
17X-6	150	148.60	159.70	11.10
17X-7	56	150.10	161.20	11.10
17X-CC	38	150.66	161.76	11.10
18X-1	150	151.60	162.70	11.10
18X-2	150	153.10	164.20	11.10
18X-3	150	154.60	165.70	11.10
18X-4	150	156.10	167.20	11.10
18X-5	150	157.60	168.70	11.10
18X-6	150	159.10	170.20	11.10
18X-7	20	160.60	171.70	11.10
18X-CC	38	160.80	171.90	11.10
19X-1	150	161.20	172.30	11.10
19X-2	150	162.70	173.80	11.10
19X-3	150	164.20	175.30	11.10
19X-4	150	165.70	176.80	11.10
19X-5	110	167.20	178.30	11.10
19X-CC	36	168.30	179.40	11.10
20X-1	150	170.90	181.43	10.53
20X-2	150	172.40	182.93	10.53
20X-3	150	173.90	184.43	10.53
20X-4	150	175.40	185.93	10.53
20X-5	150	176.90	187.43	10.53
20X-6	21	178.40	188.93	10.53
20X-CC	2	178.61	189.14	10.53
21X-CC	2	176.50	187.03	10.53
24X-1	150	199.80	210.33	10.53
24X-CC	36	201.30	211.83	10.53
25X-1	150	209.40	219.93	10.53
25X-2	150	210.90	221.43	10.53
25X-3	150	212.40	222.93	10.53
25X-4	150	213.90	224.43	10.53
25X-5	150	215.40	225.93	10.53
25X-6	150	216.90	227.43	10.53
25X-7	37	218.40	228.93	10.53
25X-CC	30	218.77	229.30	10.53
26X-1	66	219.00	229.53	10.53
26X-2	150	219.66	230.19	10.53
26X-3	150	221.16	231.69	10.53
26X-4	150	222.66	233.19	10.53
26X-5	150	224.16	234.69	10.53
26X-6	150	225.66	236.19	10.53
26X-7	128	227.16	237.69	10.53
26X-CC	36	228.44	238.97	10.53
27X-1	150	228.60	239.13	10.53
27X-2	150	230.10	240.63	10.53
27X-3	150	231.60	242.13	10.53
27X-4	150	233.10	243.63	10.53
27X-5	150	234.60	245.13	10.53
27X-6	150	236.10	246.63	10.53
27X-7	29	237.60	248.13	10.53
27X-CC	17	237.89	248.42	10.53
28X-1	150	238.20	248.73	10.53
28X-2	150	239.70	250.23	10.53
28X-3	92	241.20	251.73	10.53
28X-CC	38	242.12	252.65	10.53
29X-1	150	247.90	258.43	10.53
29X-2	150	249.40	259.93	10.53
29X-3	150	250.90	261.43	10.53
29X-4	150	252.40	262.93	10.53
29X-5	150	253.90	264.43	10.53
29X-6	123	255.40	265.93	10.53
29X-CC	31	256.63	267.16	10.53
30X-1	150	257.50	268.03	10.53
30X-2	150	259.00	269.53	10.53
30X-3	150	260.50	271.03	10.53
30X-4	150	262.00	272.53	10.53
30X-5	150	263.50	274.03	10.53
30X-6	150	265.00	275.53	10.53
30X-CC	66	266.50	277.03	10.53
31X-1	139	267.10	277.63	10.53
31X-2	150	268.49	279.02	10.53
31X-3	150	269.99	280.52	10.53
31X-4	150	271.49	282.02	10.53
31X-5	150	272.99	283.52	10.53
31X-6	150	274.49	285.02	10.53
31X-7	41	275.99	286.52	10.53
31X-CC	27	276.40	286.93	10.53
32X-1	150	276.80	287.33	10.53
32X-2	150	278.30	288.83	10.53
32X-3	150	279.80	290.33	10.53
32X-4	150	281.30	291.83	10.53
32X-5	106	282.80	293.33	10.53
32X-CC	30	283.86	294.39	10.53
33X-CC	17	286.40	296.93	10.53
34X-1	150	296.00	306.53	10.53
34X-2	150	297.50	308.03	10.53
34X-3	43	299.00	309.53	10.53
34X-CC	17	299.43	309.96	10.53
35X-CC	54	302.60	313.13	10.53
36X-1	150	305.60	316.13	10.53
36X-2	150	307.10	317.63	10.53
36X-3	150	308.60	319.13	10.53
36X-4	150	310.10	320.63	10.53
36X-5	150	311.60	322.13	10.53
36X-6	150	313.10	323.63	10.53
36X-7	153	14.60	325.13	10.53
36X-CC	36	314.75	325.28	10.53
37X-CC	76	315.20	325.73	10.53
38X-1	129	324.80	335.33	10.53
38X-CC	31	326.09	336.62	10.53
39X-1	131	334.40	344.93	10.53
39X-CC	37	335.71	346.24	10.53
40X-1	150	344.00	354.53	10.53
40X-2	129	345.50	356.03	10.53
40X-CC	41	346.79	357.32	10.53
41X-1	150	353.70	364.23	10.53
41X-2	150	355.20	365.73	10.53
41X-3	150	356.70	367.23	10.53
41X-4	150	358.20	368.73	10.53
41X-5	33	359.70	370.23	10.53
41X-CC	30	360.03	370.56	10.53
42X-1	91	363.30	373.83	10.53
42X-CC	38	364.21	374.74	10.53

Note: Depths are from the top of each section.

II is also marked by a sharp increase in magnetic susceptibility (Fig. 5) and in the sand-sized fraction, and a decrease in the clay-sized fraction (Fig. 8). Sediments of Unit II are predominantly very dark greenish gray, dark greenish gray, very dark gray, and dark gray, silty clay with sand, silty clay with sand and gravel, sand-silt-clay, and clayey silt with sand and gravel. Unit II sediments average 0.9% $CaCO_3$ (see "Organic Geochemistry" section, this chapter). Dark gray clayey inorganic calcite with silt appears as a minor lithology at the base of the unit, 364.8 to 367.0 mbsf (Sections 162-987E-1R-2 to 1R-CC). In addition, several thin clayey laminations are also present toward the base of the unit. Numerous >1-cm-sized clasts (up to 91 clasts in Core 162-987E-40X) were identified throughout this unit, with an average number of 40 clasts >1.0 cm per core. These clasts are interpreted as components of debris-flow deposits rather than as dropstones. Crystalline rocks are the dominant rock type among the clasts in this unit. Smear slide and XRD analyses indicate that quartz and feldspars are the main components of the sand- and silt-sized fraction. Amphibole and pyroxene are also present and increase slightly downcore across the boundary of Units I and II. Poor recovery and drilling disturbance yielded discontinuous magnetic susceptibility and natural gamma-ray measurements, thus limiting their usefulness as interpretive tools.

Unit III

Interval: Core 162-987E-2R through Section 23R-5
Age: upper Pliocene to lower Pliocene
Depth: 369.2 to 575.5 mbsf

The transition between Units II and III is clearly marked by a sharp downcore decrease in magnetic susceptibility and in sand-sized particles. A slight downcore increase in natural gamma radiation is also observed across this boundary. The lower boundary is marked by a strong downcore increase in magnetic susceptibility and in sand-

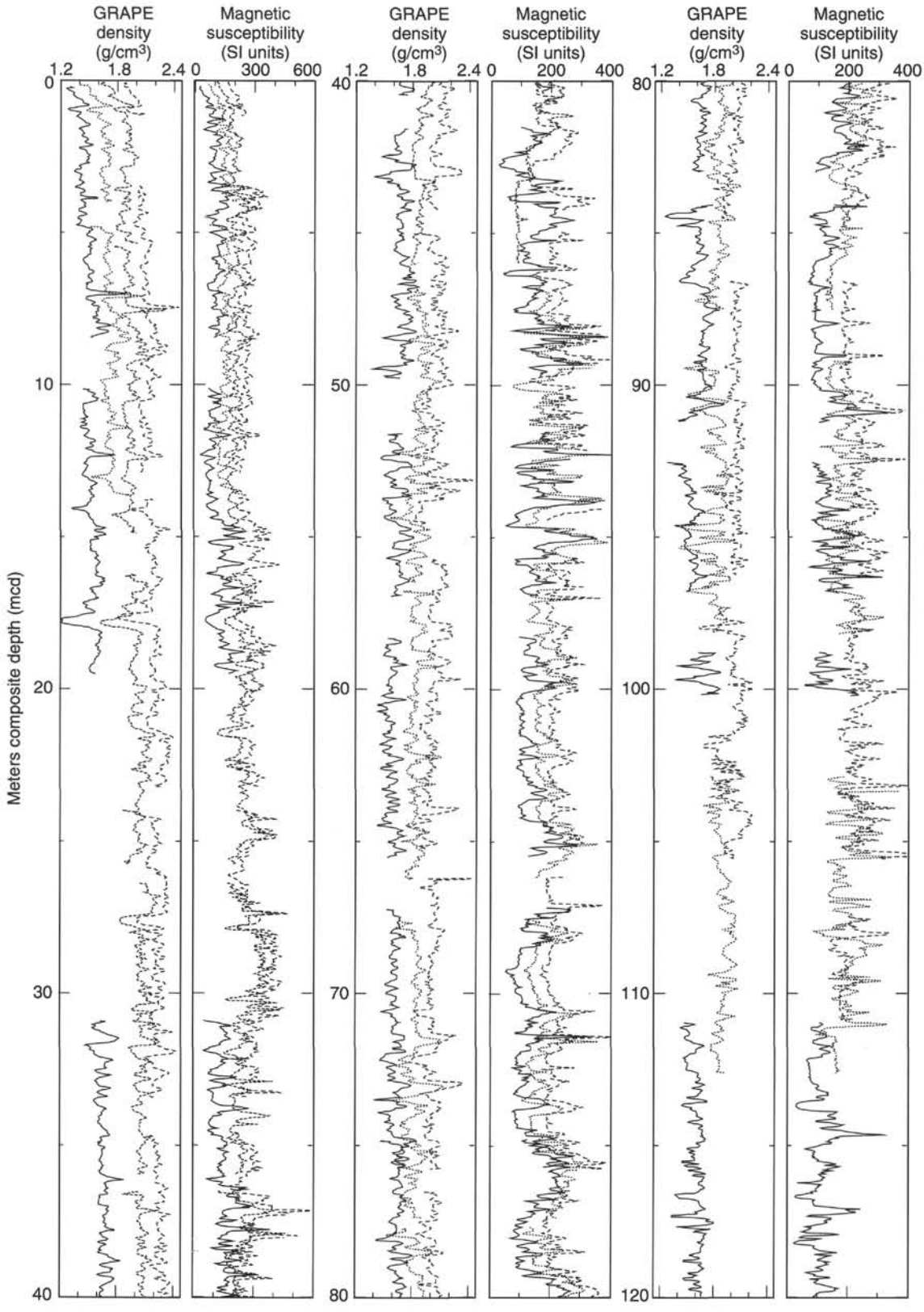

Figure 2. GRAPE density and magnetic susceptibility data from Site 987 on the mcd (meters composite depth) scale. Lines for Holes 987B (dotted), 987C (dashed), and 987D (long dashed) have been horizontally offset from line for Hole 987A (solid) for better display; therefore, values given on horizontal scale are the true values only for Hole 987A. (See also back pocket.)

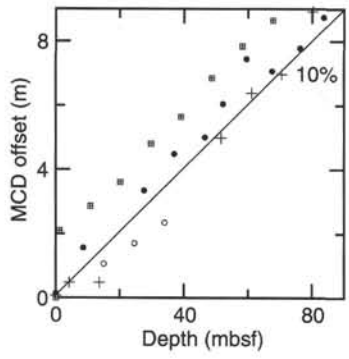

Figure 3. Depth offsets of the Site 987 mcd scale relative to mbsf depth, indicating the "growth" of the composite depth scale. Solid circles = Hole 987A, crosses = Hole 987B, open circles = Hole 987C, squares with crosses = Hole 987D.

sized content, and by a decrease in natural gamma radiation and in clay-sized fraction (Figs. 5, 8). This unit contains few >1.0 cm clasts, only averaging about two per core. These are mainly sedimentary and igneous rocks and are interpreted to be dropstones. Two subunits have been defined on the basis of smear slide and XRD analyses. Both subunits contain common thin, dark, clayey parallel laminations, and slight to moderate bioturbation occurs throughout the unit.

Subunit IIIA (369.2–465.4 mbsf) is composed of very dark gray, dark gray, and very dark greenish gray silty clay. Dark reddish, gray, and dark gray inorganic calcite with clay occurs as a minor lithology throughout the subunit. These inorganic calcite-rich layers (up to 40% $CaCO_3$) begin to be indurated toward the base of the subunit. Tilted beds occur in the middle of the subunit, 417.2 to 446.1 mbsf (Cores 162-987E-7R through 9R), and seem to be the result of processes natural rather than due to drilling disturbance.

Smear slide and XRD analyses indicate that quartz, feldspar, and inorganic calcite are still the most common components of the silt-sized fractions. Amphibole and pyroxene are also present. XRD analysis suggests that both feldspar and mica are slightly less abundant than in the previous units. The sediments are slightly to highly disturbed and are commonly fractured into drilling biscuits.

Subunit IIIB (465.4–75.5 mbsf) is defined by the downcore increase in the sand-sized fraction (Fig. 8). This subunit is mainly composed of very dark gray, dark gray, very dark greenish gray, and dark greenish gray silty clay interbedded with very dark gray and very dark greenish gray clayey silt with sand, sandy silt with clay, and clayey silt. Inorganic calcite-rich layers are less common than in Subunit IIIA. Dropstones are scattered throughout the subunit, averaging two dropstones per core. These dropstones are mainly crystalline.

Layering is common throughout this subunit and ranges from massive beds to thin subparallel laminations to rare flaser bedding. Contorted and dipping beds were also observed. Smear slide and XRD analyses reveal that quartz and feldspar are the most common terrigenous components of the silt- to sand-sized fraction. Feldspar and mica are slightly more abundant in this subunit compared with Subunit IIIA. Sulfides occur primarily as disseminated pyrite and pyrite concretions.

Unit IV

Interval: Section 162-987E-23R-5 through Core 31R
Age: lower Pliocene
Depth: 575.5 to 657.6 mbsf

The upper boundary of this unit is defined by the downcore increase in magnetic susceptibility and in sand-sized content, and by a decrease in natural gamma radiation and in clay-sized content (Fig. 5). The lower boundary of this unit is marked by a decrease in magnetic susceptibility and sand-sized content.

Table 3. Site 987 splice tie points.

Hole, core, section (cm)	Depth (mbsf)	Depth (mcd)		Hole, core, section (cm)	Depth (mbsf)	Depth (mcd)
162-987-				162-987-		
D-1H-1, 89	0.88	0.88	tie to	A-1H-1, 74	0.74	0.88
A-1H-4, 4	4.54	4.68	tie to	D-2H-1, 128	2.58	4.68
D-2H-6, 89	9.69	11.79	tie to	A-2H-2, 22	10.22	11.79
A-2H-6, 95	16.94	18.51	tie to	C-3H-2, 85	17.45	18.51
C-3H-6, 104	23.64	24.70	tie to	D-4H-1, 79	21.09	24.70
D-4H-3, 56	23.85	27.46	tie to	C-4H-1, 115	25.75	27.46
C-4H-6, 137	33.47	35.18	tie to	D-5H-1, 59	30.38	35.18
D-5H-5, 145	37.25	42.05	tie to	A-5H-1, 53	37.56	42.05
A-5H-4, 94	40.77	45.26	tie to	D-6H-1, 31	39.61	45.26
D-6H-2, 80	41.59	47.24	tie to	B-6H-1, 47	42.67	47.24
B-6H-7, 23	51.43	56.00	tie to	D-7H-1, 35	49.15	56.00
D-7H-3, 32	52.11	58.96	tie to	A-7H-1, 71	52.91	58.96
A-7H-5, 85	59.05	65.10	tie to	B-7H-6, 91	60.11	65.10
B-7H-7, 50	61.20	66.19	tie to	D-8H-1, 5	58.35	66.19
D-8H-7, 44	67.74	75.58	tie to	A-9H-1, 82	68.52	75.58
A-9H-6, 50	75.69	82.75	tie to	B-9H-4, 59	75.78	82.75
B-9H-6, 10	78.30	85.27	tie to	A-10H-1, 128	77.48	85.27
A-10H-5, 82	81.11	88.90	tie to	D-10H-2, 92	79.02	88.90
D-10H-4, 125	82.35	92.23	tie to	B-10H-3, 119	83.31	92.23
B-10H-7, 95	89.07	97.99	tie to	D-11H-2, 41	86.89	97.99
D-41X-3, 144	358.14	368.67				

Like Unit II, this unit is mainly composed of very dark gray, very dark greenish gray, very dark olive gray silty clay with sand, silty clay with sand and gravel, silty clay with gravel, and silty clay. Due to time constraints, shipboard carbonate measurements were only made to 628.8 mbsf (through Core 162-987E-28R). To this depth, carbonate content for the unit was very low, averaging 0.73% (see "Organic Geochemistry" section, this chapter). Bluish gray, greenish gray, and gray carbonate-cemented sandstone and carbonate-cemented silty sandstone occur as a minor lithology throughout the unit. These carbonate-rich intervals contain small pyrite crystals, rounded quartz, and small rock fragments and are more lithified than surrounding sediment. Various igneous, metamorphic, and sedimentary clasts <1.0 cm wide are present within the silty clay with sand matrix (Fig. 9). Gravel clasts tend to be aligned parallel to the bedding. A few clasts >1.0 cm, mainly igneous, also occur within the unit. Both thin, dark, clayey horizontal laminations and dipping beds occur at the top of the unit. Smear slide and XRD analyses indicate that quartz and feldspar are the major components of the silt- to sand-sized fraction. XRD analysis also reveals that mica, feldspar, pyroxene, and amphibole are more abundant than in the previous units. Zeolites and mixed-layer clay are also present in minor amounts.

Unit V

Interval: Cores 162-987E-31R through 52R (base of hole)
Age: Miocene to lower Pliocene
Depth: 657.6 to 859.4 mbsf

Unit V is charactered by low magnetic susceptibility and by a reduced number of gravel clasts. Sediments of Unit V are composed of very dark gray, very dark greenish gray, dark greenish gray silty clay interbedded with very dark greenish gray clayey silt, clay with silt and sand, and clayey silt with sand. Silty sand with clay and calcite occurs as a minor lithology. Two graded sandy turbidites are present in Core 162-987E-34R (676.7–686.2 mbsf). Sediments of Unit V are highly indurated and show many fine-scale structures. These structures include flaser bedding and discrete burrow traces, commonly compressed parallel to bedding. Sections with dipping beds, wavy laminae, convoluted structures, and folding, interpreted as slumps, occur throughout the unit (Fig. 10). Nonbiogenic carbonate-cemented layers and thin dark clayey laminations are also common. Silt-filled burrows and benthic foraminifers are more common toward the base of the unit. Sulfides occur mainly as pyrite concretions.

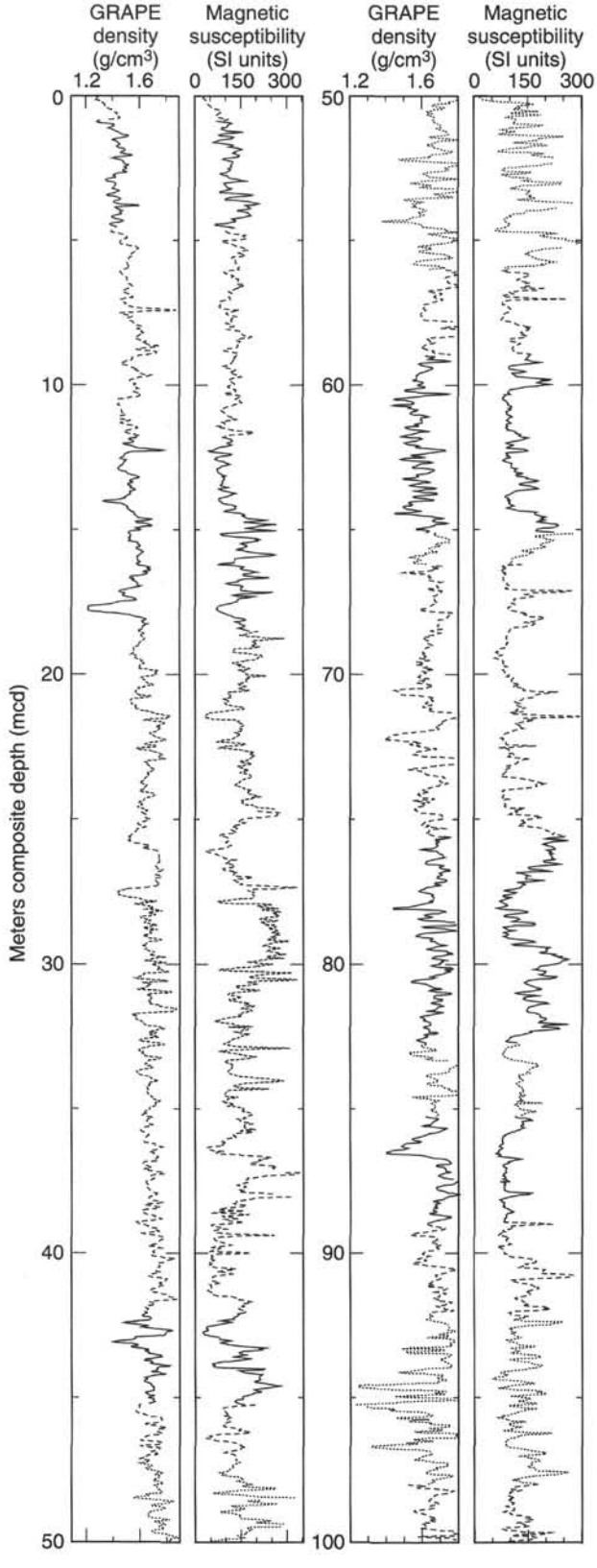

Figure 4. Spliced records of GRAPE density and magnetic susceptibility from Site 987. Tie points for forming the splice are given in Table 3. Holes are: 987A (solid), 987B (dotted), 987C (dashed), and 987D (long dashed).

Table 4. Summary table of clasts >1 cm in size found at Site 987.

Core, section, interval (cm)	Depth (mbsf)	Size (cm)	Composition	Shape
162-987A-				
1H-5, 5	6.05	2.8	Granite	Subrounded
1H-5, 7	6.07	1.8	Siltstone	Subangular
4H-3, 23	30.73	1.2	Fine-grained diorite	Subangular
4H-3, 134	31.84	1.0	Fossiliferous limestone	Subrounded
4H-3, 138	31.88	1.2	Porphyric granite	Subangular
4H-3, 140	31.90	1.8	Syenite	Subangular
4H-5, 7	33.57	1.8	Dark diorite	Angular
6H-1, 105	47.55	1.5	Light gray siltstone	Angular
7H-5, 10	58.30	3.7	Fractured pink quartzite	Rounded

Only a part of this table is reproduced here. The entire table appears on the CD-ROM (back pocket).

Smear slide analysis reveals that the sand-sized content is very low within this unit. Quartz and feldspar are the most common components of the terrigenous silt-sized fraction.

Interpretation

Turbidites, ranging from millimeter to decimeter thickness, are common within the silty clay background in the uppermost part of this site (Unit I). Turbiditic downslope sediment transport seems to be an important sedimentary process during the Pleistocene and late Pliocene.

Units II (late Pliocene) and IV (early Pliocene) are very similar. These units are characterized by increased magnetic susceptibility, bulk density, and compressional velocity, and decreased natural gamma radiation and porosity (see "Physical Properties" section, this chapter). Much of both of these units seem to be debris-flow deposits. This interpretation is supported by physical properties data and logging results (see "Physical Properties" and "Wireline Logging" sections, this chapter).

Units III (late to early Pliocene) and V (late Pliocene to Miocene) are similar to Unit I, except that the lowermost part of the Unit V is more indurated. Sediments seem to have a high hemipelagic component and seem to be less influenced by turbiditic downslope sediment transport than Units I, II, and IV.

As this site is located on a "glaciated" continental margin, the differences presented above between the two different types of deposits, those that are mass-wasting-dominated (Units II and IV), and those that are hemipelagic- and ice-rafted-debris-dominated (Units I, III, and V), may reflect variations in glacial style and/or intensity, changes in sediment source area, and/or changes in the location of a main fan depocenter. During mass-wasting-dominated intervals, coarse sediment appears to be pushed downslope or possibly concentrated in channels. During hemipelagic- and IRD-dominated intervals, finer sediments suggest less downslope transport or deposition away from a main fan-channel axis. Higher magnetic susceptibility values during mass-wasting-dominated deposition could result from changes in terrigenous source areas.

BIOSTRATIGRAPHY

The biostratigraphy of Site 987, located on the East Greenland Margin, is incomplete because of the poor preservation of all microfossil groups. Most samples from this site are barren of both siliceous and calcareous microfossils (Fig. 11). Siliceous microfossils were not observed in any samples, with the exception of rare pyritized diatom fragments in Sample 162-987E-11R-CC. Perhaps indicative of former organic material, rare to common pyrite framboids were recorded from Core 162-987E-23R to the base of the hole. Only calcareous microfossil datum could be used to provide age constraints for the sequence (see "Sedimentation Rates" section, this chapter).

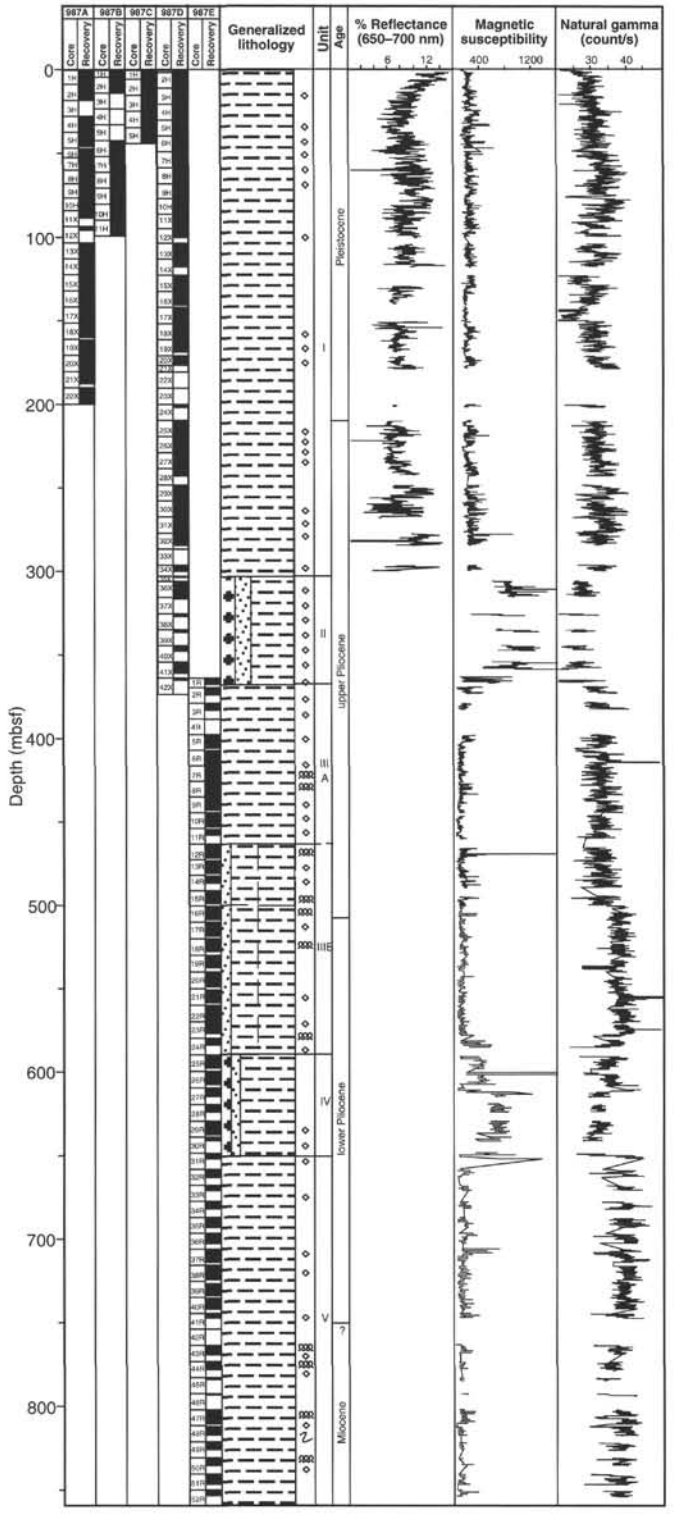

Figure 5. Core recovery, lithostratigraphy, age, spectral reflectance (red band), magnetic susceptibility, and natural gamma-ray intensity of sediments recovered in Holes 987A, 987B, 987C, 987D, and 987E. Cores containing dropstones (open diamonds) are shown in column adjacent to the lithostratigraphy. Spectral reflectance record is from Hole 987D; magnetic susceptibility and natural gamma-ray records are from both Holes 987D and 987E. (Key to symbols used in the "Generalized Lithology" column can be found in fig. 4, "Explanatory Notes" chapter, this volume.)

Calcareous Nannofossils

Calcareous nannofossils are continuously present from Cores 162-987A-1H through 5H. *Emiliania huxleyi* is present in Sample 162-987A-1H-CC, which can be placed in Zone CN15. The highest occurrence of *Pseudoemiliania lacunosa* is located in Sample 162-987A-5H-CC, and thus the top of Zone CN14a can be drawn above this sample. Calcareous nannofossils are practically absent in the sequence below Core 162-987A-5H. A few specimens of small *Reticulofenestra* were found in Samples 162-987A-14H-CC and 18H-CC. *Coccolithus pelagicus* and *Reticulofenestra pseudoumbilicus* are present in Samples 162-987E-43R-CC and 44R-CC, suggesting a general age of middle Miocene to early Pliocene. Rare nannofossils are also present in Samples 162-987E-49R-CC through 52R-CC, but no age-diagnostic species were found.

Planktonic Foraminifers

Site 987 planktonic foraminifers are generally common to abundant from the top of the sequence to Sample 162-987D-3H-CC, and preservation is good. Samples contain very rare *Neogloboquadrina pachyderma* (sinistrally coiling) from Samples 162-987A-4H-CC to 10H-CC, and are barren from Sample 162-987A-11X-CC to the bottom of the sequence (Sample 162-987E-52R-CC), except for two samples (Fig. 11). *Globigerina egelida* is recorded in Sample 162-987A-18X-CC and rare *Neogloboquadrina pachyderma* (sinistrally coiling) is observed in Sample 162-987D-19X-CC. Barren intervals prevent the use of planktonic foraminifer datums in the calculation of sedimentation rates (see "Sedimentation Rates" section, this chapter).

Benthic Foraminifers

Benthic foraminifers exhibit variable abundance and preservation at Site 987. The mudline sample (162-987A-1H-CC, 0–1 cm) contains a moderately diverse assemblage which is dominated by agglutinated taxa. Common species include *Eponides umbonatus, Epistominella exigua, Cassidulina teretis, Reophax* spp., and a roughly textured form of *Recurvoides* sp. Calcareous specimens are sporadic in their occurrence from the top of the sequence to Sample 162-987E-14R-CC, varying considerably in composition from a few abraded specimens of *Elphidium excavatum,* to clearly mixed water-depth assemblages that are dominated by either *Epistominella exigua* or *Cassidulina teretis* but also contain *E. excavatum* (e.g., Sample 162-987A-20X-CC). A barren interval occurs between Samples 162-987E-14R-CC and 46R-CC; below this depth rare agglutinated specimens are recorded. The latter include *Haplophragmoides* spp., *Spirosigmoilinella* sp., and various tubular agglutinated forms; however, these are not useful age-diagnostic taxa.

Diatoms

All samples at this site are barren of diatoms, with the exception of Sample 162-987-11R-CC. This sample contained rare, pyritized fragments of an unidentifiable centric diatom species.

Siliceous Flagellates and Radiolarians

All samples at this site are barren of siliceous flagellates and radiolarians.

PALEOMAGNETISM

At Site 987, archive halves of all cores that were not highly deformed were measured using the pass-through cryogenic magnetometer with a 5-cm measurement interval. The quality of the paleo-

Table 5. Description of the lithostratigraphic units at Site 987.

Unit	Subunit	Depth (mbsf)	Thickness (m)	Age	Lithology and characteristic features
I		0–305.6	305.6	Pleist.–late Plio.	Silty clay. Several turbidites and sandy to silty layers. Silty clay with inorganic calcite occurs as a minor lithology.
II		305.6–369.2	63.6	late Pliocene	Silty clay with sand and gravels. This unit is characterized by high magnetic susceptibility, numerous gravels and clasts, and low natural gamma radiation. Debris-flow deposits.
III		369.2–575.5	206.3	early–late Plio.	
	IIIA	369.2–465.4	96.2		Silty clay. Few tilted beds and scattered dropstones occur throughout the unit. Silty clay with inorganic calcite is interbedded as a minor lithology.
	IIIB	465.4–575.5	110.1		Silty clay interbedded with clayey silt with sand, sandy silt with clay, and clayey silt. Contorted beds and scattered dropstones occur throughout the unit.
IV		575.5–657.6	82.1	early Pliocene	Silty clay with sand and gravels. This unit is characterized by high magnetic susceptibility, numerous gravels and clasts, and low natural gamma radiation. Debris-flow deposits.
V		657.6–859.4	201.8		Silty clay. Sediment is very indurated. Scattered dropstones, dipping beds, contorted beds, folding and slumps occur throughout the unit.

magnetic data at this site was dependent on the degree of drilling disturbance. The XCB cores were particularly prone to drilling disturbance, and the magnetic inclination record was more or less incoherent in the upper part of the XCB sections. The RCB section in Hole 987E was considerably less deformed than XCB cores from the same level in Hole 987D.

Demagnetization was carried out at peak alternating fields (AF) of 25 mT for all core sections that were measured at Site 987. Magnetization intensities were in the 5–50-mA/m range after 25-mT AF demagnetization. There is no evidence for secondary magnetizations carried by iron sulfides. The natural remanent magnetization (NRM) of many cores was measured in order to establish the direction of the viscous drill-string magnetic overprint. Additional demagnetization steps at 10, 15, and 30 mT were carried out on some core sections, as time allowed (Table 6). The ubiquitous drilling-induced remanence is steeply inclined downward; however, this overprint can generally be removed by AF demagnetization at peak fields of 15–25 mT to give a "primary" magnetization component.

In Hole 987A, the inclination record is coherent to the base of the APC section (Core 987A-10H). The Brunhes/Matuyama boundary and the top of the Jaramillo Subchron can be recognized (Table 7; Fig. 12). From Core 987A-11X downward, the record is severely compromised by drilling disturbance. The top of Chron 1r.2r (the Matuyama Chron prior to the Jaramillo Subchron) is poorly defined by low inclination data (Fig. 12). The record within Chron 1r.2r improves with depth as the lithology becomes more indurated and resistant to drilling disturbance. At 195 mbsf (Core 987A-22X), the inclinations become positive close to the base of the hole (Fig. 12). We interpret this inclination change as signifying the top of the Olduvai Subchron.

Eleven APC cores were recovered from Hole 987B. A large part of the Brunhes Chron is not recorded due to lack of recovery in Core 987B-3H through 5H. The Brunhes/Matuyama boundary and the top of the Jaramillo Subchron are well defined at 72 and 89 mbsf, respectively. The record between the Brunhes and the top of the Jaramillo is compromised by drilling disturbance in Core 987B-9H and 10H.

In Hole 987C, the five APC cores record the upper part of the Brunhes Chron. The magnetic inclination record is incoherent in Core 987C-5H, at the base of the hole, due to drilling disturbance.

In Hole 987D, the base of the APC section and the entire XCB section are severely affected by drilling disturbance. Measurements of remanent magnetization were discontinued below Core 987D-36X due to the poor condition of the cores. The Brunhes/Matuyama boundary is recognized at 70 mbsf. The Jaramillo Subchron is very poorly defined in the 88–100-mbsf interval. The almost total lack of recovery in the interval between the base of Core 987D-20X and the top of Core 987D-25X resulted in loss of the Olduvai record, although the base of the Olduvai Subchron appears to be located within Core 987D-26X.

In Hole 987E, the RCB cores were in considerably better condition than the XCB cores from the same level in Hole 987D. The inclination record is fairly coherent throughout Hole 987E, although poor recovery in the first four cores compromises the record in the 360–400-mbsf interval. The Matuyama/Gauss boundary and the Gauss/Gilbert boundary are recognized at 369 and 508 mbsf, respectively (Table 6; Fig. 12). The Kaena Subchron is well defined in the 438–447-mbsf interval; however, the Mammoth is undefined and may be represented by low inclinations in the 470–485-mbsf interval. Three normal polarity subchrons within the Gilbert Chron are recognizable, with one particularly thick normal polarity subchron interpreted as the Thvera. The elevated sedimentation rates in Chron 2r.2r and Chron 3n.4n (Thvera Subchron; Fig. 13) coincide with intervals characterized by debris flows (see "Lithostratigraphy" section, this chapter).

SEDIMENTATION RATES

A sedimentary section 859 m thick was recovered at Site 987. Sedimentation rate reconstructions for Site 987 were based primarily on magnetic polarity events from Holes 987A, 987D, and 987E (see "Paleomagnetism" section, this chapter). Because the sediments at Site 987 were largely barren of fossils, biostratigraphic events were not used for sedimentation rate estimates, with the exception of the LO of *Pseudoemiliania lacunosa* at 45 mbsf (50 mcd) in Hole 987A (see "Biostratigraphy" section, this chapter). The Site 987 composite depth section (see "Composite Depths" section, this chapter) was used to relate events recorded in the five holes drilled at Site 987 to a common depth scale. To facilitate comparison between sites, sedimentation rates were estimated from age vs. depth plots (Fig. 14) by drawing straight-line segments (uniform sedimentation rate) between selected datums.

Sedimentation rates were calculated for both the meters below seafloor (mbsf) depth scale and the meters composite depth (mcd) depth scale. Table 8 and Figure 15 present sedimentation rates as a function of age and composite depth for Site 987. Magnetic polarity age control points included are the Brunhes/Matuyama, Matuyama/Gauss, and Gauss/Gilbert Chron boundaries, and the Jaramillo, Olduvai, and Kaena Subchrons. Sedimentation rates vary from ~61 mcd/m.y. from 0.78 to 0.99 Ma, to about 203 mcd/m.y. from 1.77 to 2.58 Ma.

ORGANIC GEOCHEMISTRY

The shipboard organic geochemistry program at Site 987 consisted of analyses of volatile hydrocarbons and determinations of inor-

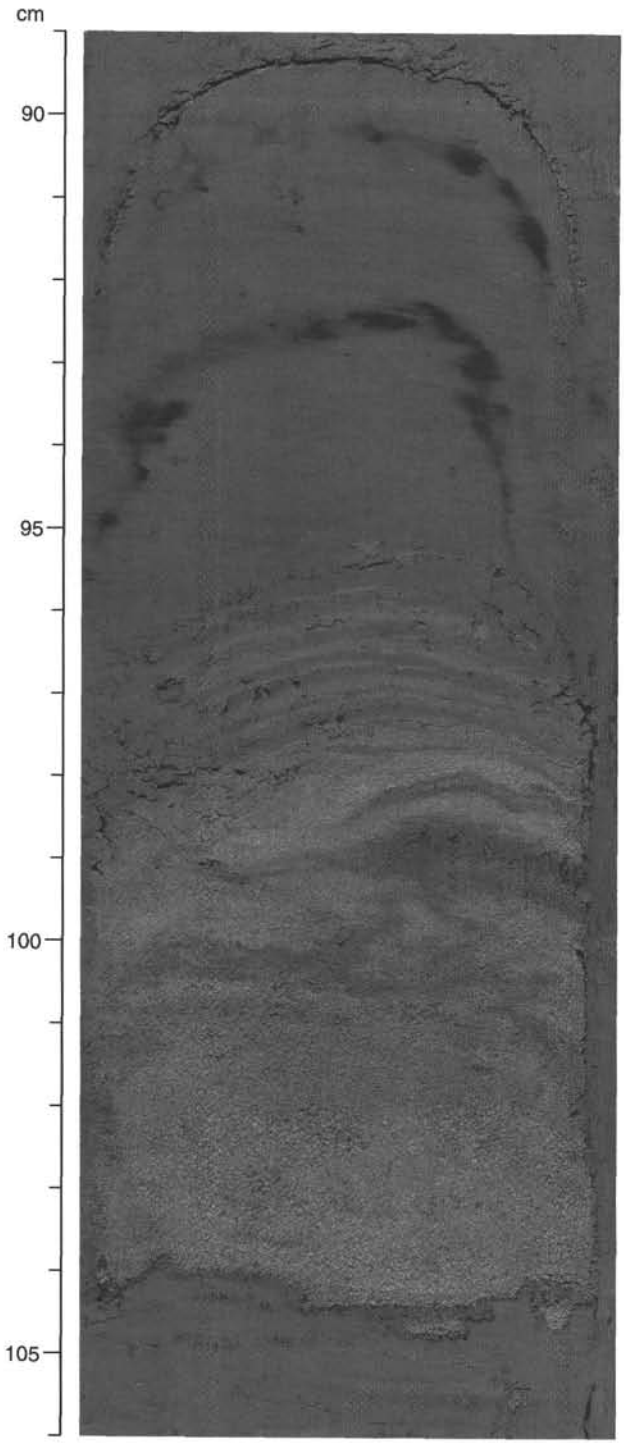

Figure 6. Photograph showing a graded sandy layer in Section 162-987B-7H-4, 89–106 cm (51.09–51.26 mbsf).

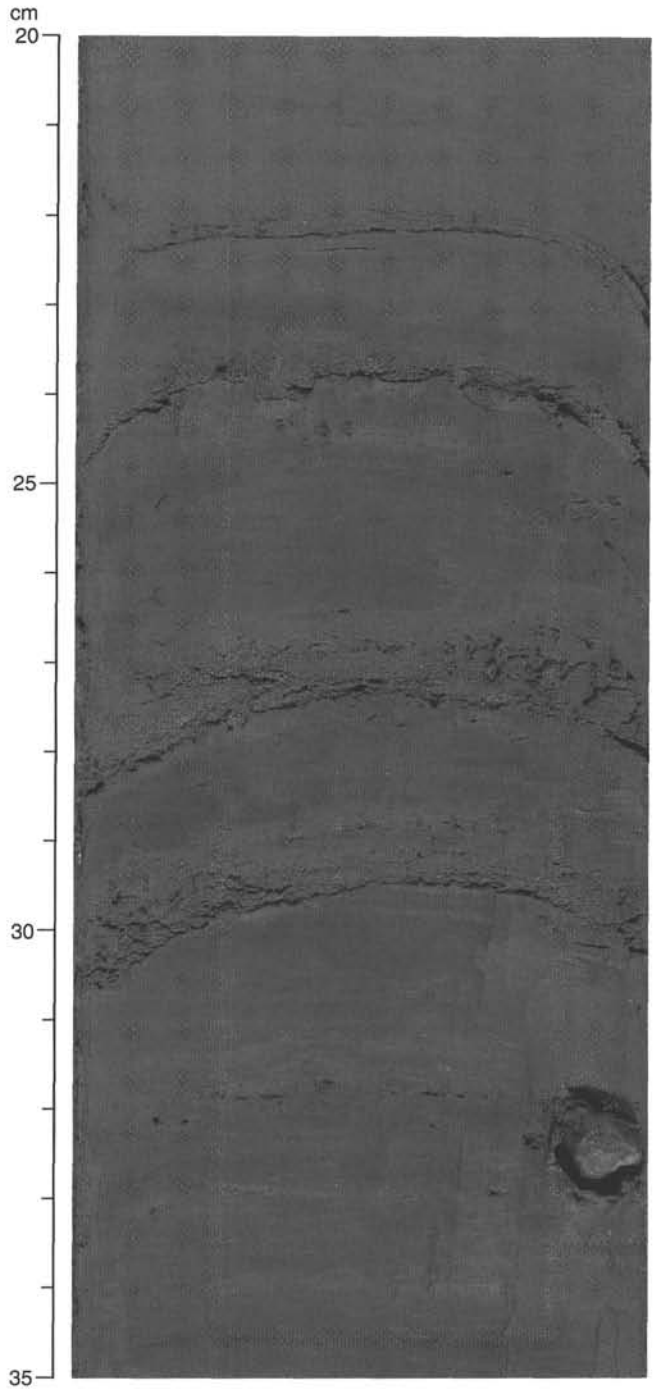

Figure 7. Photograph showing a fining- and thinning-upward sequence in Section 162-987C-4H-2, 20–35 cm (26.3–26.45 mbsf).

ganic carbon, total nitrogen, total carbon, and total sulfur (for methods, see "Explanatory Notes" chapter, this volume).

Volatile Hydrocarbons

Concentrations of headspace methane (C_1) increase abruptly at about 30 mbsf, reaching values of 68,000 ppm at 74 mbsf in Hole 987A (Fig. 16). Except in the uppermost 30 mbsf, methane contents are high throughout the sedimentary section, varying between about 4000 and 70,000 ppm (Table 9; Fig. 16). Gas hydrates should be stable down to about 180 mbsf at Site 987 (Fig. 16), based on the pressure-temperature stability field of gas hydrates (cf. Kvenvolden and Barnard, 1983), a geothermal temperature gradient of about 104°C/km (see "Physical Properties" section, this chapter), a water depth of 1684 m, and a bottom-water temperature of about 0°C. Therefore, the high concentration of methane between 30 and 180 mbsf may potentially be related to the presence of methane hydrates. This estimated depth of the gas hydrate zone corresponds to the occurrence of gas

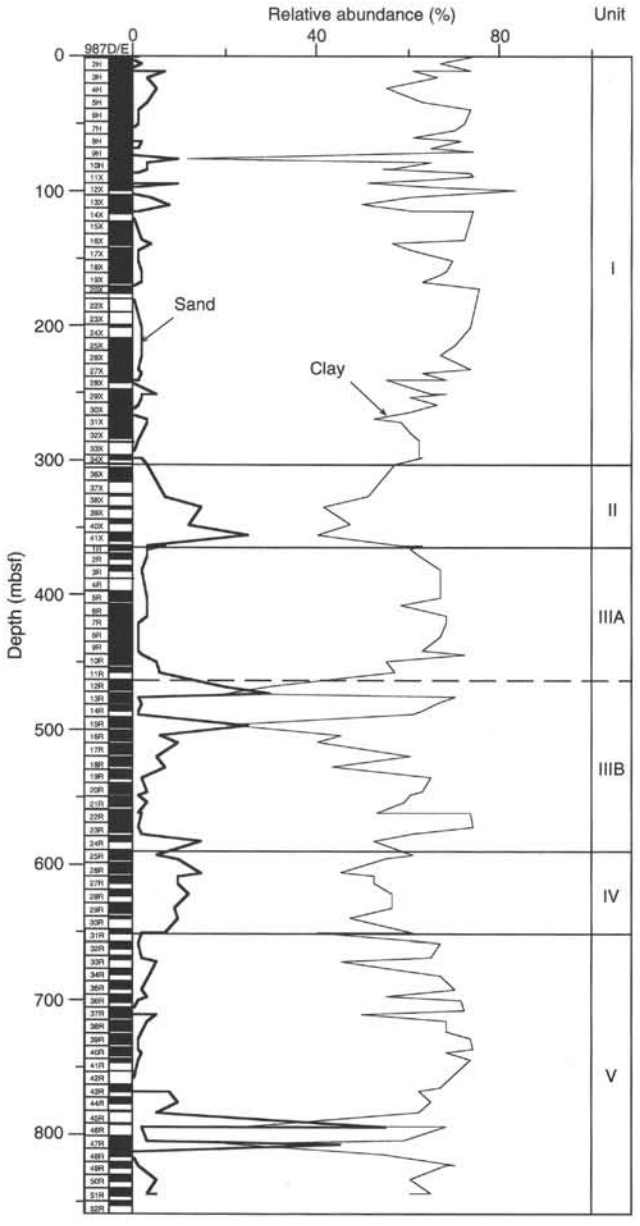

Figure 8. Core recovery and estimated relative abundances of sand-sized grains (heavy line) and clay-sized grains derived from smear slide analysis in Holes 987D and 987E.

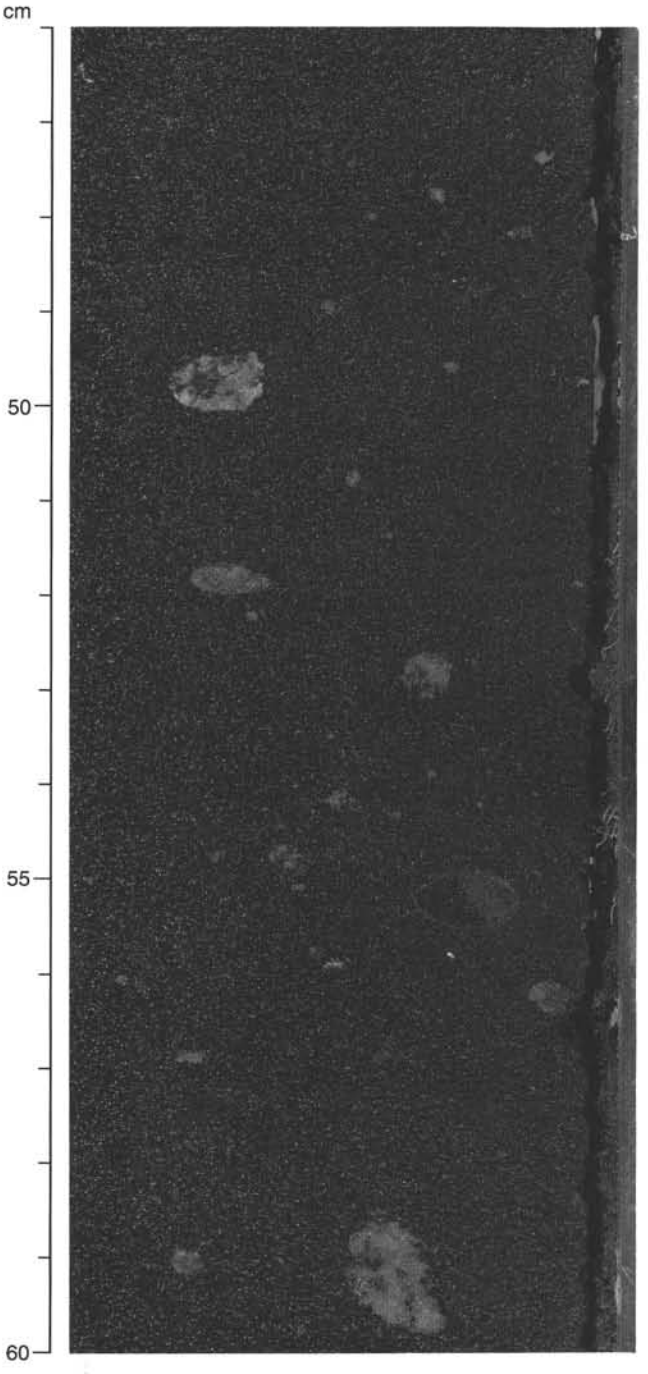

Figure 9. Photograph showing a typical debris-flow deposit with several millimeter- and centimeter-sized gravel and clasts in a silty clay with sand matrix found in Section 162-987E-26R-5, 46–60 cm (605.71–605.85 mbsf).

voids in recovered cores, which suggests degassing sediments in the core liner. However, we have no direct evidence for gas hydrates, such as a bottom-simulating reflector or recovered gas hydrates at Site 987. Likewise, chloride profiles show normal values in this interval (see "Inorganic Geochemistry" section, this chapter).

Ethane (C_2) was first detected below 34 mbsf, and generally increased with burial depth to 10–100 ppm (Fig. 16). Propane (C_3) was first detected below 109 mbsf, with low levels (reaching up to 3 ppm) in the sediment sequence at Site 987 (Fig. 16). Ethylene ($C_{2=}$) occurs in detectable amounts below 109 mbsf (Fig. 16). Higher-molecular-weight hydrocarbons (C_4 to C_6) were not detected at Site 987.

Vacutainer gas samples were obtained between 118 and 154 mbsf (Core 162-987A-14X through 18X). Concentrations of vacutainer methane are generally higher than the headspace concentrations, ranging from 87,000 to 99,000 ppm (Table 9; Fig. 16).

For safety considerations, the C_1/C_2 (methane/ethane) ratio is generally used to get quick information about the origin of the hydrocarbons. At Site 987, the headspace C_1/C_2 ratios show the normal general decrease with depth in the upper interval (above 400 mbsf), from values of >10,000 at shallow depth to values of about 1000 deeper in the sequence (Table 9; Fig. 16). Below 400 mbsf, no distinct variation of the C_1/C_2 ratio is obvious. In this interval, C_1/C_2 values range from 900 to 2000 (Fig. 16). The high C_1/C_2 ratios suggest in situ microbial production of methane from marine organic materi-

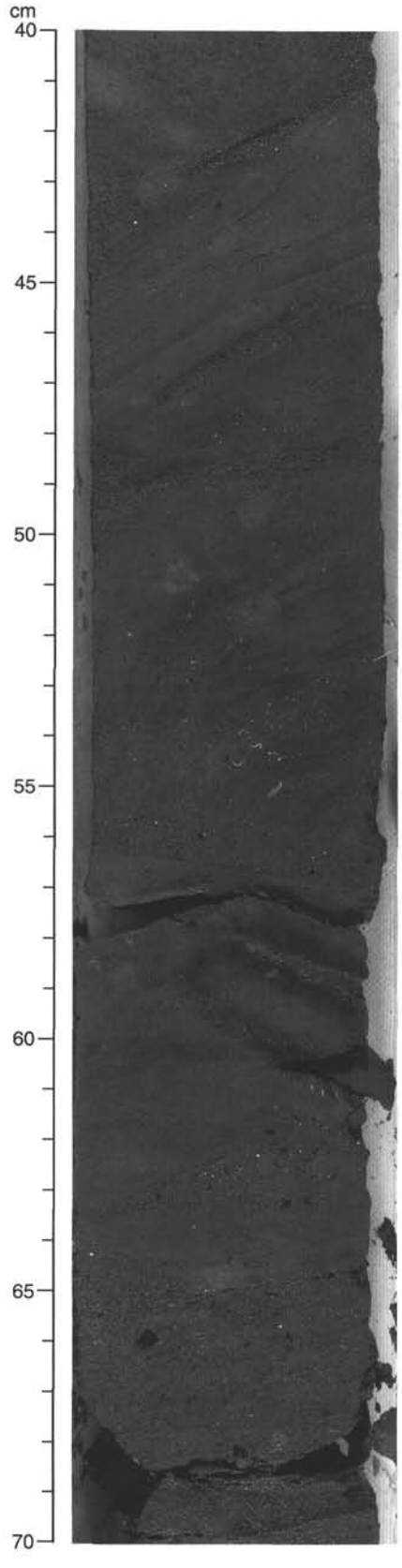

Figure 10. Photograph showing contorted bedding found in Unit V in Section 162-987E-43R-2, 40–70 cm (765.1–765.4 mbsf).

al. At Site 987, methanogenesis has begun at depths shallower than 40 mbsf, as clearly indicated by the sharp increase in methane concentrations and the contemporaneous and sharp disappearance of sulfate (see "Inorganic Geochemistry" section, this chapter).

Carbon, Nitrogen, and Sulfur Concentrations

Determinations of inorganic carbon, total carbon, total nitrogen, and total sulfur are summarized in Table 10 and presented in Figure 17. Due to the limited analytical time, shipboard $CaCO_3$ measurements could not be performed on samples below 624 mbsf in Hole 987E, and elemental analysis (TC, TN, and TS determinations) could not be performed on samples below 312 mbsf in Hole 987E. Carbonate content values in the dominant lithologies (i.e., silty clay and clayey silt) vary between 0.3% and 10% in the sedimentary sequence at Site 987. In the light-colored layers that occurred in the middle intervals (220–300 mbsf and 400–430 mbsf), carbonate contents reach values as high as 30% to 40%, reflecting nonbiogenic (inorganic) carbonate in the sediments (Fig. 17). Total organic carbon (TOC) content varies between 0.21% and 1.02% in Hole 987D, with an average value of 0.54% (Table 10; Fig. 17). Total nitrogen contents range from 0% to 0.13% (Fig. 17). Total sulfur values are low, ranging from 0% to 0.69% (Fig. 17).

Composition of Organic Matter

Total organic carbon/total nitrogen (C/N) ratios have been used to characterize the type of the organic matter. C/N ratios vary between 3.0 and 12.1 in Hole 987D, and most values range from 4 to 10 (Fig. 17), suggesting that it is marine organic matter preserved in the sediments (Fig. 18). C/N ratios of >10 occur in the upper section, between 25 and 37 mbsf (latest Pleistocene), probably reflecting the presence of small amounts of terrigenous organic material. These first rough estimates of the composition of the organic matter, however, need to be checked by shore-based organic geochemical investigations.

INORGANIC GEOCHEMISTRY

Interstitial waters were analyzed from Holes 987A and 987D to a depth of approximately 350 mbsf. Time constraints permitted only the measurement of salinity, pH, alkalinity, and chloride for Hole 987E; these results are presented in tabular format only (Table 11).

Similar to other high-sedimentation-rate sites drilled on Leg 162, sulfate concentrations decrease rapidly to zero within the top 30 m (Table 11; Fig. 19A), coinciding with an increase in methane in headspace samples (see "Organic Geochemistry" section, this chapter). Alkalinity increases rapidly in the zone of sulfate reduction from 5.9 mM at the surface to a maximum of 15.4 mM at 33.5 mbsf (Table 11; Fig. 19B). Below this level, alkalinity progressively decreases to the base of Hole 987E. Ammonia concentrations increase from 185 mM at the surface to a broad maximum of about 2880 μM between 138 and 167 mbsf (Table 11; Fig. 19C), reflecting production in both the zones of sulfate reduction and methanogenesis. Below this level, ammonia concentrations decrease toward the base of Hole 987D. The profile of dissolved phosphate exhibits two distinct peaks at 33.5 and 166.6 mbsf. The upper and larger of the two peaks is associated with the alkalinity maximum at the base of the sulfate reduction zone, and probably reflects the release of phosphate from organic matter. The lower peak is associated with the ammonia maximum (Table 11; Fig. 19D).

Except for the top 33.5 mbsf where calcium decreases slightly, calcium generally increases and magnesium decreases downhole (Table 11; Fig. 19E), reflecting the in situ alteration of volcanic material and chemical interaction with oceanic basement. The rate of change in both calcium and magnesium increases below about 200 mbsf and the slope of the Ca vs. Mg relationship is −1.4, which is typ-

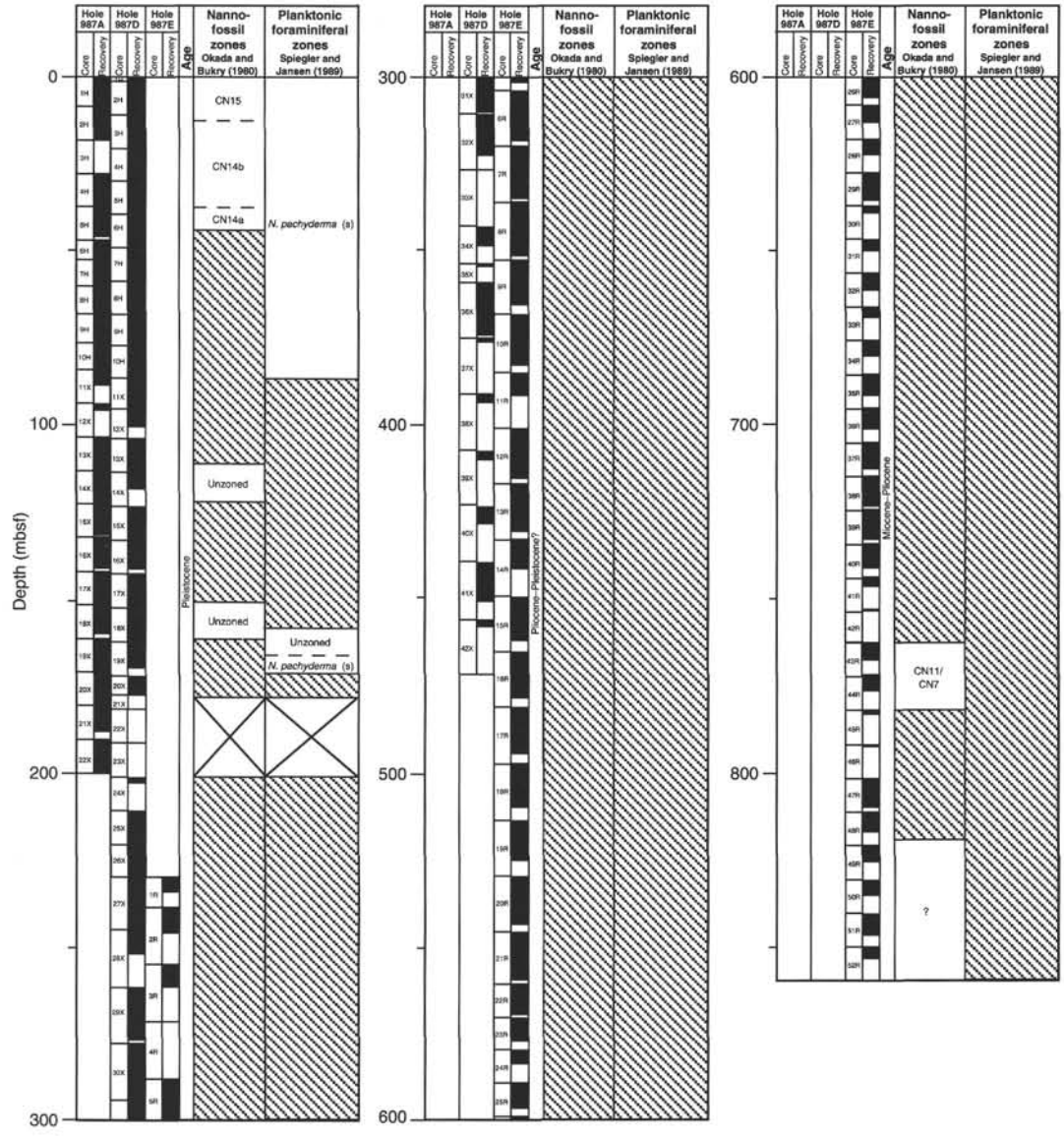

Figure 11. Biostratigraphic summary, Site 987. Hatched intervals indicate absence of fossils. An "X" indicates interval with no recovery. Age information is based on planktonic foraminifer and nannofossil biostratigraphy.

ical of sites located on basaltic oceanic crust (Fig. 19F; McDuff, 1981).

Potassium concentrations decrease downhole from about 12 mM near the surface to 1.2 mM at the bottom of Hole 987D (Table 11; Fig. 19G), reflecting uptake during the alteration of oceanic basement and volcanic material in the sediment column. The lithium profile displays complex behavior and is sigmoidal in shape (Table 11; Fig. 19H); concentrations decrease downhole in the top 33.5 mbsf, then increase to a maximum between 215 and 241 mbsf, and finally decrease toward the bottom of Hole 987D.

Chloride concentrations are relatively constant down to 450 mbsf, averaging 563 mM (Table 11; Fig. 19I), slightly greater than the IAPSO standard (559 mM). Below 450 mbsf, chloride decreases to a minimum of 514 mM at 721 mbsf, and then increases slightly toward the base of Hole 987E (Table 11). Similar to Site 986, this decrease in chloride below 450 mbsf may be related to dehydration reactions of clay minerals (e.g., smectite to illite), although post-cruise clay mineralogical studies will be needed to test this hypothesis. Heat flow at Site 987 is also moderately high, with estimates ranging from 75° to 96.5°C/km (see "Physical Properties" section, this chapter). Sodium concentrations are near seawater values at the top of the core and remain relatively high until about 200 mbsf, where they begin to decrease abruptly, reaching minimum values of 446 mM near the base of Hole 987D (Table 11; Fig. 19I). This decrease may reflect the uptake of sodium during the formation of Na-bearing zeolites. Salinity decreases rapidly downhole in the upper 33.5 mbsf, reflecting the removal of sulfate in the zone of sulfate reduction, and then values remain relatively constant to the bottom of Hole 987D (Table 11; Fig. 19J). In Hole 987E, salinity decreases below 400 mbsf in concert with the decreases in chloride, reaching minimum values of 30 between 460 and 720 mbsf (Table 11). This dilution of interstitial waters is probably related to the dehydration of clay minerals.

Silica concentrations exhibit a twin-peak maximum between 138 and 215 mbsf (Table 11; Fig. 19K), which probably reflects alteration of volcanic material or dissolution of siliceous microfossils. Strontium concentrations are relatively constant and average 77 µM in the

Table 6. Summary of pass-through cryogenic magnetometer measurements at Site 987.

Measurement	Core sections
	162-987A-
NRM	2H-4, 2H-5, 2H-6, 4H-5, 4H-6, 7H-3, 7H-4, 7H-5, 8H-2 through 8H-5, 9H-2 through 9H-5, 10H-4, 10H-5, 11X-2, 12X-1, 16X-2
15 mT	2H-6
25 mT	1H-1 through 21X-5, 22X-2 through 22X-6
30 mT	2H-6, 9H-3, 10H-4, 10H-5, 10H-2, 11X-1, 13X-2, 13X-6, 14X-4 through 15X-5, 17X-1, 17X-3, 18X-1, 19X-1
	162-987B-
NRM	9H-3, 9H-6, 10H-4, 11H-2
15 mT	9H-3, 10H-4
25 mT	1H-1 through 11H-7
30 mT	9H-3, 9H-6, 11H-1, 11H-6
	162-987C-
25 mT	1H-1 through 5H-7
30 mT	3H-3, 5H-1, 5H-3
	162-987D-
NRM	9H-4, 10H-3 through 10H-6, 13X-4, 13X-6, 15X-5, 15X-6, 16X-4, 16X-5, 18X-1, 19X-2, 19X-3, 25X-2, 26X-3 through 26X-6, 27X-2, 27X-3, 27X-4, 29X-5
15 mT	15X-5, 15X-6, 16X-4
25 mT	1H-1 through 14X-3, 15X-5 through 25X-6, 26X-2, 26X-3, 26X-5, 26X-6, 26X-7, 27X-2 through 29X-3, 29X-5 through 36X-1, 36X-4 36X-5, 36X-6
30 mT	8H-6, 9H-4, 10H-6, 11H-3, 13X-1, 13X-2, 13X-6, 14X-1, 14X-2, 14X-3, 16X-1, 16X-2, 16X-5, 28X-1, 30X-1 through 30X-5, 31X-6, 32X-3, 32X-5, 34X-2
	162-987E-
NRM	2R-2, 2R-3, 3R-2, 3R-3, 5R-1, 5R-2, 5R-3, 5R-6, 6R-1 through 6R-5, 9R-5, 10R-1, 10R-4, 10R-5, 11R-1 through 12R-5, 13R-1 through 15R-2, 16R-1 through 20R-2, 20R-4 through 23R-5, 27R-1, 27R-2, 27R-3, 38R-4 through 40R-5, 41R-2, 43R-2 through 52R-2
10 mT	25R-2 through 27R-1, 28R-1 through 29R-1, 29R-3 through 30R-1, 31R-2, 32R-1, 32R-2, 32R-3, 33R-1 through 38R-4, 41R-1, 43R-1
15 mT	1R-2, 18R-2, 18R-3, 25R-1, 51R-2, 51R-4, 52R-1, 52R-2
25 mT	1R-1 through 2R-3, 3R-2 through 5R-3, 5R-6, 6R-1 through 25R-5, 26R-2 through 52R-2
30mT	1R-3, 11R-2, 13R-1, 13R-4, 14R-3, 16R-3, 17R-2, 19R-3, 25R-4, 29R-5, 32R-2, 35R-1, 35R-2, 35R-3, 36R-5, 36R-6, 48R-2, 49R-1, 52R-1, 52R-2

top 167 mbsf, and then increase downhole, reaching maximum values of 139 µM at the base of Hole 987D (Table 11; Fig. 19L). This indicates a downhole source of strontium that is perhaps derived from the alteration of volcanic material and/or basement since there is no biogenic carbonate available for recrystallization (although inorganic carbonate layers in the sediments at this site may have recrystallized from biogenic carbonates).

PHYSICAL PROPERTIES

The main objectives of the physical properties measurements at Site 987 relate to the variability of high-latitude continental margin processes in response to glacial-interglacial variations, and are similar to those for Site 986 (see "Site 986" chapter, this volume). Drilling at the two sites, 986 and 987, provides a good database for comparative studies of margin processes adjacent to two of the main late Cenozoic ice sheets, the Greenland and the Svalbard–Barents Sea ice sheets.

Physical properties measurements at Site 987 included index properties, bulk density as measured by the GRAPE, *P*-wave velocity using the PWL and on split cores, undrained shear strength, using both the motorized vane and a fall-cone device, magnetic susceptibility, natural gamma radiation, and thermal conductivity. Downhole temperature measurements were carried out at four depths (32.7, 51.7, 70.7, and 80.2 mbsf) in Hole 987A, using the APC temperature device.

Laboratory methods and procedures are described in the "Explanatory Notes" chapter (this volume). The index properties, compressional velocities, and shear strength data from Site 987 are presented in Tables 12–15, while maximum, minimum, and mean values of the same parameters for each geotechnical unit are presented in Table 16. Thermal conductivities are reported in Table 17.

Results

In establishing a geotechnical stratigraphy for Site 987, we have used laboratory measurements from Holes 987D and 987E. As at Site 986, the presence of gas in the sediments below approximately 30 mbsf (see "Organic Geochemistry" section, this chapter) made velocity measurements problematic. Because several cores had to be drained by drilling holes through the liner at ~10-cm intervals, the liner was no longer in fluid contact with the sediment. With the additional problems caused by disturbance of XCB and RCB cores, *P*-wave velocities could not be measured with the PWL sensor on the MST below 38 mbsf. Furthermore, velocity measurements on split-core sections and discrete samples also failed to a large extent between 70 and 300 mbsf (Table 13; Fig. 20) because of high signal attenuation in the samples. As at Site 986, the most likely explanation for this is the presence of pore voids which are not water-saturated, and possible microcracks caused by gas expansion. For the same reasons, the velocity measurements done in the upper 30 mbsf are most likely too low, and have, as a consequence, been corrected by +3% when used for time-depth conversion in the seismic sections. This correction makes the velocities match those measured downhole during wireline logging (see "Wireline Logging" section, this chapter). Within the above limitations, we have defined four geotechnical units, G1 to G4, at Site 987 (Fig. 20), based on downhole trends in physical properties.

Geotechnical Unit G1 (0–304 mbsf)

Most physical properties of this unit generally show normal increasing or decreasing trends with depth, in response to increased overburden. Based on the change in slope of the index properties, the unit has been divided in two subunits at 30 mbsf (Fig. 20). A slightly lower grain density in geotechnical Subunit G1A than in G1B (Table 16) indicates a possible change in mineralogy across the boundary. Constant laboratory-measured *P*-wave velocities between 1500 and 1550 m/s throughout Unit G1 are most likely a result of gas expansion and escape. Undrained shear strength shows a steady increase with depth and follows a normal trend for terrigenous sediments (Tables 14, 15; Fig. 20). Below approximately 250 mbsf, the sediment became too brittle for accurate shear strength measurements to be made.

Geotechnical Unit G1 corresponds to lithostratigraphic Unit I, a silty clay with frequent thin turbidites (see "Lithostratigraphy" section, this chapter). It also corresponds to seismic Units EG-I and EG-II. The reflector separating these seismic units forms a distinct unconformity further upslope, to the west of Site 987, but appears conformable at the site. The physical properties do not show any sign of an erosional hiatus at this horizon.

Geotechnical Unit G2 (304–370 mbsf)

This unit is characterized by a distinct increase in bulk density, grain density, compressional velocity, and magnetic susceptibility, and a corresponding decrease in porosity, as well as in natural gamma-ray counts (see "Lithostratigraphy" section, this chapter; Table 16; Fig. 20). Grain densities increase from an average of 2.65 g/cm^3 to an average of 2.72 g/cm^3. This unit corresponds to lithostratigraphic Unit II and the upper part of seismic Unit EG-III, and represents a silty clay with sand and gravel, most likely a series of debris flows.

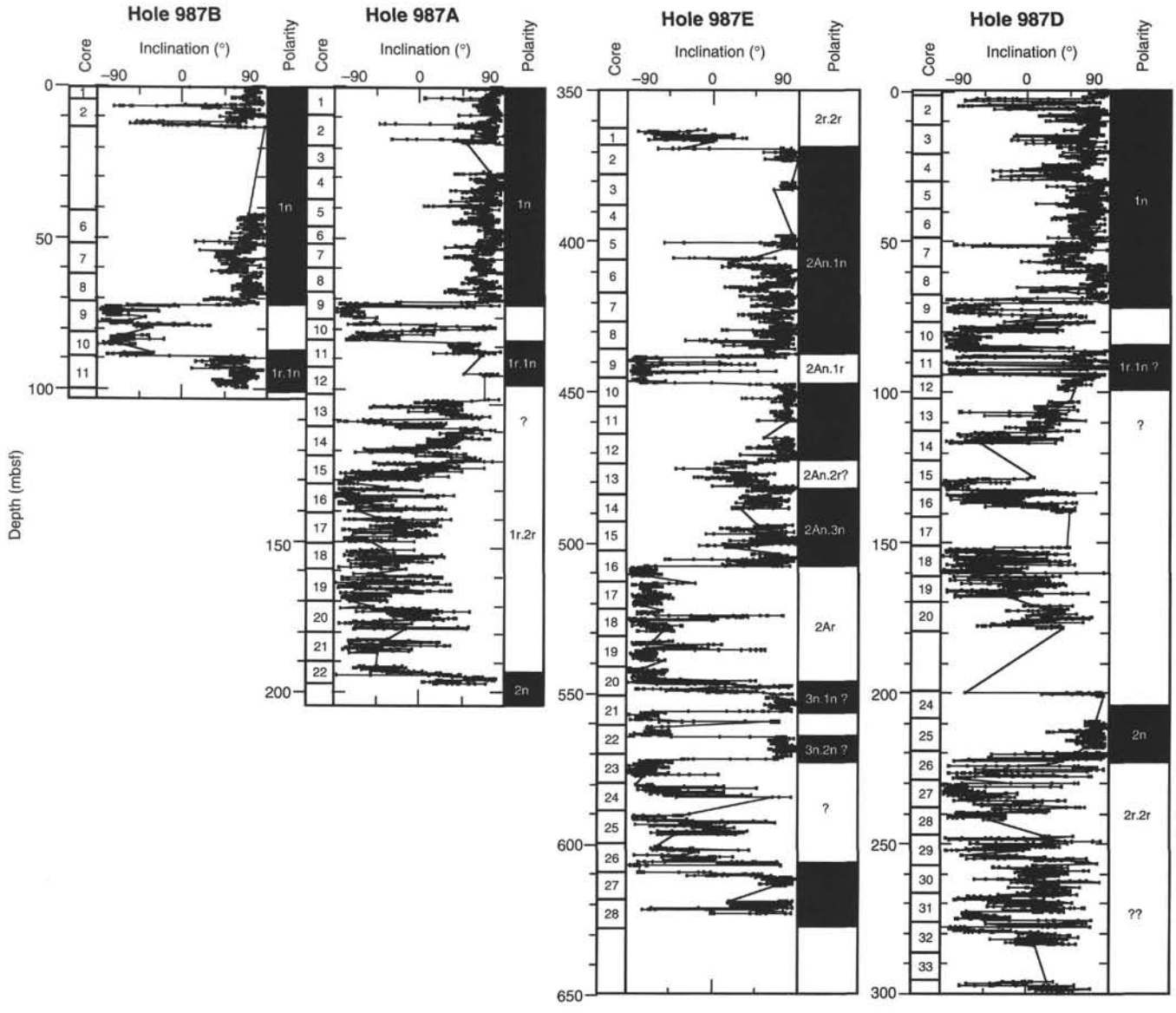

Figure 12. Inclination of the magnetization vector vs. depth (mbsf) for Holes 987A, 987B, 987D, and 987E after demagnetization at peak alternating fields of 25 mT.

Geotechnical Unit G3 (370–580 mbsf)

Again, normal, depth-related trends of index properties and *P*-wave velocities are the main characteristics of geotechnical Unit G3. The index properties follow approximately the same slope as that of Unit GIB (Fig. 20), only interrupted by the anomalous values of the interpreted debris flows of Unit G2. This indicates similar sediments in geotechnical Subunit G1B and Unit G3, which is confirmed by lithostratigraphy. Unit G3 corresponds to lithostratigraphic Unit III (divided in Subunits IIIA and IIIB), and to seismic stratigraphic Units EG-III and EG-IV. The change from lithostratigraphic Subunit IIIA to IIIB, which marks a slight increase in the amount of interbedded sand layers and corresponds to seismic Reflector R3, shows no apparent response in the physical properties (Fig. 20).

Geotechnical Unit G4 (580–650 mbsf)

Similar to geotechnical Unit G2, this unit shows an increase in bulk density, compressional velocity, magnetic susceptibility, and grain density, and a corresponding decrease in porosity and natural gamma radiation values (see "Lithostratigraphy" section, this chapter). Because the changes occur at a greater depth, the relative changes are smaller than in Unit G2 due to the effect of greater compaction. Geotechnical Unit G4 corresponds to lithostratigraphic Unit IV and to the upper part of seismic Subunit EG-VA, both having the same characteristics as Unit G2; silty clay with sand and gravel, and high-amplitude seismic reflectors above a more transparent interval. This suggests that the physical properties of geotechnical Unit G4 reflect debris-flow deposits.

Geotechnical Unit G5 (650–859 mbsf, total depth)

Bulk density, porosity, and compressional velocity show somewhat anomalous trends with depth in this unit, with slightly increasing values of porosity and decreasing velocity and bulk density (Fig. 20). As both magnetic susceptibility values and natural gamma-ray counts show constant values, the trends most likely reflect predominantly more fine-grained sediments and the increased effect of ce-

Table 7. Polarity chron interpretation of magnetostratigraphy from Site 987.

Core, section, interval (cm)	Depth (mbsf)	Interpreted boundary	Age (Ma)	Comments
162-987A-				
9H-3, 130	72.00	Brunhes/Matuyama	0.78	
10H-2, 40	78.00	Jaramillo (top)	0.99	Poorly defined
22X-4, 110	194.00	Olduvai (top)	1.77	
162-987B-				
9H-2, 0	72.20	Brunhes/Matuyama	0.78	Section break
10H-7, 100	89.10	Jaramillo (top)	0.99	
162-987D-				
4H-2, 10	70.60	Brunhes/Matuyama	0.78	
26X	219–228	Olduvai (bottom)	1.95	Poorly defined
162-987E-				
2R-1, 25	369.45	Matuyama/Gauss	2.58	
9R-2, 60	438.50	Kaena (top)	3.04	
10R-1, 130	447.40	Kaena (bottom)	3.11	
16R-3, 120	508.00	Gauss/Gilbert	3.58	
20R-5, 35	548.55	Cochiti (top) ?	4.18	Chron uncertain
21R-4, 10	556.40	Cochiti (bottom) ?	4.29	Chron uncertain
22R-3, 15	564.55	Nunivak (top) ?	4.48	Chron uncertain
23R-1, 125	572.25	Nunivak (bottom) ?	4.62	Chron uncertain

Note: The interpretation of the magnetostratigraphy below the Gauss/Gilbert boundary is uncertain and must await shore-based work.

mentation. The latter is also seen as an increased frequency of well-cemented beds of nonbiogenic carbonate (see "Lithostratigraphy" section, this chapter).

Discussion

The physical properties of the cored sediments at Site 987 reflect variations between hemipelagic deposition of silty clays and downslope, gravity-driven processes forming dense, coarse-grained deposits. The latter is, by volume, less important. The variations caused by the probable debris-flow deposits are superimposed on a normal compactional trend with increasing effective overburden. The lowermost part of the hole, below 650 mbsf, forms an exception, which may be due to an increased amount of clay-sized grains and cementation. As Site 987 is located on a glaciated continental margin, the observed variations are most likely a response to changing glacial style between different periods through the Pliocene and Pleistocene. The units with increased sand and gravel contents, which we interpret to represent debris-flow deposits, may form when grounded glaciers reach the shelf break. Changes in grain density may indicate a change in sediment source area during such periods.

Compared to Site 986, on the Svalbard continental margin, the component of debris-flow deposits relative to the total cored sedimentary section appears much less at Site 987. This is supported by both lithological data and seismic stratigraphy (see "Lithostratigraphy" and "Seismic Stratigraphy" sections, this chapter) and may reflect important differences in the style of glaciation between the two areas. However, the seismic character shows lateral changes, with more high-amplitude stratification, as well as pinch-out of wedge-shaped units farther upslope of Site 987 (see "Seismic Stratigraphy" section, this chapter). Thus, the differences seen between the deposits at Sites 986 and 987 may also reflect the slightly more distal position of Site 987, relative to the base of the slope, and possibly also the difference in slope gradient between the two margins.

Heat Flow

The main objective of the downhole temperature measurements at this site was to add to the very sparse heat-flow database for this part of the Norwegian-Greenland Sea. A total of 76 measurements of thermal conductivity were carried out in the upper cores of Holes 987A, 987B, and 987D, to a maximum depth of 109 mbsf (Table 17).

The temperature measurements were of good quality, with a very low noise level, and yielded a thermal gradient of 96.5°C/km (Figs. 21, 22). Extrapolation of the downhole temperatures gives a bottom water temperature of –0.99°C, which is in good correspondence with physical oceanographic data (CTD-casts) from this region (S. Østerhuis, pers. comm., 1996). Using an average measured thermal conductivity of 1.278 W/(m·K) provides a heat-flow estimate of 123.3 mW/m^2 at Site 987. Compared to Site 986, at the Svalbard Margin, the slightly lower heat-flow value measured at Site 987 is consistent with an older crust at the latter site. The bottom of Hole 987E, which terminated within a few meters of basement (see "Seismic Stratigraphy" section, this chapter), has an age estimate of 6–7 Ma (see "Paleomagnetism" section, this chapter).

WIRELINE LOGGING

Operations

At Site 987, Hole 987E was logged with three tool strings, the Quad combination (Quad combo), Formation MicroScanner (FMS), and the Geological High-resolution Magnetometer tool (GHMT) (Table 18). Hole 987E was completed at ~860 mbsf (2542 mbrf) and the hole was conditioned by a "wiper trip" to remove drilling debris prior to logging. The wiper trip for Hole 987E was very difficult and took almost 17 hours to complete. Due to expected difficult logging conditions, it was decided that logging would be done in two sections. For the lower section, the pipe was placed at ~425 mbsf. Unfortunately, the Quad tool string could not be advanced farther than 490 mbsf. After two attempts at moving the pipe past bridges, logging efforts in the lower section (440–860 mbsf) were terminated. The pipe was then pulled to a depth of 77 mbsf and logging continued in the upper portion (77–495 mbsf) of the borehole. All three tool strings were run successfully over this upper section. Following the last logging run with the FMS tool, a series of wireline heave compensation tests was carried out for LDEO-BRG. See "Explanatory Notes" chapter (this volume) and Borehole Research Group (1994) for a complete description of all tool strings and associated acronyms.

Hole conditions during logging of upper section were quite variable. Caliper data from both the Quad combo and FMS tool strings in Hole 987E indicated that hole diameter varied between 20 and 35 cm over some sections, especially the ~60-m interval of the hole containing a thick debris-flow unit (300–369 mbsf). The natural gamma-ray tool (NGT) was used to determine the mudline in Hole 987E through the drill pipe during the last run of the Quad tool string. The mudline was measured at ~1682.4 mbrf by running the NGT very slowly near estimated driller's depth and recording where a spike occurred when seawater was encountered. This mudline value was used to depth-shift all raw data from the three tool strings to mbsf from mbrf. There was no difference between the driller's estimated depth and the mudline measurement from logging. Table 18 provides a complete summary of logging operations conducted at this site.

Core-to-Log Data Comparisons

Magnetic Susceptibility

The magnetic susceptibility log data obtained by the GHMT at this site correlate well with the magnetic susceptibility measured on the cores (Fig. 23). The log data provide a much more continuous record and a stronger signal than the core measurements. Comparison of the two data sets suggests that the log susceptibility measurements provide a much more consistent record over the upper section of Hole 987E and should be used in place of core data.

Susceptibility measurements range between 30 and 1600 SI units with no obvious cyclicity. The overall pattern is fairly random with abrupt changes in values that may correspond to depositional processes and/or sediment type (i.e., debris flow, turbidite, or hemipe-

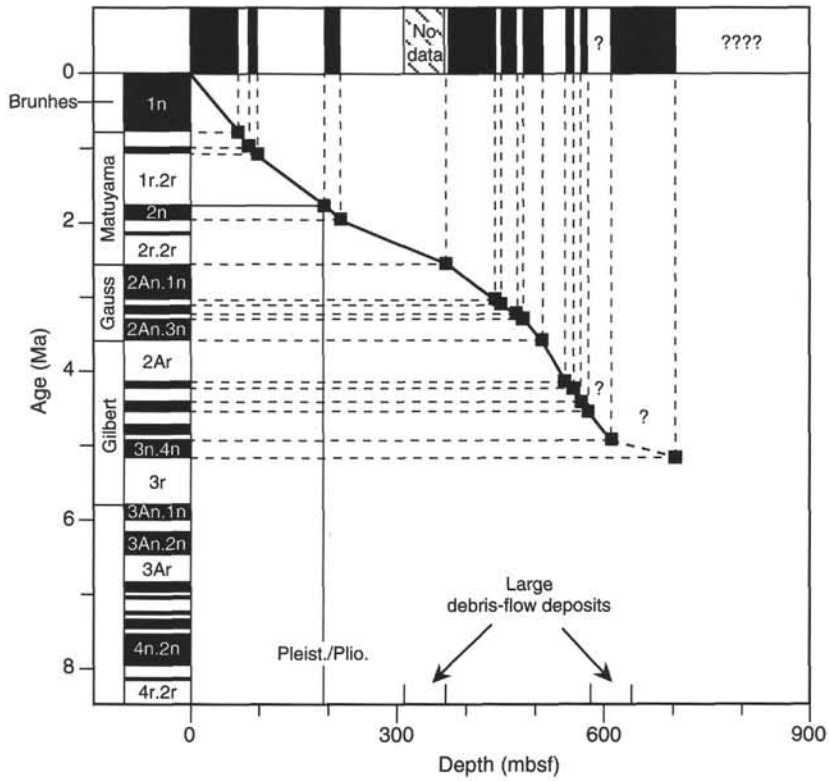

Figure 13. Correlation of Site 987 magnetostratigraphy to the geomagnetic polarity time scale of Cande and Kent (1995).

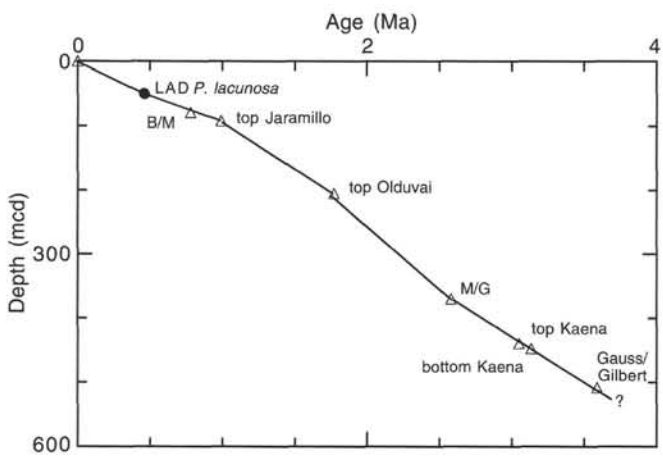

Figure 14. Site 987 age vs. depth (mcd) curve based on biostratigraphic and magnetostratigraphic datums. Solid circle = nannofossil datum; open triangles = magnetostratigraphic datums. M/G = Matuyama/Gauss.

lagic sediment). The sections of core corresponding to inferred debris-flow layers, 205–210 and 300–369 mbsf, typically show high magnetic susceptibility, in contrast to debris flows at Site 986. Like Site 986, however, the magnetic susceptibility readings are uniform across the layers, making it easy to establish the upper and lower boundaries of flows. The main reason for this is not clear but is probably related to composition of debris.

Velocity

Sonic log data were collected in Hole 987E by the Long-Spaced Sonic (LSS) tool, which was run as part of the standard Quad tool string. In Hole 987E, sonic log data were collected between 79 and 464 mbsf. Compressional-wave transit-time measurements were recorded for source-receiver spacings of 8, 10, and 12 ft (2.438, 3.048, and 3.658 m). Measurements at 10-ft spacing were recorded by two separate source-receiver pairs, resulting in a total of four different transit-time measurements at each depth.

Noise spikes were edited out of the data from the 8-ft and 10-ft source-receiver spacings and a depth-derived, borehole-compensated sonic log (DTLN) was recalculated from these data. Figure 24A shows a comparison of the recalculated log with the original DTLN transit times computed during logging.

The recalculated log shows that a steady decrease in interval transit time (increase in velocity) is interrupted by two layers with sharp boundaries and anomalous high velocities. These layers occur in the intervals 205–210 mbsf and 300–369 mbsf. The downhole velocities are shown in Figure 24B, together with laboratory measurements from the same holes and an empirical velocity-vs.-depth function for deep-sea turbidite successions. Velocities on the recalculated sonic log are close to those on the empirical function for turbidites of Hamilton (1979), except in the anomalous high-velocity layers. Other log data show that the thick, high-velocity layer between 300 and 369 mbsf is also characterized by high density, high resistivity, and high magnetic susceptibility, and it is thought to be a large debris flow or stack of debris flows (see "Lithostratigraphy" section, this chapter). Above 300 mbsf the log velocities are considerably higher than those recorded by the sparse laboratory measurements made between 85 and 300 mbsf. Laboratory measurements were not possible through most of this interval because of very high acoustic signal attenuation in the core samples thought to be a result of gas expansion during recovery (see "Physical Properties" section, this chapter). Within the high-velocity layer between 300 and 369 mbsf, the log velocities are consistently lower than the laboratory measurements, while below 369 mbsf the log velocities and laboratory measurements are similar. The observation that the log velocities are actually

Table 8. Age control points, Site 987.

Event	Age (Ma)	987A (mbsf)	987A (mcd)	987B (mbsf)	987B (mcd)	987D (mbsf)	987D (mcd)	987E (mbsf)	987E (mcd)	Avg. depth (mbsf)	Avg. depth (mcd)	Rate (mbsf/m.y.)	Rate (mcd/m.y.)
Top of section	0.00	0.00	0.00	0.00	0.00	0.00	0.00			0.00	0.00		
												98.39	108.15
LO *P. lacunosa* (N)	0.46	45.26	49.75							45.26	49.75		
												82.31	91.91
Brunhes/Matuyama	0.78	72.00	79.06	72.20	79.17	70.60	79.25			71.60	79.16		
												56.90	60.69
Jaramillo (top)	0.99	78.00	85.79	89.10	98.02					83.55	91.91		
												141.60	144.80
Olduvai (top)	1.77	194.00	204.85							194.00	204.85		
												216.60	203.21
Matuyama/Gauss	2.58							369.45	369.45	369.45	369.45		
												146.91	146.91
Kaena (top)	3.05							438.50	438.50	438.50	438.50		
												111.25	111.25
Kaena (base)	3.13							447.40	447.40	447.40	447.40		
												131.74	131.74
Gauss/Gilbert	3.59							508.00	508.00	508.00	508.00		

Notes: Ages are from Berggren et al. (1995). N = calcareous nannofossil.

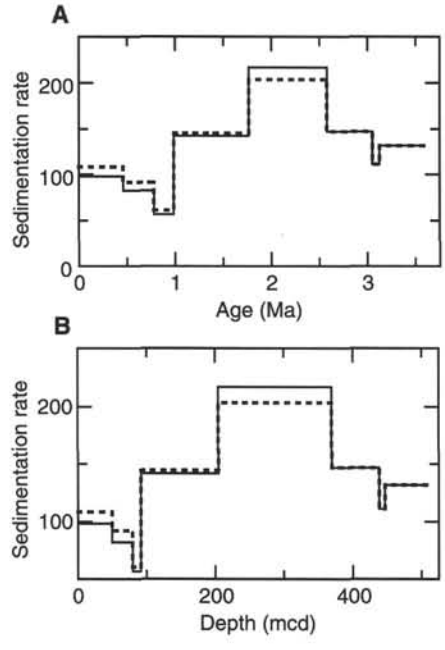

Figure 15. Site 987 sedimentation rates vs. age (**A**) and vs. composite depth (**B**). Solid lines indicate rates in mbsf/m.y.; dashed lines indicate rates in mcd/m.y.

lower than the laboratory measurements within the high-velocity layer may indicate that fractures or other discontinuities reduce the average velocity of the layer to less than the velocities measured on core samples.

Density

Bulk density data in Hole 987E were collected by the Hostile-environment Litho-Density Tool (HLDT), which was run as part of the standard Quad tool string. In addition to making the standard bulk density (RHOB) and photoelectric effect measurements (PEF) every 15 cm, the tool was run in high-resolution mode, producing additional bulk density (HRHO) and photoelectric effect (HPEF) data at 2.5-cm spacing. In Hole 987E, density log data were collected between 78 and 478 mbsf. The reliability of the density log data is reduced in the uppermost 7 m because the caliper was closed before pulling the tool into the drill pipe.

In Hole 987E, the caliper (Fig. 24C) showed that hole diameter was irregular and many intervals were washed out. In many of the washed-out intervals, anomalous low-density readings were obtained, indicating that the density tool was probably not in consistent contact with the borehole wall. The wireline log bulk density data are shown with GRAPE data and laboratory wet bulk density measurements on discrete samples in Figure 24C. Laboratory wet bulk density measurements are all close to the higher end of the range of values on the density log, which supports the view that the lower values on the log are suspect. The high-velocity layer between 300 and 369 mbsf, interpreted as a debris flow or flows (see above, and "Lithostratigraphy" section, this chapter), is also prominent on the density log as a high-density layer. The borehole diameter is almost constant across this layer, hardly any larger than the diameter of the drill bit, so the log density measurements are considered to be reliable.

FMS Imaging

FMS imaging in the upper portion of Holes 987E revealed a fairly homogenous, moderately well-layered hemipelagic sediment sequence with one very large debris flow at 300 to 369 mbsf (lithostratigraphic Unit II) and small turbidite layers between 77 and 500 mbsf. The entire logged interval corresponds roughly to lithostratigraphic Units I, II, and a portion of Unit III. This thick debris-flow unit corresponds to seismic Reflector R2 (see "Lithostratigraphy" and "Seismic Stratigraphy" sections, this chapter), and stands out dramatically on almost all the wireline log responses. It corresponds to a small borehole diameter and areas of very good FMS images. In addition, the natural gamma-ray and especially the resistivity log data depict these layers very clearly (Fig. 25A, -B). The deep resistivity log responds primarily to the water content of the sediments, with higher resistivity corresponding to lower water content. The high resistivity, coarse, poorly sorted sediments, low water content, and little internal structure are all consistent with a debris-flow interpretation. The natural gamma-ray log response is relatively constant across the debris flow, showing significantly less variablity than in the intervals above and below.

Downhole Temperature Measurements

Borehole fluid temperature measurements were recorded in Hole 987E using the Lamont temperature logging Tool (TLT). The TLT was run at the base of the Quad tool string, which was the first logging run, and both downhole and uphole profiles were acquired. The

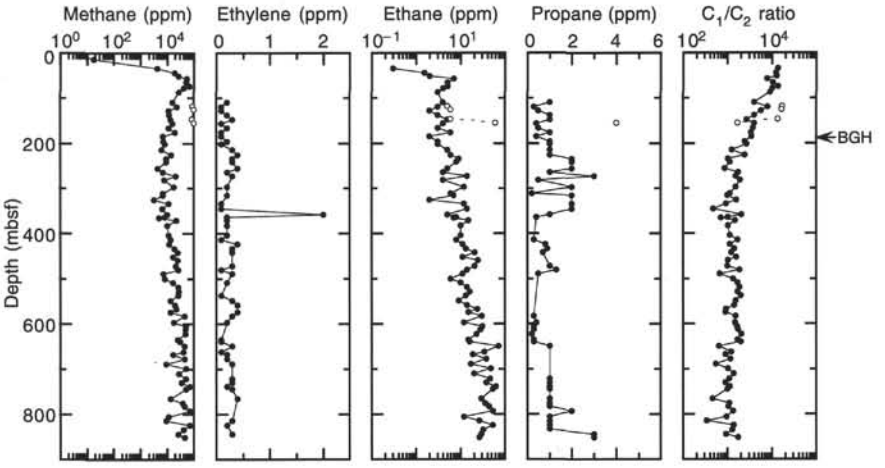

Figure 16. Profiles of headspace and vacutainer methane, ethylene, ethane, and propane concentrations and methane/ethane (C_1/C_2) ratio at Site 987. Solid symbols = headspace data; open symbols = vacutainer data. "BGH" indicates the calculated base of stable gas hydrate at Site 987, which is estimated based on the pressure-temperature stability field of gas hydrates (cf. Kvenvolden and Barnard, 1983).

maximum recorded temperature at 490 mbsf in Hole 987E was 18°C. The unusually low temperatures are probably due to circulation of cold seawater used to clean drilling debris from the hole prior to logging.

SEISMIC STRATIGRAPHY

The drilling proposal for EGM-4 (Site 987) was based on a multichannel seismic line (GGU82-12) acquired in 1982 by the Geological Survey of Greenland (GGU). This is an east-west-trending dip line across the flank of the Scoresbysund Fan. The proposed site was located near the base of slope, 16 km from the eastern end of the line. The site survey was designed to duplicate Line GGU82-12, which was acquired without GPS navigation, and then do a crossing line over the site. However, because the site was close to the ice edge, the survey was started farther west, at approximately 16°18′E, and ran westward along the extension of Line GGU82-12, at 70°30′N, with an option to define a site to the east of the proposed site EGM-4. Because of the ice situation at EGM-4, in addition to severe icing and subsequent failure of the water guns, a new position was chosen, approximately 13 km east of EGM-4 (Fig. 26). Site 987 is located at shotpoint 2928 on Line 987-S1 (Fig. 27), which is approximately equivalent to shotpoint 2530 of Line GGU82-12 (Fig. 28).

A single 80-in.^{3} water gun was used as a source, and both the 3.5-kHz and 12-kHz PDR systems were run during the survey (see "Explanatory Notes" chapter, this volume). Although the total survey length was nearly 40 nmi, there are large data gaps due to gun failure (Fig. 27). Three different guns were used, and this caused an unfortunate difference in source signature over the length of the survey. This is well exemplified by the different character of the seafloor reflector between the two portions of the line shown in Figure 27. The most likely reason for this is different towing depths for the individual guns. A consequence of the water-gun problems was that no crossing line was run over the site.

Hole 987E was logged down to 480 mbsf (see "Wireline Logging" section, this chapter) and compressional velocities taken from the laboratory measurements and used in the time-depth conversions are checked against the velocities from the downhole measurements. The laboratory velocity values shallower than 300 mbsf are increased by approximately 3% to compensate for the effects of core expansion during recovery (see "Physical Properties" section, this chapter). Seismic unit thicknesses and depth to reflectors in mbsf are shown in Figure 29.

Description of Seismic Stratigraphic Units

Five seismic units were defined, based on the data acquired during the site survey, Line 987-S1, and the pre-cruise Line GGU82-12. The upper unit EG-I (2.375–2.590 seconds two-way traveltime [s TWT] in the seismic section) is characterized by low-amplitude parallel internal reflections, often forming bands of narrow reflectors. While the reflecting bands are continuous over the length of the line, individual reflectors appear discontinuous and may have a slight relief. In the lower resolution Line GGU82-12, the overall character of this unit is transparent, but with discontinuous, hummocky internal structures (Fig. 28). Upslope, however, the seismic character becomes more stratified. Another feature characteristic of this unit is westward thinning. It has its maximum thickness (within the surveyed area) at Site 987 and thins rapidly upslope. The basal reflector of the unit, R1, is a distinct unconformity when followed westward, where it shows both erosional truncation of underlying reflectors, and onlap of internal reflectors within Unit EG-I. A lateral change in the character of Reflector R1 is also indicated by the present site survey line (Fig. 27). With an interval velocity of 1.65 km/s, the thickness of seismic Unit EG-I is 177 m.

With the exception of at least one strong reflector in the upper part which interferes with the response of Reflector R1, the seismic character of seismic Unit EG-II (2.590–2.735 s TWT) is not significantly different from that of the upper unit. Below the strong reflector(s), there are similar low-amplitude, slightly undulating reflectors. Internal reflectors downlap on the base of the unit, Reflector R2, but the latter reflector does not appear to truncate underlying reflectors. Using an interval velocity of 1.75 km/s, the thickness of seismic Unit EG-II is 127 m.

Seismic Unit EG-III (2.735–2.895 s TWT) is characterized by high-amplitude, conformable reflectors at and west of Site 987. Eastward from the site, the unit thins and the deeper internal reflectors, in particular, appear weaker. However, since there were problems with the water guns along this line, and guns had to be changed frequently, an effect of different source signatures cannot be excluded. Farther westward, along Line GGU82-12, Unit EG-III exhibits the greatest thickening of all drilled seismic units, becoming 0.7 s thick beneath the shelf break. The basal reflector of this unit, R3, is a distinct unconformity when followed westward, where it is overlain by downlapping reflectors of Unit EG-III, and shows truncation of underlying reflectors. From both laboratory and wireline measurements of compressional velocity, the upper 50 ms of Unit EG-III has a distinctly higher velocity (2.6 km/s) than the lower 110 ms (1.9 km/s) (Fig. 29).

Table 9. Results of headspace and vacutainer gas analyses of Hole 987A, 987D, and 987E samples.

Core, section, interval (cm)	Depth (mbsf)	C_1 (ppm)	$C_{2=}$ (ppm)	C_2 (ppm)	$C_{3=}$ (ppm)	C_3 (ppm)	C_1/C_2	C_1/C_{2+}
Headspace								
162-987A-								
1H-5, 0–5	6.03	7						
2H-5, 0–5	14.53	18						
4H-5, 0–5	33.53	4,157		0.3			13,410	13,410
5H-7, 0–5	44.33	18,328		1.5			12,219	12,219
6H-4, 0–5	51.03	25,595		2			12,798	12,798
7H-4, 0–5	56.73	54,037		7			7,720	7,720
8H-5, 0–5	65.73	52,248		5			10,450	10,450
9H-5, 0–5	73.73	67,760		5			13,552	13,552
10H-3, 0–5	78.48	40,009		4			10,002	10,002
11X-3, 0–5	86.73	27,612		3			9,204	9,204
13X-5, 0–5	109.03	15,688	0.2	4		1.0	3,922	3,017
14X-5, 0–5	118.73	23,986	0.1	3		0.3	7,995	7,055
15X-5, 0–5	128.23	11,563	0.1	2		0.5	5,782	4,447
16X-5, 0–5	137.83	11,934	0.2	3		1.0	3,978	2,841
17X-5, 0–5	147.43	13,300	0.3	5		1.0	2,660	2,111
18X-5, 0–5	157.03	15,686	0.1	4		0.4	3,922	3,486
19X-5, 0–5	166.73	11,141	0.2	3		0.5	3,714	3,011
20X-5, 0–5	176.33	20,162	0.1	6		1.0	3,360	2,840
21X-4, 0–5	184.43	7,013	0.1	2		0.4	3,507	2,805
22X-6, 0–5	195.95	7,330	0.2	3		1.0	2,443	1,745
162-987D-								
24X-CC, 0–5	201.33	8,065	0.1	3		1.0	2,688	1,967
25X-5, 0–5	215.43	6,157	0.3	5		1.0	1,231	977
26X-6, 0–5	225.69	14,455	0.4	6		1.0	2,409	1,953
27X-5, 0–5	234.63	9,127	0.3	9		2.0	1,014	808
28X-3, 0–5	241.23	9,031	0.3	8		2.0	1,129	877
29X-6, 0–5	255.43	4,386	0.4	5	0.1	2.0	877	585
30X-6, 0–5	265.03	7,050	0.2	4		1.0	1,763	1,356
31X-5, 0–5	273.02	21,087	0.3	14		3.0	1,506	1,219
32X-4, 0–5	281.33	7,595		4		0.5	1,899	1,688
34X-2, 0–5	297.53	18,071	0.2	12		2.0	1,506	1,273
36X-5, 0–5	311.63	6,805		6		0.2	1,134	1,098
37X- CC, 0–5	315.23	6,839	0.2	7		2.0	977	743
38X-1, 0–5	324.83	3,162		2			1,581	1,581
39X-1, 0–5	334.43	11,213	0.1	12		2.0	934	794
40X-2, 0–5	345.53	6,620	0.1	14		2.0	473	411
41X-4, 0–5	358.23	10,446	2.0	5	1.4	1.0	2,089	1,111
42X-1, 0–5	363.33	8,259	0.2	8		0.4	1,032	960
162-987E-								
1R-2, 0–5	364.83	4,975		7			711	711
2R-2, 0–5	370.73	22,135	0.2	15			1,476	1,456
3R-3, 0–5	381.83	10,078	0.2	10			1,008	988
5R-5, 0–5	404.03	11,418	0.2	10			1,142	1,119
6R-5, 0–5	413.63	13,349	0.1	8		0.3	1,669	1,589
7R-5, 0–5	423.23	12,421	0.4	11		0.8	1,129	1,018
8R-5, 0–5	432.83	18,766	0.3	13		0.9	1,444	1,322
9R-5, 0–5	442.43	25,282	0.3	21	0.2	0.7	1,204	1,139
10R-5, 0–5	452.13	17,107		11			1,555	1,555
11R-3, 0–5	458.83	25,282		25			1,011	1,011
12R-5, 0–5	471.43	20,509	0.3	21		1.0	977	920
13R-5, 0–5	481.03	25,773	0.1	14		1.3	1,841	1,674
14R-4, 0–5	489.03	7,272	0.3	11		0.5	661	616
15R-5, 0–5	500.23	8,047		6			1,341	1,341
16R-4, 0–5	508.33	16,929	0.2	10			1,693	1,660
17R-5, 0–5	519.43	25,934		14			1,852	1,852
18R-5, 0–5	529.03	27,117		16			1,695	1,695
19R-4, 0–5	537.13	25,440	0.1	13			1,957	1,942
20R-5, 0–5	548.23	13,713	0.3	9			1,524	1,475
21R-5, 0–5	557.83	19,934	0.4	14			1,424	1,384
22R-5, 0–5	567.43	22,352		24			931	931
23R-3, 0–5	574.03	13,227	0.4	15			882	859
24R-2, 0–5	582.13	45,858	0.3	30	0.2	0.3	1,529	1,489
25R-5, 0–5	596.33	17,816	0.2	12		0.4	1,485	1,414
26R-5, 0–5	605.28	50,217		31		0.3	1,620	1,604
27R-3, 0–5	612.53	49,072		28		0.3	1,753	1,734
28R-3, 0–5	622.07	47,489		23		0.2	2,065	2,047
29R-5, 0–5	634.83	25,107	0.1	15		0.3	1,674	1,630
30R-2, 0–5	639.88	31,346	0.1	16		0.3	1,959	1,911
31R-2, 0–5	649.47	46,612	0.3	72		1.0	647	636
32R-4, 37–42	662.07	41,487	0.1	34			1,220	1,217
33R-2, 0–5	668.73	17,000	0.2	19			895	885
34R-2, 0–5	678.31	44,845	0.2	38			1,180	1,174
35R-3, 0–5	689.30	9,347	0.3	17			550	540
36R-3, 0–5	698.96	49,556		48			1,032	1,032
37R-5, 0–5	710.81	27,301		20			1,365	1,365
38R-5, 0–5	721.19	49,750	0.3	46		1.0	1,082	1,052
39R-5, 0–5	730.93	33,594	0.3	38		1.0	884	855
40R-4, 0–5	739.03	69,996	0.2	62		1.0	1,129	1,108
41R-2, 0–5	745.41	51,541	0.3	52		1.0	991	967
43R-3, 0–5	766.23	13,338	0.4	29		1.0	460	439
44R-3, 0–5	775.83	38,112		35		1.0	1,089	1,059
45R-1, 0–5	782.53	44,841		43		1.0	1,043	1,019
46R-1, 75–80	792.88	70,787		53		2.0	1,336	1,287
47R-4, 0–5	806.33	11,494		12		1.0	958	884
48R-4, 0–5	814.20	8,976	0.3	26		1.0	345	329
49R-3, 0–5	823.93	70,372	0.2	52		1.0	1,353	1,323

Table 9 (continued).

Core, section, interval (cm)	Depth (mbsf)	C_1 (ppm)	$C_{2=}$ (ppm)	C_2 (ppm)	$C_{3=}$ (ppm)	C_3 (ppm)	C_1/C_2	C_1/C_{2+}
50R-3, 0–5	833.73	41,411		32		1.0	1,294	1,255
51R-4, 0–5	844.44	26,476	0.3	29		3.0	913	820
52R-2, 0–5	851.31	45,970		26		3.0	1,768	1,585
Vacutainer 162-987A-								
14X-5, 49–50	118.20	87,025		5			17,405	17,405
15X-3, 131–132	125.52	99,410		6			16,568	16,568
17X-5, 65–66	147.06	82,546		6			13,758	13,758
18X-3, 131–132	154.32	99,410		60		4	1,657	1,553

Notes: C_1 = methane, $C_{2=}$ = ethylene, C_2 = ethane, $C_{3=}$ = propylene, C_3 = propane, C_1/C_2 = methane/ethane ratio, and C_1/C_{2+} = methane/other hydrocarbon gases ratio.

Probably because of seismic interference, however, there is no distinct reflector showing the division. Because of this, and the distinct lateral changes observed in Unit EG-III, the upper high-velocity interval has not been defined as a separate subunit. Using an average interval velocity of 2.15 km/s, the thickness of this unit is 172 m.

Seismic Unit EG-IV (2.895–3.015 s TWT) displays distinct internal reflectors in the western part of Line 987-S1. East of Site 987, however, the internal reflectors become weak and discontinuous. As seen from the regional Line GGU82-12, this unit, as well as the one below, shows less increase in thickness toward the west compared to the units above. At the site, Unit EG-IV has a thickness of 0.120 s, which equals 120 m using an interval velocity of 2.0 km/s. The basal reflector of the unit, Reflector R4, is a prominent seismic reflector that marks a difference in seismic character above and below, as well as truncating underlying reflectors.

The lowermost seismic unit above acoustic basement at Site 987, Unit EG-V (3.015–3.235 s TWT), has been divided in two subunits, EG-VA and EG-VB, bounded by Reflector R5 (Figs. 27, 29). Subunit EG-VA is characterized by strong but discontinuous reflections. Reflector R5 does not form a distinct, continuous reflector at Site 987, but is defined as the base of Subunit EG-VA. Farther west, however, Reflector R5 is a prominent reflector as well as an unconformity. Below Reflector R5, at approximately 3.130 s TWT, the seismic character changes to the structureless and transparent character of Subunit EG-VB, which continues to the basement reflector at 3.235 s. The compressional velocity of the upper 45 ms of Subunit EG-VA is 2.6 km/s, while the average velocity for the rest of seismic Unit EG-V is 2.4 km/s. This gives a total thickness of 264 m (see the following discussion of basement depth).

Discussion

The main seismic stratigraphic boundaries at Site 987 show, with some exceptions, a good correspondence with both lithostratigraphy and geotechnical stratigraphy (see "Lithostratigraphy" and "Physical Properties" sections, this chapter).

Seismic Units EG-I and EG-II correspond to lithostratigraphic Unit I and geotechnical Unit G1. Reflector R1, however, does not appear to be associated with any change in lithology or physical properties. This may explain the lateral, east-west changes observed in the character of both Unit EG-I and Reflector R1, and could indicate that the changes are caused by varying amounts of downslope, gravity-driven sediment transport in the form of turbidites and debris flows. Lithostratigraphic Unit I consists of hemipelagic silty clay with frequent but relatively thin sand layers interpreted as turbidites. Hence, from the seismic character, an upslope increase in both frequency and thickness of turbidites, possibly also grading into debris flows, would be expected.

Reflector R2 corresponds to the upper boundary of lithostratigraphic Unit II, a silty clay with sand and gravel, and geotechnical Unit G2, which are 60 m thick and characterized by high velocities and densities (see "Lithostratigraphy" and "Physical Properties" sections, this chapter). The character of this upper part of seismic Unit EG-III, as well as the physical properties and the lithological character of the sediments, point at debris flows as the likely depositional mechanism. Further support for this is found in comparison with results of the drilling at Site 986 on the Svalbard Margin (see "Site 986" chapter, this volume). The lower part of seismic Unit EG-III shows low-amplitude reflectors corresponding to lithostratigraphic Subunit IIIA and the upper part of geotechnical Unit G3, which are silty clays with normal depth-related trends in physical properties.

Reflector R3 was a main target for the proposed drilling at EGM-4. This reflector shows the same lateral change in character as that observed for Reflector R1, being more distinct to the west of the site and farther upslope (Figs. 27, 28). The transition between seismic Units EG-III and EG-IV, across Reflector R3, does not involve a change in the physical properties but, lithostratigraphically, Reflector R3 corresponds to the boundary between Subunits IIIA and IIIB marked by an increase of interbedded sandy layers. Therefore, Reflector R3 most likely marks the end of a period of increased downslope sediment transport in the form of turbidites and/or debris flows, which had stronger influence on the sediments farther upslope than at Site 987.

Reflector R4 forms the most prominent seismic reflector at Site 987, and it corresponds approximately to the boundary between lithostratigraphic Subunits IIIB and IV and geotechnical Units G3 and G4. As for Reflector R2, Reflector R4 defines the top of an approximately 70-m-thick sandy, gravelly silty clay with distinctly raised densities and seismic velocities. This unit (lithostratigraphic Unit IV) is interpreted to represent debris flows and this interval corresponds to the upper part of the reflective upper half of seismic Unit EG-V. Although the debris-flow unit is the main cause for Reflector R4, the seismic character of seismic Subunit EG-VA continues below the interpreted debris-flow deposit. Laboratory measurements of *P*-wave velocity (see "Physical Properties" section, this chapter) show a larger variation in values above 710 mbsf than below. This may explain the seismic character of Subunit EG-VA, and also indicate a transitional period with increased downslope transport before onset of the main debris-flow activity of lithostratigraphic Unit IV. Seismic Subunit EG-VB represents relatively homogeneous silty clays giving rise to the seismically structureless character of this subunit.

Using *P*-wave velocities measured in the laboratory for seismic Unit EG-V (see "Physical Properties" section, this chapter), acoustic basement is shallower than the bottom of Hole 987E. Therefore, higher velocities than actually measured are used in the time-depth conversion of the lower part of Subunits EG-VA and EG-VB, to result in a basement depth below 860 mbsf. By comparison of velocities measured in the laboratory with those measured downhole, in indurated sediments at this site, as well as in other sites during Leg 162, it is unlikely that the laboratory measured velocities deviate more than 0.1–0.2 km/s from the true velocities. An explanation for not having reached basement in Hole 987E is, therefore, a basement relief that is not detected by the seismic data of Line 987-S1 (Fig. 27), in addition to a possible slight offset of the hole relative to the seismic

Table 10. Summary of organic geochemical analyses of Hole 987D and 987E samples.

Core, section, interval (cm)	Depth (mbsf)	IC (%)	$CaCO_3$ (%)	TC (%)	TOC (%)	TN (%)	TS (%)	C/N	C/S
162-987D-									
1H-1, 62–63	0.62	0.18	1.5	0.65	0.47	0.09	0.00	5.1	
2H-1, 36–37	1.66	0.92	7.7	1.16	0.24	0.07	0.00	3.3	
2H-6, 110–112	9.90	0.33	2.7	0.66	0.33	0.08	0.00	4.3	
3H-1, 52–53	11.32	0.25	2.1	0.51	0.26	0.09	0.00	3.0	
3H-5, 32–33	17.12	0.32	2.7	0.95	0.63	0.09	0.05	6.9	11.7
4H-4, 61–62	25.41	0.54	4.5	1.29	0.75	0.07	0.11	10.2	6.6
5H-2, 34–35	31.64	0.80	6.7	1.33	0.53	0.08	0.69	6.7	0.8
5H-5, 110–111	36.90	0.61	5.1	1.63	1.02	0.08	0.08	12.1	13.2
6H-1, 36–37	39.66	0.18	1.5	0.60	0.42	0.11	0.00	3.7	
6H-6, 43–44	47.23	1.35	11.2	1.87	0.52	0.08	0.00	6.5	
7H-1, 48–49	49.28	0.23	1.9	0.59	0.36	0.08	0.00	4.5	
7H-7, 31–32	58.11	0.43	3.6	0.71	0.28	0.07	0.00	3.8	
8H-2, 119–120	60.99	1.03	8.6	1.39	0.36	0.07	0.00	5.4	
8H-5, 110–111	65.40	1.09	9.1	1.45	0.36	0.07	0.11	5.3	3.3
9H-4, 124–125	73.54	0.29	2.4	0.81	0.52	0.09	0.04	5.6	13.6
9H-5, 91–92	74.71	0.60	5.0	0.95	0.35	0.08	0.00	4.2	
10H-1, 140–141	78.00	0.98	8.2	1.37	0.39	0.08	0.00	4.9	
10H-3, 28–29	79.88	0.92	7.7	1.27	0.35	0.08	0.00	4.5	
10H-5, 36–37	82.96	0.15	1.2	0.74	0.59	0.11	0.00	5.1	
11H-3, 48–49	88.46	1.34	11.2	1.79	0.45	0.07	0.00	6.1	
11H-6, 94–95	93.42	0.21	1.7	0.61	0.40	0.10	0.00	4.2	
12X-2, 49–50	96.79	0.40	3.3	0.73	0.33	0.10	0.00	3.4	
12X-3, 49–50	98.29	0.04	0.3	0.59	0.55	0.12	0.36	4.6	1.5
13X-1, 80–81	104.20	0.15	1.2	0.76	0.61	0.11	0.00	5.3	
13X-5, 80–81	110.20	0.09	0.7	0.67	0.58	0.12	0.07	4.9	8.3
14X-1, 89–90	113.89	0.30	2.5	0.84	0.54	0.07	0.10	7.5	5.2
14X-3, 80–81	116.53	1.28	10.7	1.49	0.21	0.07	0.00	3.1	
15X-4, 138–139	128.48	0.14	1.2	0.70	0.56	0.10	0.00	5.8	
15X-5, 91–92	129.51	0.59	4.9	0.98	0.39	0.09	0.09	4.3	4.2
15X-6, 94–95	131.04	0.17	1.4	0.96	0.79	0.11	0.14	7.3	5.5
16X-1, 60–61	132.90	0.26	2.2	0.75	0.49	0.11	0.08	4.5	6.2
16X-5, 60–61	138.90	0.08	0.7	0.94	0.86	0.12	0.00	7.2	
17X-7, 10–11	150.20	0.32	2.7	0.77	0.45	0.09	0.00	5.1	
18X-1, 90–91	152.50	0.07	0.6	0.60	0.53	0.12	0.11	4.6	4.9
18X-5, 119–120	158.79	0.45	3.7	0.90	0.45	0.09	0.00	4.8	
19X-1, 51–52	161.71	0.14	1.2	1.14	1.00	0.13	0.00	7.7	
19X-5, 58–59	167.78	0.07	0.6	0.67	0.60	0.12	0.36	4.8	1.7
20X-1, 51–52	171.41	0.33	2.7	0.99	0.66	0.12	0.00	5.8	
20X-5, 35–36	177.25	0.88	7.3	1.39	0.51	0.08	0.00	6.6	
24X-1, 113–114	200.93	0.10	0.8	0.75	0.65	0.12	0.00	5.4	
25X-1, 47–48	209.87	0.15	1.2	0.74	0.59	0.10	0.00	5.7	
25X-6, 135–136	218.25	0.98	8.2	1.45	0.47	0.10	0.00	4.9	
26X-3, 76–77	221.92	0.47	3.9	1.11	0.64	0.09	0.00	7.1	
26X-4, 135–136	224.01	1.82	15.2	2.67	0.85	0.09	0.00	9.6	
27X-2, 107–108	231.17	0.10	0.8	1.09	0.99	0.11	0.00	9.1	
27X-6, 114–115	237.24	0.16	1.3	1.01	0.85	0.10	0.05	8.6	16.9
28X-1, 29–30	238.49	0.36	3.0	1.11	0.75	0.10	0.00	7.4	
28X-2, 116–117	240.86	0.60	5.0	1.23	0.63	0.08	0.43	7.5	1.5
29X-1, 124–125	249.14	0.07	0.6	0.46	0.39	0.10	0.00	3.8	
29X-4, 46–47	252.86	0.80	6.7	1.05	0.25	0.08	0.00	3.1	
30X-3, 131–132	261.81	0.09	0.7	0.98	0.89	0.13	0.07	6.7	12.4
30X-CC, 55–56	267.05	4.09	34.1	4.43	0.34	0.06	0.00	5.4	
31X-3, 93–94	270.92	0.05	0.4	0.63	0.58	0.10	0.00	5.6	
31X-5, 79–80	273.78	0.42	3.5	1.14	0.72	0.12	0.09	6.0	8.0
31X-5, 147–148	274.46	0.97	8.1	1.90	0.93	0.10	0.00	9.8	
32X-1, 111–112	277.91	3.80	31.7	4.19	0.39	0.07	0.00	5.7	
32X-2, 114–115	279.44	0.25	2.1	0.91	0.66	0.10	0.37	6.8	1.8
32X-4, 48–49	281.78	0.12	1.0	0.86	0.74	0.11	0.00	6.8	
34X-1, 128–129	297.28	1.25	10.4	1.53	0.28	0.06	0.00	4.5	
34X-3, 23–24	299.23	0.09	0.7	0.69	0.60	0.11	0.00	5.3	
36X-2, 51–52	307.61	0.17	1.4	0.52	0.35	0.00	0.00		
36X-5, 51–52	312.11	0.14	1.2	0.53	0.39	0.06	0.09	6.4	4.3
162-987E-									
2R-3, 98–99	367.28	0.04	0.3						
5R-2, 83–84	400.33	3.07	25.6						
5R-5, 113–114	405.13	0.21	1.7						
6R-2, 94–95	410.04	5.06	42.1						
6R-4, 116–117	413.26	0.21	1.7						
7R-1, 99–100	418.19	3.71	30.9						
7R-4, 33–34	422.03	0.10	0.8						
8R-1, 21–22	427.01	2.44	20.3						
8R-2, 134–135	429.64	0.14	1.2						
9R-1, 119–120	437.59	0.12	1.0						
9R-5, 53–54	442.93	0.79	6.6						
10R-2, 77–78	448.37	0.16	1.3						
10R-5, 63–64	452.73	0.10	0.8						
11R-1, 27–28	456.07	0.07	0.6						
11R-3, 90–91	459.70	0.12	1.0						
12R-3, 115–116	469.55	0.12	1.0						
12R-5, 118–119	472.58	0.06	0.5						
13R-2, 103–104	477.53	0.10	0.8						
13R-3, 54–55	478.54	0.11	0.9						
13R-4, 68–69	480.18	0.13	1.1						
14R-2, 67–68	486.77	0.14	1.2						
14R-4, 21–22	489.21	0.06	0.5						
15R-1, 77–78	494.97	0.14	1.2						
15R-5, 73–74	500.93	0.05	0.4						

Table 10 (continued).

Core, section, interval (cm)	Depth (mbsf)	IC (%)	$CaCO_3$ (%)	TC (%)	TOC (%)	TN (%)	TS (%)	C/N	C/S
16R-2, 110–111	506.40	0.06	0.5						
17R-2, 73–74	515.63	1.50	12.5						
17R-4, 71–72	518.61	0.64	5.3						
17R-5, 64–65	520.04	0.16	1.3						
18R-1, 57–58	523.57	0.08	0.7						
18R-3, 44–45	526.44	0.16	1.3						
19R-1, 50–51	533.10	0.05	0.4						
19R-4, 70–71	537.80	0.06	0.5						
20R-1, 50–51	542.70	0.07	0.6						
20R-4, 45–46	547.15	0.05	0.4						
22R-1, 29–30	561.69	0.05	0.4						
22R-6, 87–88	569.77	0.06	0.5						
23R-1, 72–73	571.72	0.05	0.4						
23R-4, 100–101	576.50	0.04	0.3						
24R-1, 131–132	581.91	0.04	0.3						
24R-3, 62–63	584.22	0.12	1.0						
25R-2, 96–97	592.76	0.07	0.6						
25R-4, 70–71	595.50	0.15	1.2						
26R-2, 106–107	602.40	0.09	0.7						
26R-6, 67–68	607.43	0.06	0.5						
27R-1, 81–82	610.31	0.05	0.4						
27R-3, 78–79	613.28	0.10	0.8						
28R-1, 120–121	620.40	0.09	0.7						
28R-3, 116–117	623.36	0.11	0.9						
	Average:	0.52	4.3	1.11	0.54	0.09	0.06	5.8	6.6
	Maximum:	5.06	42.1	4.43	1.02	0.13	0.69	12.1	16.9
	Minimum:	0.04	0.3	0.46	0.21	0.00	0.00	3.0	0.8

Notes: IC = inorganic carbon, $CaCO_3$ = calcium carbonate, TC = total carbon, TOC = total organic carbon, TN = total nitrogen, TS = total sulfur, C/N = total organic carbon/total nitrogen ratios, and C/S = total organic carbon/total sulfur ratio.

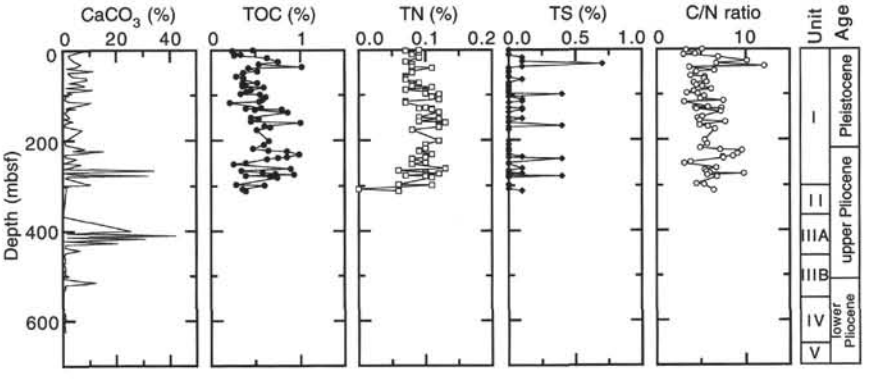

Figure 17. Calcium carbonate ($CaCO_3$), total organic carbon (TOC), total nitrogen (TN), and total sulfur (TS) contents, TOC/TN (C/N) ratio, lithostratigraphic unit, and age at Site 987.

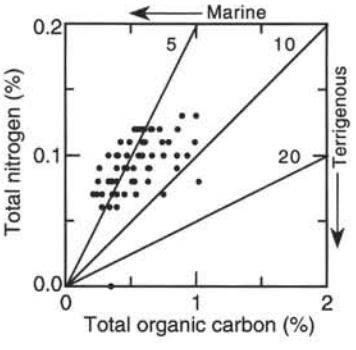

Figure 18. Total organic carbon vs. total nitrogen at Site 987. Lines show C/N ratios of 5, 10, and 20.

line, within the range of the dynamic positioning system and the GPS accuracy.

In summary, the seismic stratigraphy at Site 987 appears to reflect variations in the frequency and amount of gravity-driven sediment transport from the East Greenland Shelf, which is in accordance with the site being located at the northeastern flank of the Scoresbysund glacial fan. Intervals of more frequent debris flows form the most distinct seismic reflectors but do not seem to be the volumetrically most important deposits. This differs from Site 986 on the Svalbard Margin, where the greater part of the drilled section apparently consisted of debris flows (see "Site 986" chapter, this volume).

Results of the shipboard paleomagnetic studies indicate a late Miocene age for the lowermost drilled sediments, immediately above basement. In a previous seismic interpretation of Line GGU82-12, Larsen (1990) assigned a middle to late Miocene age to the part of the seismic section between basement and Reflector R3, late Miocene to the equivalent of seismic Unit EG-III, late Miocene–Pliocene above Reflector R2 and Pleistocene only for the upper approximately 50 mbsf. A main result of drilling at Site 987 is, therefore, that new and younger ages can be assigned to the main buildup of the Scoresbysund Fan. Based on Line GGU82-12, and also shown by Larsen (1990), the main phase of fan construction took place after Reflector R3 time, which we date at approximately lower upper Pliocene. The depocenter for the period prior to this is located below the present-day middle to inner shelf.

REFERENCES

Berggren, W.A., Hilgen, F.J., Langereis, C.G., Kent, D.V., Obradovich, J.D., Raffi, I., Raymo, M.E., and Shackleton, N.J., 1995. Late Neogene chronology: new perspectives in high-resolution stratigraphy. *Geol. Soc. Am. Bull.*, 107:1272–1287.

Borehole Research Group, 1994. *Wireline Logging Services Guide:* Palisades, NY (Lamont-Doherty Earth Observatory, Columbia Univ.).

Cande, S.C., and Kent, D.V., 1995. Revised calibration of the geomagnetic polarity timescale for the Late Cretaceous and Cenozoic. *J. Geophys. Res.,* 100:6093–6095.

Eldholm, O., Thiede, J., Taylor, E., et al., 1987. *Proc. ODP, Init. Repts.,* 104: College Station, TX (Ocean Drilling Program).

Fronval, T. and Jansen, E., in press. Late Neogene paleoclimates and paleoceanography in the Iceland-Norwegian Sea: evidence from the Iceland and Vøring Plateaus, ODP Leg 151 and 104. *In* Thiede, J., Myhre, A.M., Firth, J.V., Johnson, G.L., and Ruddiman, W.F. (Eds.), *Proc. ODP, Sci. Results,* 151: College Station, TX (Ocean Drilling Program).

Funder, S., 1989. Development of climate, glaciation and ocean circulation. *In* Fulton, R. (Ed.), *Quaternary Geology of Canada and Greenland.* Geol. Soc. Am., Geol. of North Am. Ser., K-1:783–792.

Hamilton, E.L., 1979. Sound velocity gradients in marine sediments. *J. Acoust. Soc. Am.,* 65:909–922.

Jansen, E., Bleil, U., Henrich, R., Kringstad, L., and Slettemark, B., 1988. Paleoenvironmental changes in the Norwegian Sea and Northeast Atlantic during the last 2.8 m.y.: Deep Sea Drilling Project/Ocean Drilling Program Sites 610, 642, 643, and 644. *Paleoceanography,* 3:563–581.

Jansen, E., and Sjøholm, J., 1991. Reconstruction of glaciation over the past 6 Myr from ice-borne deposits in the Norwegian Sea. *Nature,* 349:600–603.

Kvenvolden, K.A., and Barnard, L.A., 1983. Gas hydrates of the Blake Outer Ridge, Site 533, Deep Sea Drilling Project Leg 76. *In* Sheridan, R.E., Gradstein, F.M., et al., *Init. Repts. DSDP,* 76: Washington (U.S. Govt. Printing Office), 353–365.

Larsen, H.C., 1990. The East Greenland Shelf. *In* Grantz, A., Johnson, G.L., and Sweeney, J.F. (Eds.), *The Arctic Ocean Region.* Geol. Soc. Am., Geol. of North Am. Ser., L:185–210.

Larsen, H.C., Saunders, A.D., Clift, P.D., et al., 1994. *Proc. ODP, Init. Repts.,* 152: College Station, TX (Ocean Drilling Program).

Larsen, H.C., Saunders, A.D., Clift, P.D., Beget, J., Wei, W., Spezzaferri, S., and the ODP Leg 152 Scientific Party, 1994. Seven million years of glaciation in Greenland. *Science,* 264:952–955.

McDuff, R.E., 1981. Major cation gradients in DSDP interstitial waters: the role of diffusive exchange between seawater and upper oceanic crust. *Geochim. Cosmochim. Acta,* 45:1705–1713.

Myhre, A.M., Thiede, J., Firth, J.V., et al., 1995. *Proc. ODP, Init. Repts.,* 151: College Station, TX (Ocean Drilling Program).

Okada, H., and Bukry, D., 1980. Supplementary modification and introduction of code numbers to the low-latitude coccolith biostratigraphic zonation (Bukry, 1973; 1975). *Mar. Micropaleontol.,* 5:321–325.

Spiegler, D., and Jansen, E., 1989. Planktonic foraminiferal biostratigraphy of Norwegian Sea sediments: ODP Leg 104. *In* Eldholm, O., Thiede, J., Taylor, E., et al., *Proc. ODP, Sci. Results,* 104: College Station, TX (Ocean Drilling Program), 681–696.

Vogt, P.R., 1986. Geophysical and geochemical signatures and plate tectonics. *In* Hurdle, B.G. (Ed.), *The Nordic Seas:* New York (Springer-Verlag), 413–662.

Wolf, T.C.W., and Thiede, J., 1991. History of terrigenous sedimentation during the past 10 m.y. in the North Atlantic (ODP Legs 104 and 105 and DSDP Leg 94). *Mar. Geol.,* 101:83–102.

Ms 162IR-110

Note: For all sites drilled, core description forms ("barrel sheets") and core photographs can be found in Section 3, beginning on page 391. Forms containing smear slide data can be found in Section 4, beginning on page 1147. All processed logs (including FMS, dipmeter, temperature data, high-resolution density and neutron data, and sonic waveforms not shown in printed form) are on the CD-ROM enclosed in the back pocket of this volume. Also on the CD-ROM are all tables from this chapter (including an extended coring summary table) and shipboard measurements (files containing GRAPE density, *P*-wave velocity, natural gamma radiation, magnetic susceptibility, index properties, and spectral reflectance data).

Table 11. Composition of interstitial waters in Holes 987A, 987D, and 987E.

Core, section, interval (cm)	Depth (mbsf)	Na (mM)	K (mM)	Li (μM)	Mg (mM)	Ca (mM)	Sr (μM)	Cl (mM)	SO_4 (mM)	NH_4 (μM)	Si (μM)	PO_4 (μM)	pH	Alkalinity (mM)	Salinity
162-987A-															
1H-4, 145–150	5.95	484	11.7	43.6	47.4	9.3	82	558	23.0	185	207	8.9	7.68	5.898	35.0
2H-4, 145–150	14.45	483	10.4	25.8	46.2	6.8	75	561	15.0	669	313	10.3	7.81	9.292	33.0
4H-4, 145–150	33.45	485	8.3	16.9	40.9	2.9	72	566	0.0	1009	285	53.0	7.95	15.347	32.0
6H-3, 145–150	50.95	486	6.5	16.9	39.3	3.8	73	564	0.0	1393	194	7.0	8.16	14.632	31.5
9H-4, 145–150	73.65	487	4.7	18.9	41.2	5.0	79	570	0.0	2015	250	7.8	7.96	14.293	32.0
13X-4, 145–150	108.95	480	3.7	23.9	38.4	6.1	76	559	0.8	2529	291	5.9	7.97	12.301	32.5
16X-4, 145–150	137.75	484	3.4	32.9	37.0	6.4	76	565	0.2	2876	527	10.0	7.81	9.090	32.0
19X-4, 140–150	166.60	478	2.7	37.9	36.9	8.3	82	564	0.0	2883	356	23.3	7.82	7.867	32.0
22X-5, 140–150	195.82	483	2.5	46.1	32.7	11.3	101	567	0.0	2536	509	4.9	7.86	6.985	32.0
162-987D-															
25X-4, 145–150	215.35	469	2.3	51.1	32.7	15.1	108	561	0.3	2377	455	3.0	7.88	5.567	32.0
28X-2, 140–150	241.10	466	1.6	50.2	28.7	20.9	123	563	0.1	2044	265	1.9	8.05	3.877	32.0
31X-4, 140–150	272.89	460	1.3	49.2	20.2	31.4	129	563	0.0	1443	222	2.1	7.06	2.298	32.5
34X-1, 140–150	297.40	457	1.2	41.3	11.0	43.3	134	565	0.4	1139	239	1.9	7.89	1.714	33.0
40X-1, 140–150	345.40	446	1.2	31.3	3.7	55.0	139	562	1.1	1371	176	2.1	8.29	0.641	32.0
162-987E-															
1R-1, 140–150	364.70							559					8.13	1.081	33.0
5R-3, 140–150	402.40							556					8.77	2.511	33.0
8R-4, 140–150	432.70							560					8.18	3.264	32.0
11R-2, 140–150	458.70							541					8.47	2.373	30.0
14R-2, 140–150	487.50							549					8.47	1.784	31.0
17R-4, 140–150	519.30							541					8.31	1.307	31.0
20R-4, 140–150	548.10							539					8.75	1.128	32.0
23R-2, 135–150	573.85							542					8.74	1.211	31.5
26R-4, 135–150	605.10							545							31.0
29R-5, 130–145	636.10							527					8.75	1.387	31.0
32R-4, 42–57	662.09							519					8.95	1.804	30.0
35R-2, 135–150	689.12							525					9.13	1.754	30.0
38R-4, 137–150	721.03							514					8.88	1.534	30.0
41R-1, 114–128	745.24							522					8.77	1.405	30.0
44R-2, 135–150	775.65							526					8.87	1.367	31.0
47R-3, 133–150	806.13							540					8.62	1.104	32.0
50R-2, 145–160	833.55							533					8.80	1.256	30.5

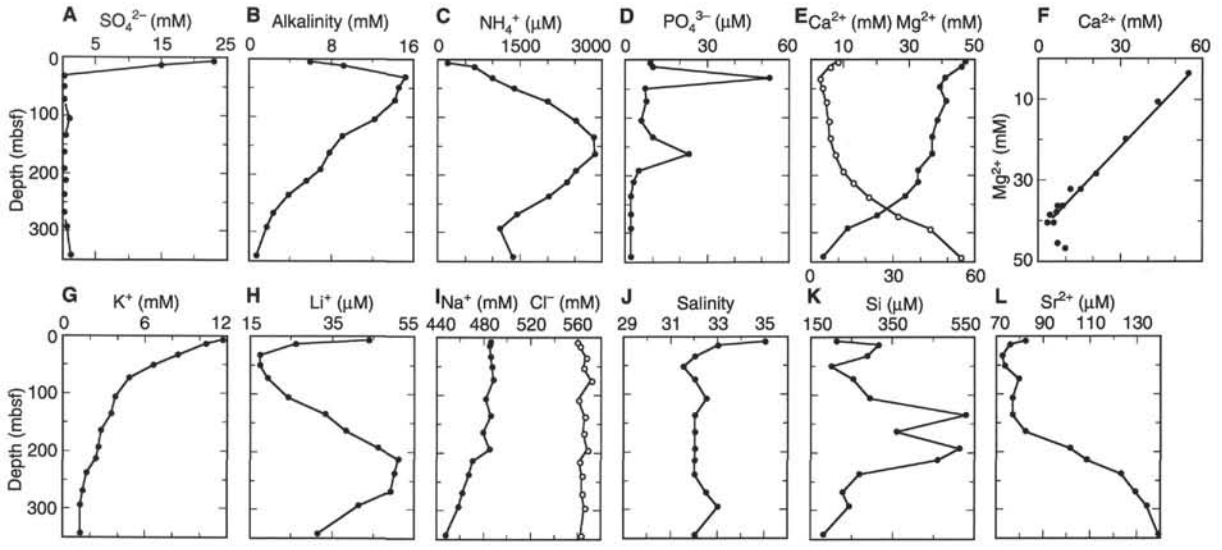

Figure 19. Vertical profiles of sulfate (**A**), alkalinity (**B**), ammonium (**C**), phosphate (**D**), calcium and magnesium (**E**), calcium vs. magnesium (**F**), potassium (**G**), lithium (**H**), sodium and chloride (**I**), salinity (**J**), silica (**K**), and strontium (**L**) in Holes 987A and 987D.

Table 12. Index properties of samples from Holes 987D and 987E.

Core, section, interval (cm)	Depth (mbsf)	Water content (wet %)	Water content (dry %)	Wet bulk density Method C (g/cm^3)	Grain density Method C (g/cm^3)	Dry bulk density Method C (g/cm^3)	Porosity Method C (%)	Void ratio Method C
162-987D-								
2H-1, 120–122	2.50	44.3	79.6	1.55	2.64	0.87	67.3	2.05
2H-2, 35–37	3.15	34.2	52.0	1.72	2.64	1.13	57.3	1.34
2H-2, 120–122	4.00	40.5	68.0	1.61	2.64	0.96	63.6	1.75
2H-3, 35–37	4.65	40.6	68.4	1.63	2.73	0.97	64.6	1.82
2H-3, 120–122	5.50	41.4	70.7	1.59	2.61	0.93	64.3	1.80
2H-4, 28–30	6.08	34.8	53.3	1.69	2.59	1.10	57.4	1.35
2H-4, 121–123	7.01	37.9	61.1	1.65	2.64	1.02	61.1	1.57
2H-5, 32–34	7.62	31.6	46.3	1.76	2.65	1.21	54.5	1.20
2H-5, 107–109	8.37	39.2	64.5	1.64	2.68	1.00	62.7	1.68

Only part of this table is reproduced here. The entire table appears on the CD-ROM (back pocket).

Table 13. Compressional-wave velocity measurements from Holes 987D and 987E.

Core, section, interval (cm)	Depth (mbsf)	Velocity (m/s)	Temperature (°C)	Direction
162-987D-				
1H-1, 20	0.20	1503	20.2	y
1H-1, 95	0.95	1517	20.3	y
2H-1, 44	1.74	1504	19.4	y
2H-1, 121	2.51	1499	19.2	y
2H-2, 21	3.01	1536	19.5	y
2H-2, 115	3.95	1526	19.8	y
2H-3, 26	4.56	1515	19.3	y
2H-3, 117	5.47	1503	19.2	y
2H-4, 26	6.06	1564	19.0	y

Note: For explanation of measurement directions, see "Explanatory Notes" chapter (this volume).

Only part of this table is reproduced here. The entire table appears on the CD-ROM (back pocket).

Table 14. Undrained shear strength measurements from Hole 987D.

Core, section, interval (cm)	Depth (mbsf)	Undrained shear strength (kPa)	Spring no.
162-987D-			
1H-1, 20	0.20	3.9	1
1H-1, 95	0.95	5.1	1
2H-1, 45	1.75	11.1	1
2H-1, 121	2.51	6.8	1
2H-2, 116	3.96	7.3	1
2H-3, 27	4.57	8.2	1
2H-3, 118	5.48	11.5	1
2H-4, 123	7.03	7.5	1
2H-5, 32	7.62	9.9	1

Only part of this table is reproduced here. The entire table appears on the CD-ROM (back pocket).

Table 15. Undrained shear strength measured by the fall-cone device, Hole 987D.

Core, section, interval (cm)	Depth (mbsf)	Cone type (g/degree)	Penetration (mm)	Undrained shear strength (kPa)
162-987D-				
1H-1, 20	0.20	60/60	7.5	2.65
1H-1, 95	0.95	60/60	11.0	1.18
2H-1, 45	1.75	60/60	5.0	5.88
2H-1, 121	2.51	60/60	6.0	4.12
2H-2, 22	3.02	60/60	6.0	4.12
2H-2, 116	3.96	60/60	4.5	7.25
2H-3, 27	4.57	100/30	9.8	10.30
2H-3, 118	5.48	100/30	9.5	11.00
2H-4, 125	7.05	60/60	4.0	9.21
2H-4, 25	6.05	60/60	4.0	9.21

Only part of this table is reproduced here. The entire table appears on the CD-ROM (back pocket).

Table 17. Thermal conductivity measurements from Holes 987A, 987B, and 987D.

Core, section, interval (cm)	Depth (mbsf)	Thermal conductivity (W/[m·K])	Standard error (W/[m·K])
162-987A-			
1H-2, 75	2.25	1.236	0.00670
1H-3, 75	3.75	1.111	0.00552
1H-5, 75	6.75	0.994	0.00324
1H-6, 35	7.85	1.654	0.00442
2H-3, 75	12.25	1.214	0.00272
2H-5, 75	15.25	1.070	0.00226
4H-1, 75	28.25	1.421	0.00267
4H-3, 75	31.25	1.317	0.00407
4H-5, 75	34.25	1.364	0.00241

Only part of this table is reproduced here. The entire table appears on the CD-ROM (back pocket).

Table 16. Summary statistics of the physical properties for the geotechnical units and subunits at Site 987.

	Water content (%)			Porosity (%)		
Unit	Min.	Max.	Mean	Min.	Max.	Mean
G1A	25.8	60.5	35.8	47.2	73.1	58.1
G1B	11.2	39.0	26.0	25.2	63.0	47.4
G2	9.2	24.4	14.7	21.1	46.2	31.3
G3	5.4	26.6	19.5	13.3	48.5	36.7
G4	10.3	29.3	13.3	23.7	52.9	28.8
G5	12.6	26.5	17.2	27.5	48.5	35.2

	Void ratio			Wet bulk density (g/cm^3)		
Unit	Min.	Max.	Mean	Min.	Max.	Mean
G1A	0.89	3.87	1.50	1.34	1.87	1.70
G1B	0.34	1.70	0.93	1.65	2.31	1.89
G2	0.30	0.86	0.46	1.94	2.40	2.20
G3	0.20	0.90	0.64	1.87	2.54	2.04
G4	0.30	1.10	0.43	1.85	2.37	2.24
G5	0.38	0.94	0.55	1.87	2.25	2.10

	Dry bulk density (g/cm^3)			Grain density (g/cm^3)		
Unit	Min.	Max.	Mean	Min.	Max.	Mean
G1A	0.53	1.39	1.10	2.54	2.78	2.65
G1B	1.01	2.06	1.40	2.58	2.80	2.67
G2	1.46	2.16	1.88	2.65	2.83	2.73
G3	1.37	2.40	1.64	2.55	2.80	2.68
G4	1.31	2.13	1.95	2.61	2.84	2.74
G5	1.38	1.95	1.74	2.57	2.82	2.68

	Velocity (m/s)		
Unit	Min.	Max.	Mean
G1A	1481	1653	1550
G1B	1491	2315	1585
G2	2210	2977	2600
G3	1776	4150	1972
G4	2020	4761	2615
G5	1914	2823	2151

	Vane strength (kPa)			Core strength (kPa)		
Unit	Min.	Max.	Mean	Min.	Max.	Mean
G1A	4	36	14.4	1.2	235.2	59.7
G1B	12	104	47.7	131.3	158.8	142.1

Table 18. Logged depth intervals in Hole 987E for Quad combo, GHMT, and FMS runs.

String	Run	Depth interval logged (mbsf)	Depth interval logged (mbrf)	Tools
Quad combo:	Up	489.0–77.0	2171.0–1761.0	NGT/SDT/CNT-G/HLDT/DIT/TLT
	Up*	176.0–111.0	1860.0–1795.0	NGT/SDT/CNT-G/HLDT/DIT/TLT
Start time:	1530 hr (8/31/95)—after failed logging attempts in lower section			
Stop time:	2000 hr			
Logging speeds:	375m/hr down log			
	275m/hr up log			
(Mudline measured at 1682.4 mbrf with NGT)				

String	Run	Depth interval logged (mbsf)	Depth interval logged (mbrf)	Tools
GHMT:	Up	483.0–77.0	2165.0–1762.0	NGT/GHMT
	Up*	216.0–116.0	1900.0–1800.0	NGT/GHMT
Start time:	2000 hr			
Stop time:	2315 hr			
Logging speed:	550m/hr			

String	Run	Depth interval logged (mbsf)	Depth interval logged (mbrf)	Tools
FMS:	Up*	410.0–202.0	2092.0–1886.0	NGT/FMS/GPIT
	Up	412.0–77.0	2094.0–1761.0	NGT/FMS/GPIT
Start time:	2315 hr			
Stop time:	0205 hr (9/1/95)—logging completed			
Logging speed:	460 m/hr			
Wireline heave compensation testing:				
Start time:	0230 hr			
Stop time:	0330 hr (9/1/95)			
Wiper trip:	Hole conditioning prior to logging			
Start time:	1500 hr (8/30/95)—logging started			
Stop time:	0800 hr (8/31/95)			
Total logging time: 36.5 hr				
Estimated time: ~36–38 hr				

Notes: Depths are in meters below seafloor (mbsf) and meters below rig floor (mbrf). * = repeat section for quality control. For tool abbreviations, see note below table 19, "Site 986" chapter (this volume).

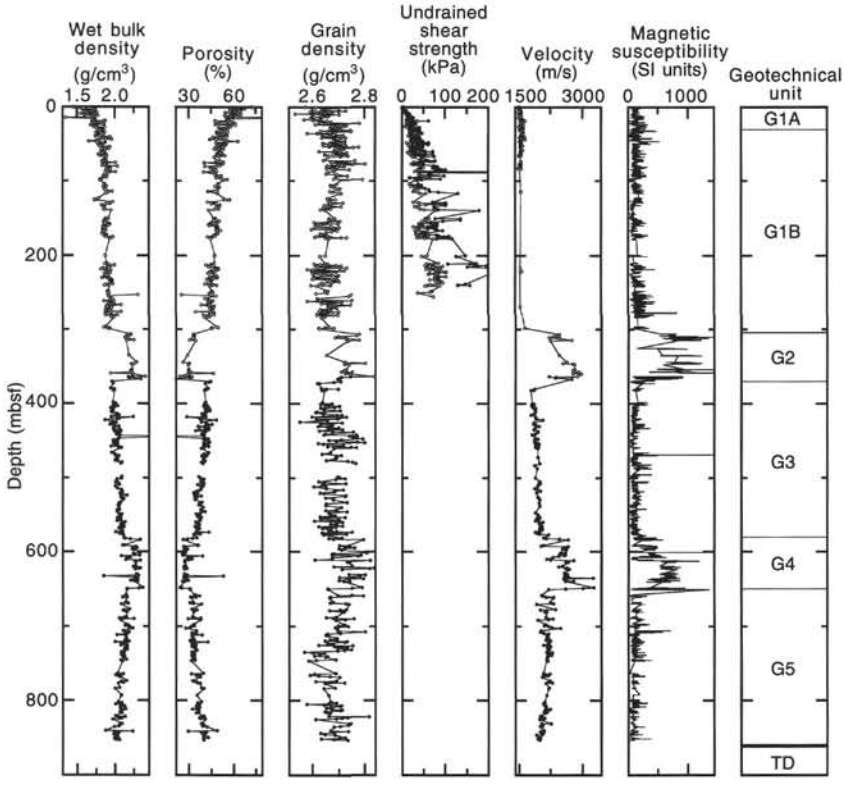

Figure 20. Geotechnical stratigraphy of Site 987, with vertical profiles of wet bulk density, porosity, grain density, *P*-wave velocity, undrained shear strength, and magnetic susceptibility. Open and solid circles represent measurements from Holes 987D and 987E, respectively. Undrained shear strength measurements were made only in Hole 987D, and here the open and solid circles mark motorized vane and fall-cone values, respectively.

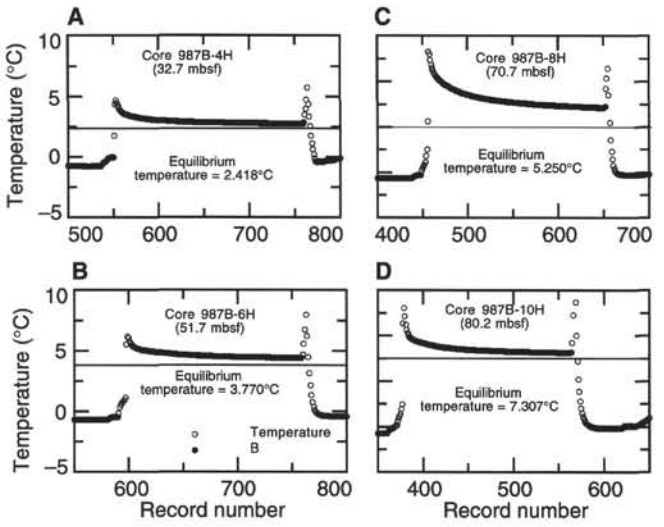

Figure 21. **A–D.** Downhole temperature measurements and calculated equilibrium temperatures from Hole 987B.

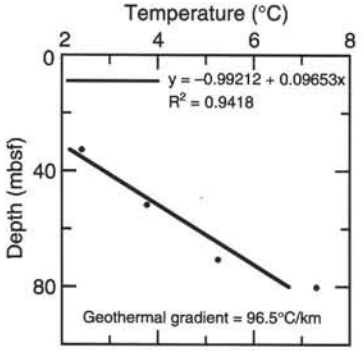

Figure 22. Calculated geothermal gradient for Hole 987B.

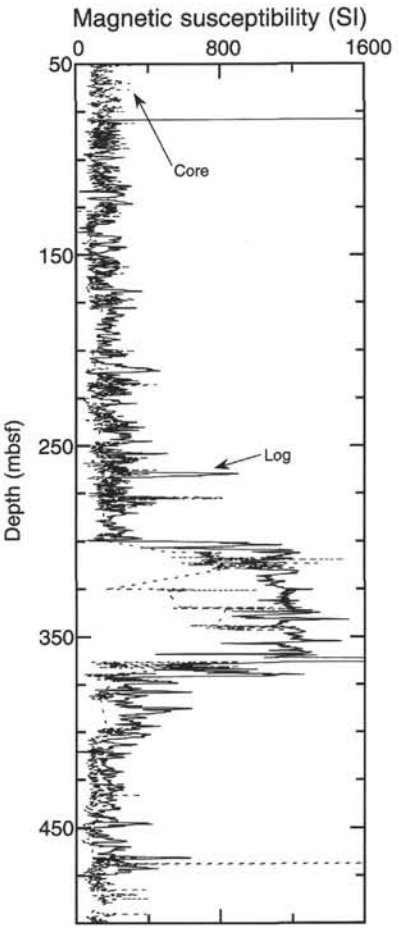

Figure 23. Comparison of log magnetic susceptibility data with magnetic susceptibility core measurements (dashed line) from Hole 987E. Depth scales for both data sets are given in meters below seafloor (mbsf). No depth shifts were applied to the data.

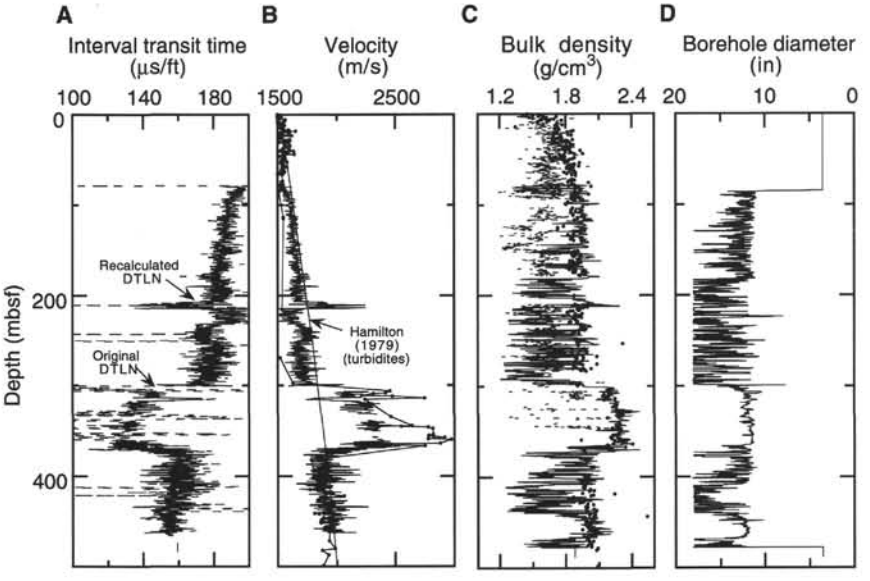

Figure 24. **A.** Comparison of original depth-derived, borehole-compensated sonic logs (DTLN) from Hole 987E, computed during logging, with the same log recalculated after removal of noise spikes from the original transit-time data. **B.** Comparison of seismic velocities from recalculated sonic log with laboratory velocity measurements on core samples (line with solid circles) and the empirical velocity-vs.-depth functions for turbidite successions from Hamilton (1979). **C.** Comparison of wireline log bulk density measurements (solid line) with GRAPE bulk density measurements (dashed line) and gravimetric wet bulk density measurements (line with solid circles). **D.** Downhole caliper measurements show the washed-out zones that account for the very low densities observed.

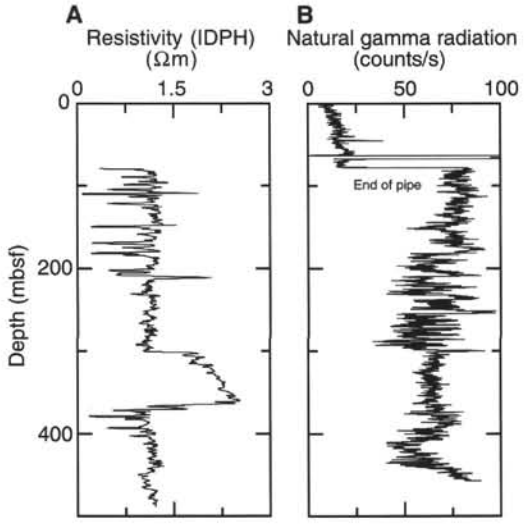

Figure 25. **A.** Downhole resistivity measurements from Site 987 clearly define the sharp boundaries of the debris-flow layer between 300 and 369 mbsf. **B.** Downhole natural gamma-ray measurements at Site 987. Note the similar wireline response of natural-gamma-ray log to debris-flow layers.

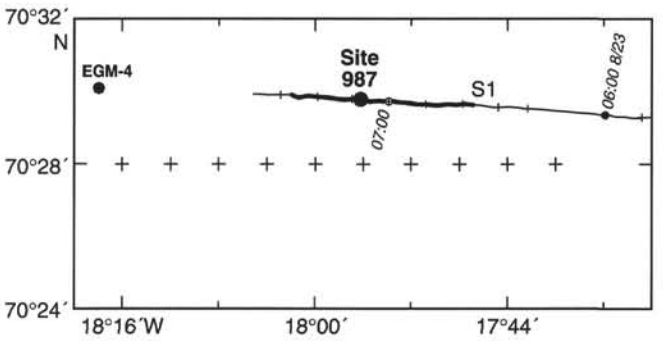

Figure 26. Map showing the proposed site EGM-4 and the site survey near Site 987. Note that the line started farther east at 17°16′E, but only the portion nearest the site is shown here and is discussed in this chapter. Bold line marks profile shown in Figure 27.

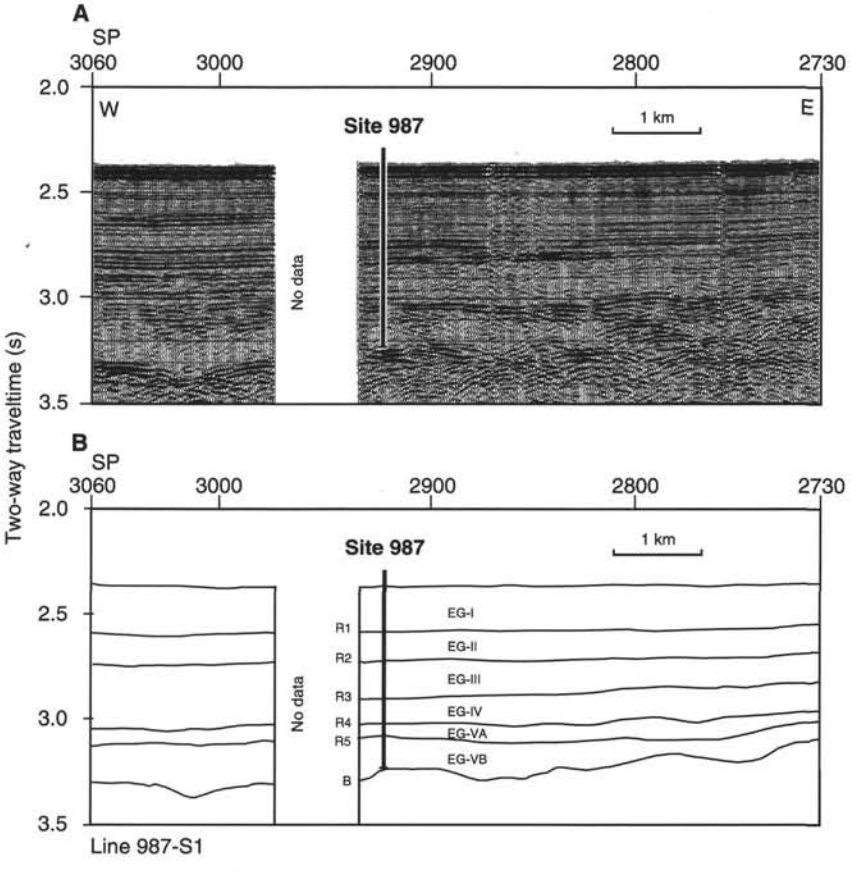

Figure 27. **A.** Part of seismic Line 987-S1, crossing Site 987. **B.** Line interpretation of seismic Line 987-S1. See Figure 26 for location.

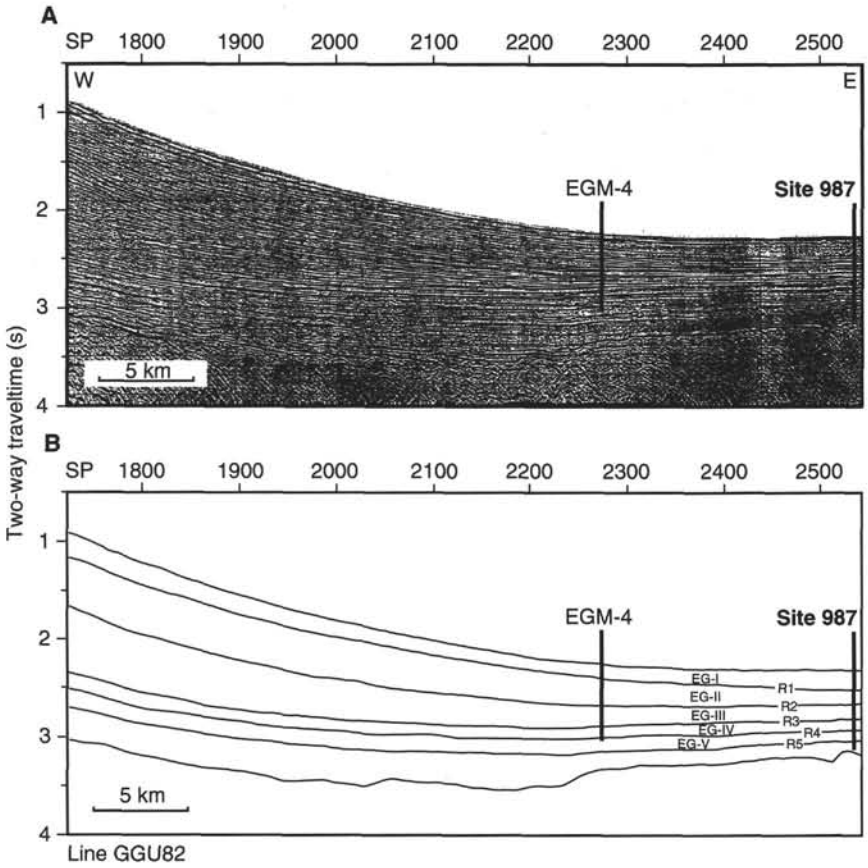

Figure 28. **A.** Portion of pre-cruise seismic Line GGU82-12, showing the proposed site EGM-4 and Site 987. **B.** Line interpretation of seismic Line GGU82-12. See Figure 26 for location of the sites.

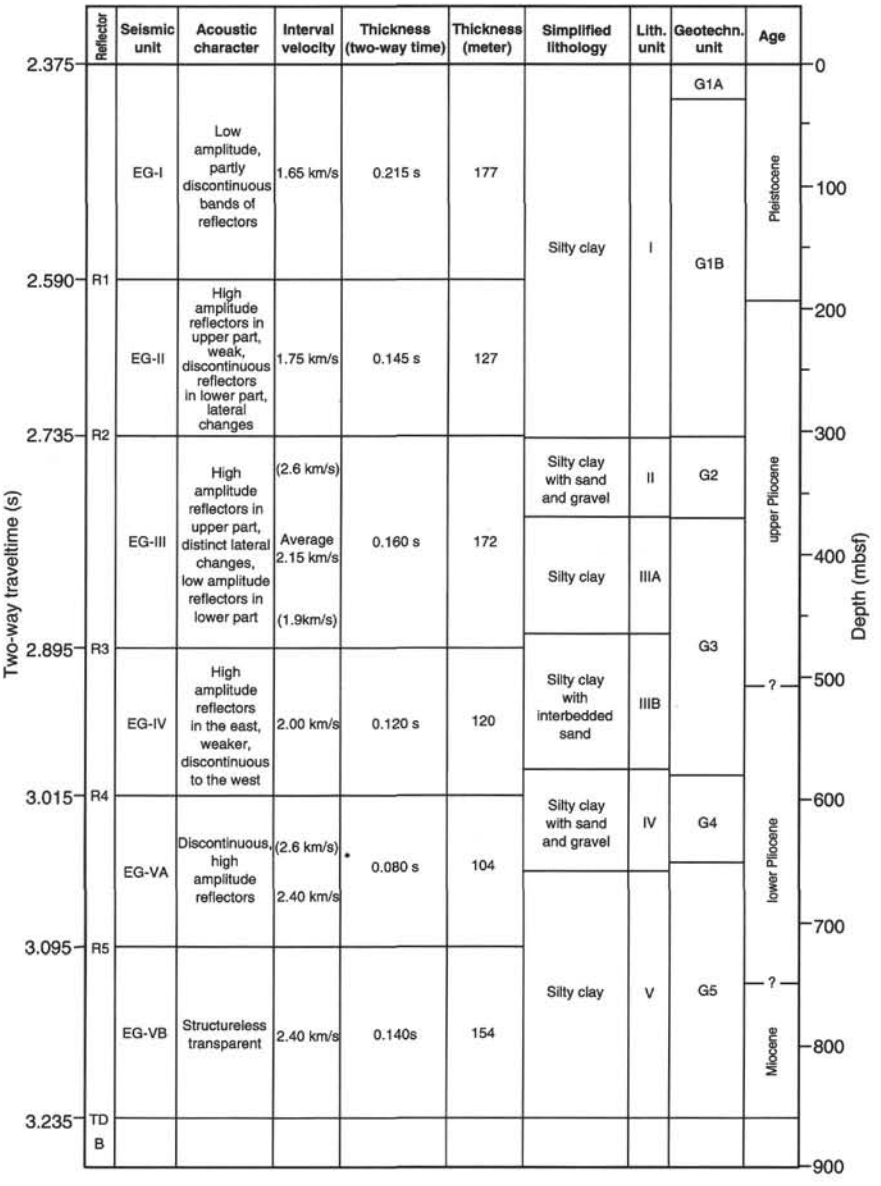

Figure 29. Correlation of the seismic stratigraphy with lithostratigraphy and geotechnical stratigraphy. TD = total depth; B = basement.

SHORE-BASED LOG PROCESSING

Hole 987E

Bottom felt: 1684.2 mbrf
Total penetration: 363.3 mbsf
Total core recovered: 308.8 m (62.3%)

Logging Runs

Logging string 1: DIT/SDT/HLDT/CNTG/NGT
Logging string 2: GHMT/NGT
Logging string 3: FMS/GPIT/NGT (2 passes)
Wireline heave compensator was used to counter ship's heave.

Bottom-Hole Assembly

The following bottom-hole/pipe/casing assembly (BHA) depths are as they appear on the logs after differential depth shift (see "Depth shift" section) and depth shift to the seafloor. As such, there might be a discrepancy with the original depths given by the drillers on board. Possible reasons for depth discrepancies are ship's heave, use of wireline heave compensator, and drill string and/or wireline stretch.

DIT/SDT/HLDT/CNTG/NGT: BHA at ~78 mbsf.
GHMT/NGT: BHA at mbsf ~78 mbsf.
FMS/GPIT/NGT: BHA at ~77.5 mbsf (pass 1).
FMS/GPIT/NGT: Did not reach BHA.

Processing

Depth shift: Original logs have been interactively depth shifted with reference to NGT from DIT/SDT/HLDT/CNTG/NGT main run, and to the seafloor (–1682 m). Note that the depth of the seafloor as seen on the logs differs from the "bottom felt" depth given by the drillers (–2.2 m).

Gamma-ray processing: Data have been processed to correct for borehole size and type of drilling fluid.

Acoustic data processing: The array sonic tool was operated in standard depth-derived borehole compensated mode including long-spacing (8–10–10–12 ft) logs. The logs have been processed to eliminate some of the noise and cycle skipping experienced during the recording.

Quality Control

Data recorded through bottom-hole assembly, such as the neutron porosity and gamma-ray data above 78 mbsf, should be used qualitatively only because of the attenuation on the incoming signal. Invalid gamma-ray spikes were recorded at 63–67 mbsf.

Hole diameter was recorded by the hydraulic caliper on the HLDT tool (CALI) and the caliper on the FMS string (C1 and C2).

Note: Details of standard shore-based processing procedures are found in the "Explanatory Notes" chapter (this volume). For further information about the logs, please contact:

Crstina Broglia
Phone: 914-365-8343
Fax: 914-365-3182
E-mail: chris@ldeo.columbia.edu

Elizabeth Pratson
Phone: 914-365-8313
Fax: 914-365-3182
E-mail: beth@ldeo.columbia.edu

Hole 987E: Natural Gamma Ray-Resistivity-Sonic Logging Data

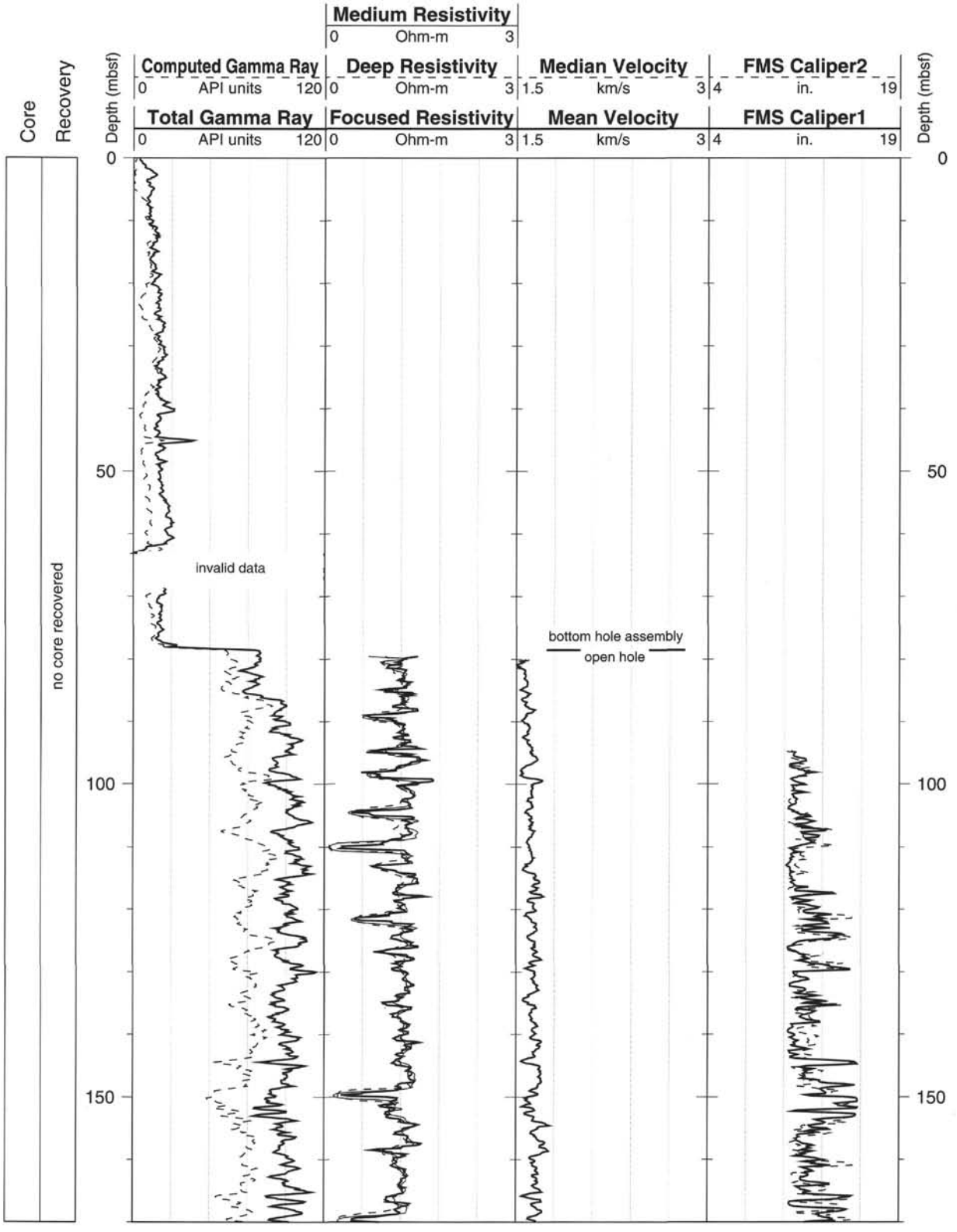

Hole 987E: Natural Gamma Ray-Resistivity-Sonic Logging Data (cont.)

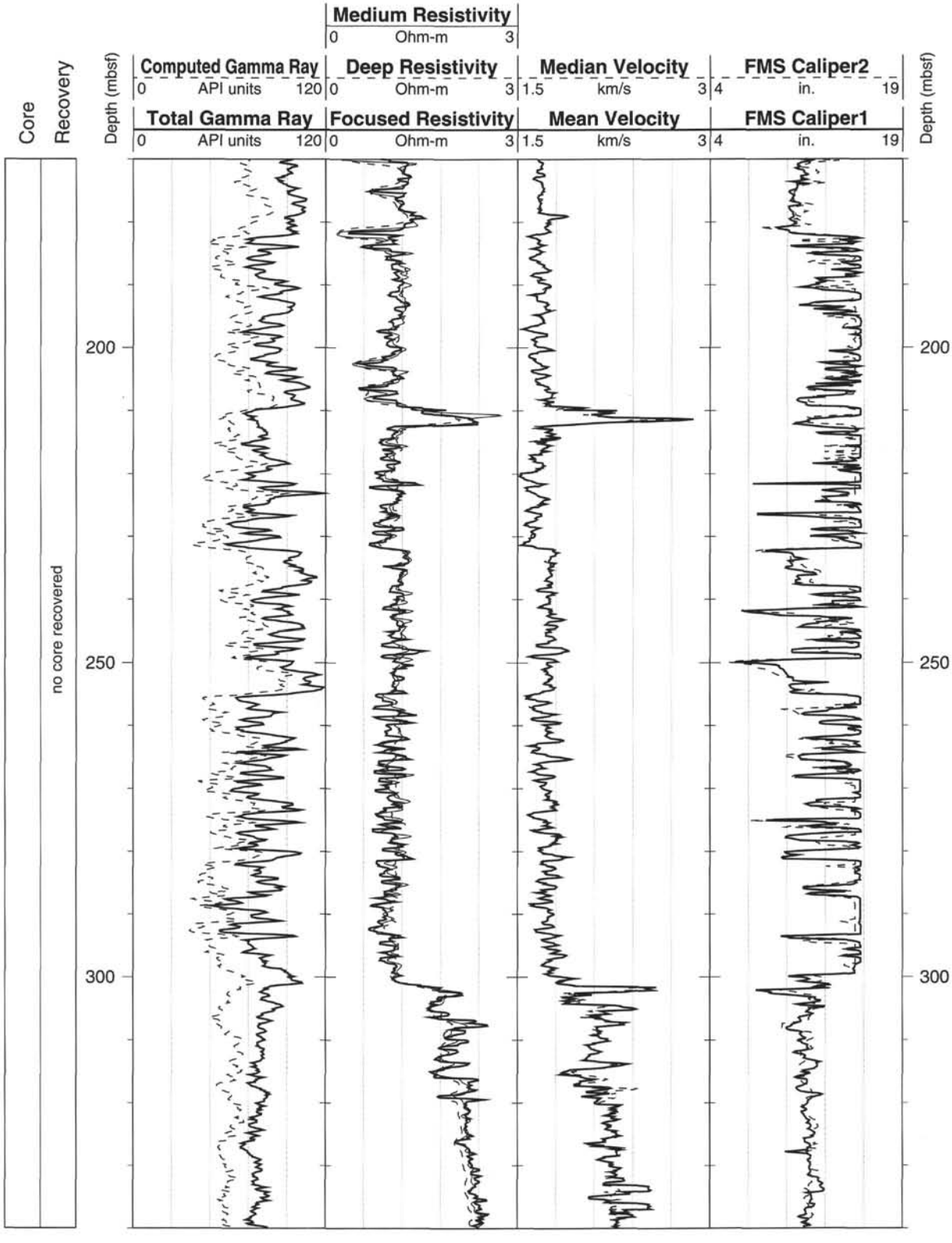

Hole 987E: Natural Gamma Ray-Resistivity-Sonic Logging Data (cont.)

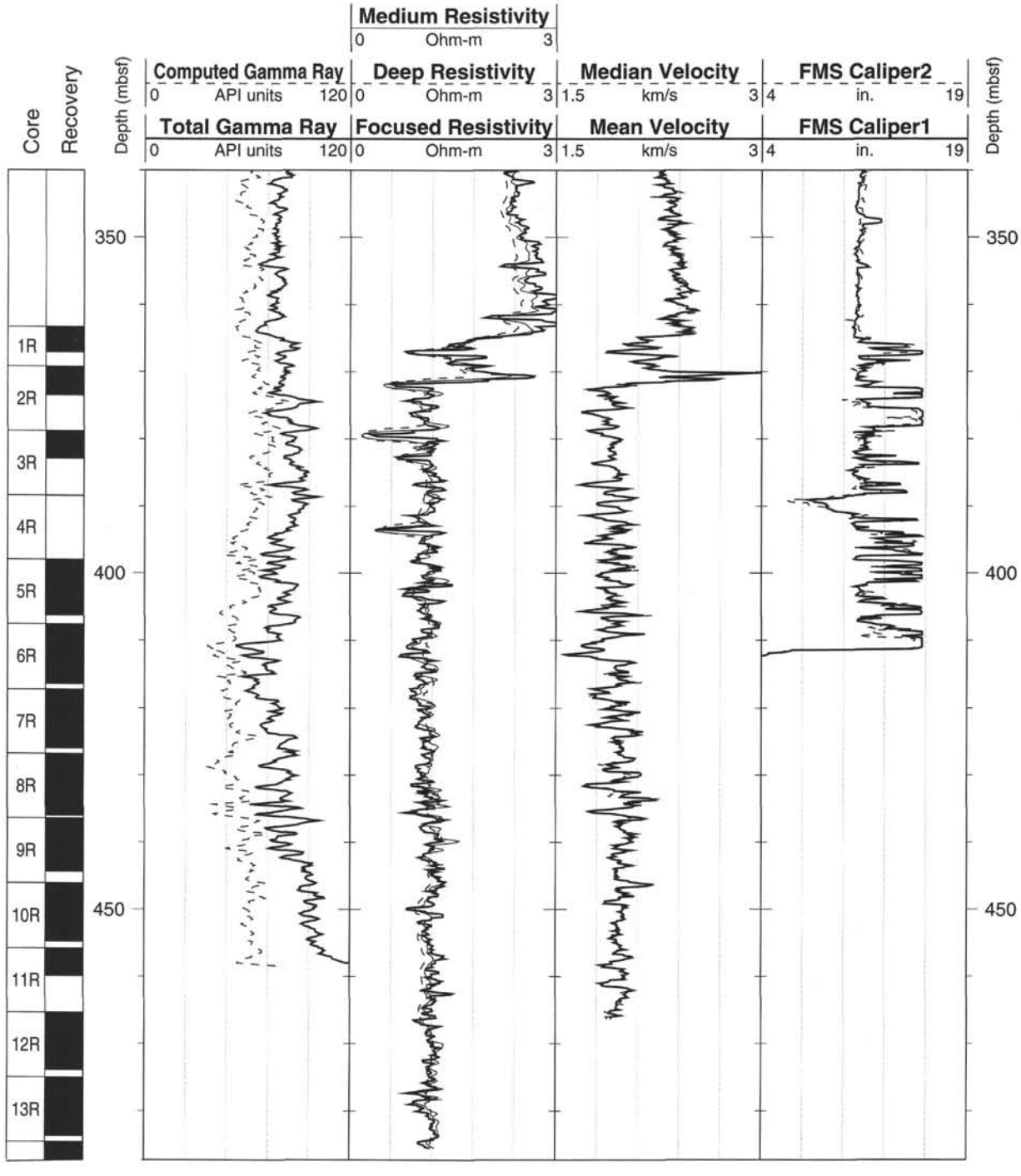

Hole 987E: Natural Gamma Ray-Density-Porosity Logging Data

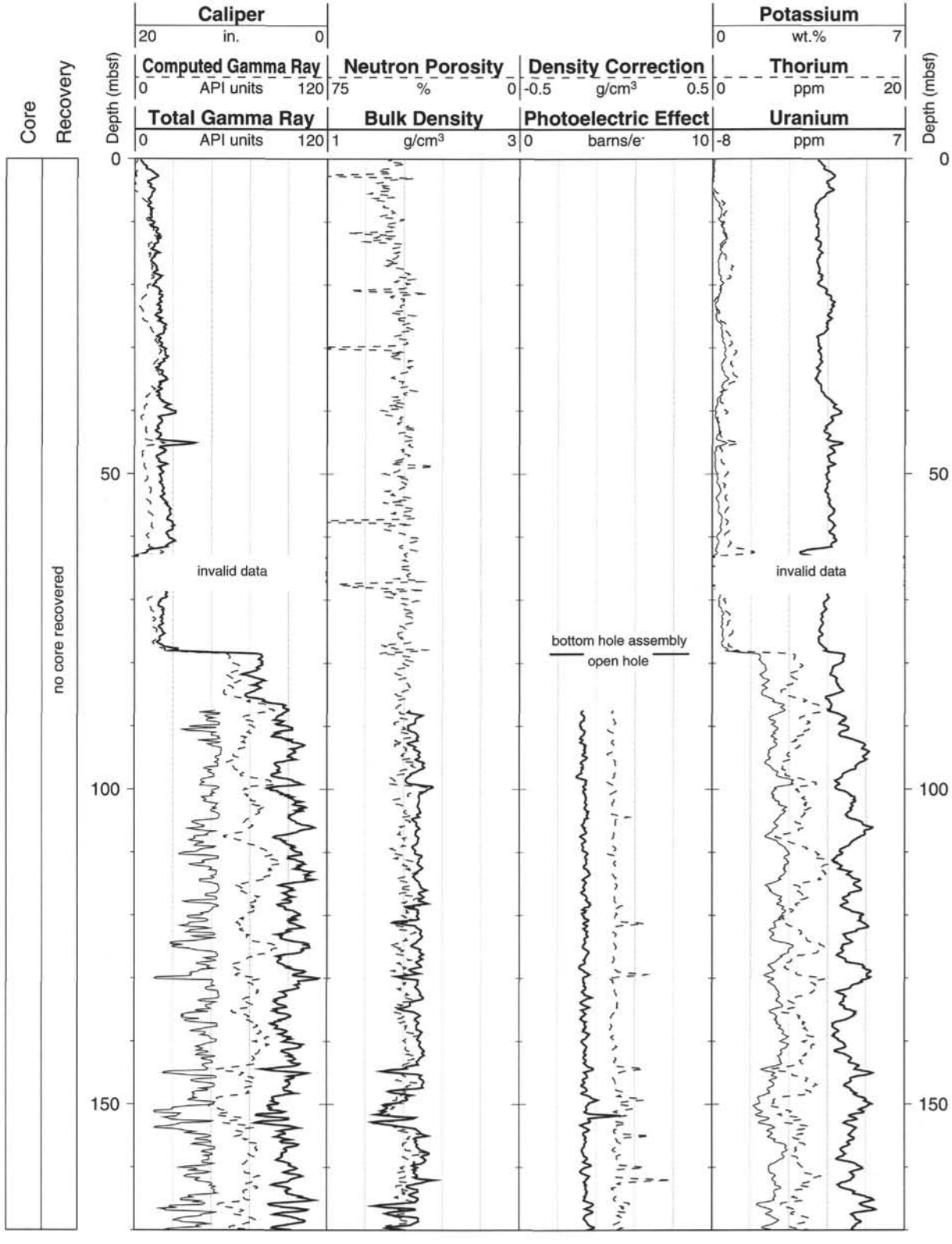

Hole 987E: Natural Gamma Ray-Density-Porosity Logging Data (cont.)

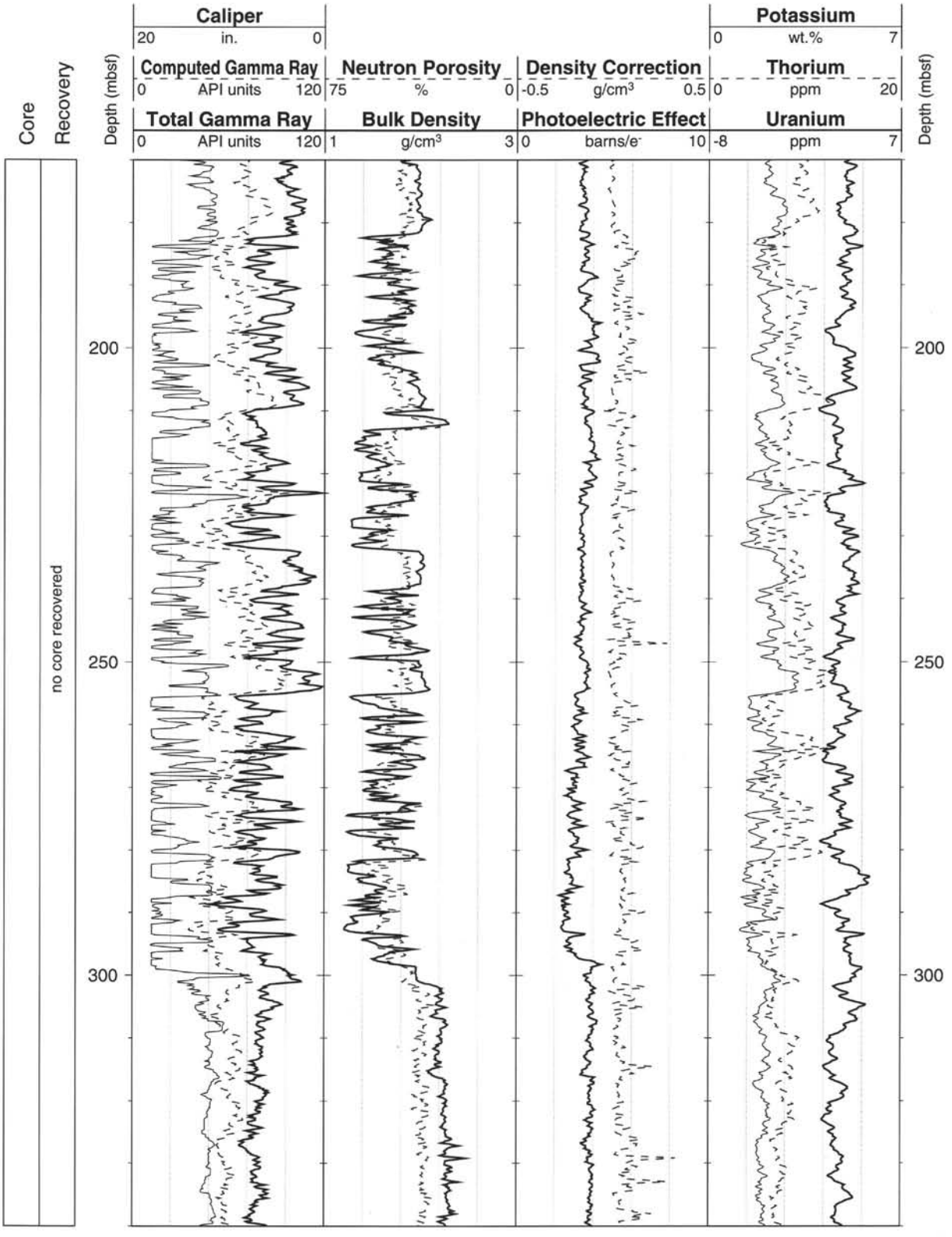

Hole 987E: Natural Gamma Ray-Density-Porosity Logging Data (cont.)